

High-resolution magnetic susceptibility data interpretation in a well through the Miocene of the Vienna Basin

8/13/2015

Delft University of Technology

JUAN NOBILE

High-resolution magnetic susceptibility data interpretation in a well through the Miocene of the Vienna Basin

by
JUAN NOBILE
4321960

A thesis submitted in partial fulfillment of the requirements for the
degree of

MASTER OF SCIENCE
IN PETROLEUM ENGINEERING AND GEOSCIENCES

at the

DELFT UNIVERSITY OF TECHNOLOGY
2015

Delft University Of Technology
Department Of
Petroleum Engineering and Geosciences

The thesis of Juan Nobile is approved by the Thesis Examining
Committee

Dated: August 13th, 2015

Prof. Dr. Stefan Luthi
(Supervisor TU DELFT)

Prof. Dr. Giovanni Bertotti
(TU DELFT)

Dr. Auke Barnhoorn
(TU DELFT)

Prof. Dr. Gert Jan Weltje
(KU Leuven)

ACKNOWLEDGMENTS

Primarily I would like to thank God for giving me the strength needed along this difficult and risky stage in my life.

I am grateful to Prof. Dr. Stefan Luthi for his technical support during the whole project. He proposed me this thesis work and guided me through until the project was successfully completed. His feedback and inputs were extremely valuable and always available even with his extremely busy agenda. Also thanks for the finance aid when needed.

Also, I would like to express my sincere gratitude to my committee members Dr. Auke Barhoorn and Prof. Dr. Giovanni Bertotti because they participated very actively and were involved at all times asking and providing feedback. Thanks as well to Prof. Dr. Gert Jan Weltje who accepted the invitation for being part of the thesis committee.

I would like to thank also many people who directly or indirectly helped me in the process: Arno Mulder, Jack Voncken, Ralf Haak, Marlijn Ammerlaan, Lydia Broekhuijsen-Bentvelzen, and in general all the staff personnel involved somehow in my project.

I would like to thank the Emeritus Scientist from the USGS, Dr. Dennis Eberl, who voluntarily helped me out with a critical part of my thesis, as well to his colleague David Metge who also helped in the process of getting the soil samples in the US for the study.

I am very thankful with Professor Brooks Ellwood, who is one of the most important researchers in this topic and gave me important feedback. Also thanks to Dr. Torrence and Dr. Compo who developed a long time ago the programming code used in this work and gave me few hints for its use.

My endless gratitude goes definitively to my parents, my brother and sister for their support and telling me the right words at the right time.

To my daughter Francesca because even though she was only five years when I started, she understood better than others the reason why I was doing this.

And last but not least, thanks to my beloved wife, who decided to change her life and quit to her dreams for following mine. She suffered as I did and this degree is as much yours as mine. Thanks for everything Gorda. I have no words to express how thankful I feel right now.

TABLE OF CONTENTS

TABLE OF CONTENTS	VI
LIST OF FIGURES	VIII
LIST OF TABLES	X
CHAPTER 1: INTRODUCTION	1
CHAPTER 2: GEOLOGICAL SETTING	3
REGIONAL GEOLOGY	3
VIENNA BASIN	4
TECTONIC EVOLUTION	4
DEPOSITIONAL SYSTEMS AND BASIN FILLING	5
BADENIAN (16.4. -13 MA)	5
SARMATIAN (13 -11.5 MA)	5
PANNONIAN (11.5 - 7.1 MA)	6
STUDY AREA	7
SPANNBERG-21	7
CHAPTER 3: MAGNETIC SUSCEPTIBILITY	9
DEFINITION	9
DIAMAGNETIC MATERIALS	9
PARAMAGNETIC MINERALS	9
FERROMAGNETIC MINERALS	10
ORIGIN OF MAGNETIC SUSCEPTIBILITY IN ROCKS	11
FACTORS CONTROLLING MS	11
GREIGITE AND MAGNETITE	13
MAGNETIC PROPERTIES OF SEDIMENTS	13
MARINE SEDIMENTS	13
TERRESTRIAL SEDIMENTS	13
CYCLOSTRATIGRAPHY	14
THE ORIGIN OF THE CYCLES	14
MILANKOVITCH CYCLES	15
WAVELET ANALYSIS	15
CHAPTER 4: METHODOLOGY	16

PREVIOUS WORKS	16
BASICS OF PALEOMAGNETISM	16
ORIGIN OF THE DOWNHOLE MAGNETIC TOOL (GHMT*)	16
PALEOMAGNETIC LOGGING TOOL	16
DATA ACQUISITION	16
LABORATORY DATA	17
LOGGING DATA	17
CURRENT WORKS	20
CROSS-PLOTS	20
ACID TEST	21
XRD/XRF ANALYSIS	21
TIME-SERIES ANALYSIS	27
CHAPTER 5: RESULTS	29
LOG DESCRIPTION	29
CORRELATION MATRIX	32
XRD/XRF	35
SPECTRAL ANALYSIS	40
DISCUSSION OF RESULTS	43
ORIGIN OF THE MAGNETIC SUSCEPTIBILITY SIGNAL	43
DEPOSITIONAL ENVIRONMENTS	45
GRAIN SIZE	45
IRON EFFECT	47
BADENIAN LOW RESPONSE	48
PROVENANCE OF THE SEDIMENTS	48
DETRITAL INPUT	49
DISSOLUTION	49
ELEMENTAL RATIOS ANALYSIS	51
WAVELET ANALYSIS	54
CHAPTER 6: CONCLUSIONS	56
CHAPTER 7: RECOMMENDATIONS	58
REFERENCES	59
APPENDICES	68
GLOSSARY OF TERMS	87

LIST OF FIGURES

Figure 1: Situation of the Vienna Basin within the Alpine-Carpathian thrust belt (from OMV, 1992)	3
Figure 2: Stratigraphic overview of the Vienna Basin fill. Time axis not to scale. From (Holzel et al., 2010)	4
Figure 3: Evolution of the Vienna Basin through the Mid-Badenian times. a) sea level low stand, erosion of Lower Badenian strata. Build up of large low stand delta complexes: Zwerndorf, Zistersdorf and Andlersdorf. b) transgression, retreat of deltas, transgressive 16 TH , carbonate platforms. c) highstand, shale and <i>Matzen Haupt Marker</i> . Deltas are pushed back to basin limit. d) FSST, Progradation of Zistersdorf delta complex (15 and 14 TH). Deposition of 15Z2TH basin floor fan (from OMV, 2007). Red star indicates the location of the well.	6
Figure 4: Stratigraphy of the Vienna Basin. From (Hamilton et al., 1999).	7
Figure 5: Location of the well Spannberg-21. Red circle indicates the location of the well in the 15Z2TH fan (modified from OMV, 2007). Schematic representation of the basin floor fan and the sediments supply source.	7
Figure 6: Palaeogeography and Facies distribution during the Karpatian, Badenian, and Pannonian times in the Vienna Basin. Straight red arrows mean uplift/subsidence. Bent red arrows mean directions of overthrust. Black arrows indicate direction of main sediment transport (from OMV, 1992).	8
Figure 7: Diamagnetic and paramagnetic material without magnetic field (A) and with magnetic field (B).	9
Figure 8: Ferromagnetic, ferromagnetic, and antiferromagnetic material.	10
Figure 9: Mass Susceptibility of some diamagnetic minerals (left), paramagnetic minerals (<i>center</i>), ferrimagnetic, and ferromagnetic minerals (<i>right</i>). From Schon (2011)	10
Figure 10: Mineral contributions to rock susceptibility, note that 100 % of mafic silicates contribute less than 1% of magnetite. From (Hrouda et al., 2009).	11
Figure 11: Graphic visualization of magnetic susceptibility values for the most common (<i>top</i>) paramagnetic, diamagnetic, and (<i>bottom</i>) ferrimagnetic, ferromagnetic, and antiferromagnetic minerals. Compilation from (Schon, 2011) and (Opdyke and Channel, 1996). Values may vary depending on the sources.	14
Figure 12: Distribution of magnetic minerals found by Koolen (2010) vs. Depth.	18
Figure 13: Summary table with results of the 32 samples analyzed by Koolen (2010).	19
Figure 14: Criteria used for choosing the samples for semiquantitative analysis. <i>Left:</i> Sarmatian unit, <i>Right:</i> Badenian unit.	22
Figure 15: Superposition of the 32 samples analyzed by Koolen (2010) in the GR vs. MS plot used for the correlation matrix. This shows the wide distribution of magnetic minerals with depth. Purple: greigite + pyrite found. Black: magnetite + greigite found. Red: magnetite. Blue: greigite.	23
Figure 16: Superposition of the 32 samples chosen by Koolen (2010) in the GR vs. MS plot used for the correlation matrix. These plots were helpful for the further samples selection.	24
Figure 17: Samples chosen for the analysis. In total 6 samples. The criteria is fully explained in the text.	25
Figure 18: Mortar and samples analyzed. This was the methodology applied in the first XRD/XRF preparation.	25
Figure 19: Matching patterns performed by Rock Jock Excel program.	26
Figure 20: Logging data from Spannberg-21 - 8 ^{1/2} " section. Orange dashed line marks the Pannonian-Sarmatian transition. Red dashed line marks the Sarmatian-Badenian transition. From left to right: GR, PEF, RES_BS, RES_BM, MS, RHOB, TNPH.	30
Figure 21: Correlation matrix plots generated. <i>Top</i> plots are GR vs. MS. <i>Bottom</i> plots are PEF vs. MS. The specific pattern is observed in zone MS2 (500-860 mts) corresponding to Lower Pannonian and the other zone MS5 (1300-1590 mts) corresponding to Badenian.	33
Figure 22: <i>Top</i> plot shows GR vs. MS in the top interval. In this zone the pattern observed in the zones from MS1 to MS4 is not evident. <i>Bottom</i> plot shows the MS vs. Depth for the same interval. Red line indicates the limit between Upper Pannonian and Middle Pannonian.	34

Figure 23: Magnetic susceptibility and GR comparison. The light green curve in the left track is the GR. The middle track is depth in meters. The red curve in the third track is MS. <i>Top</i> is Pannonian, <i>Center</i> is Sarmatian, and <i>Bottom</i> is Badenian. _____	35
Figure 24: Non-clays content in every sample according to the semiquantitative analysis. The clear increasing trend with depth is observed. _____	37
Figure 25: Smectite vs Illite content expressed in weight percentage in the samples according to the semiquantitative XRD analysis. For sample locations see Table 8. _____	38
Figure 26: Plot showing the content of diamagnetic minerals present in every sample. A clear increasing trend with depth is observed. Sample 5 shows the highest value. _____	38
Figure 27: Diamagnetic and paramagnetic minerals vs. depth. _____	39
Figure 28: Wavelet analysis contour maps and global wavelet spectra indicating the periodicities in each interval. Dashed orange line indicates the 95% confidence level. Both time and depth domains along the magnetic susceptibility response are shown. <i>a)</i> Upper and Middle Pannonian; <i>b)</i> Middle and Lower Pannonian. Modified MATLAB code from Torrence and Compo (1997) _____	41
Figure 29: Wavelet analysis contour maps and global wavelet spectra indicating the periodicities in each interval. Dashed orange line indicates the 95% confidence level. Both time and depth domains along the magnetic susceptibility response are shown. <i>c)</i> Upper Sarmatian; <i>d)</i> Lower Sarmatian. Modified MATLAB code from Torrence and Compo (1997) _____	42
Figure 30: <i>Top</i> plot indicates the direct relationship between MS and detrital input. Detrital data are obtained from the XRF analysis. <i>Bottom</i> plot indicates the inverse relationship between MS and carbonate content. Data are also obtained from XRF. _____	43
Figure 31: <i>Top left</i> shows carbonate content and MS response. <i>Top right</i> shows titanium content and MS response. <i>Bottom left</i> indicates marine -terrestrial ratio (Ca/Ti) and MS response vs. depth. <i>Bottom right</i> shows titanium vs. calcium vs. depth. This helps to visualize the relationship between high/low MS values and the calcium/terrigenous content. _____	44
Figure 32: <i>Left:</i> MS vs. Depth along the Pannonian unit showing the decreasing trend of MS values towards the top. The trend is discussed in the text. <i>Right:</i> It is also a MS vs. Depth plot, but the MS values does not show any increase or decrease trend. UP stands for Upper Pannonian, MP Middle Pannonian, LP Lower Pannonian, US Upper Sarmatian, LS Lower Sarmatian. _____	46
Figure 33: A plot of three mineral groups versus depth, based on the XRF results. _____	48
Figure 34: Detrital elements correlation. _____	49
Figure 35: <i>Left</i> plot (modified from Koolen, 2010) shows ARM/MS and ARM/SIRM vs. depth. Red dashed line marks the start of the Badenian. <i>Right</i> plot shows MS vs. ARM with a positive correlation coefficient indicating a change of the magnetic grains with depth. ARM and SIRM show a clear indicative of the low concentration of magnetic minerals in the Badenian. Plots generated using the data acquired by Koolen (2010). ARM/SIRM is expressed in A/mts. MS is expressed in $*10^{-6}$ SI. _____	50
Figure 36: Simplified model illustrating the progressive dissolution of SD and PSD magnetite (dark/grey area/line) and the formation of SP/SD greigite (light grey line/area)., followed by the delay before greigite grows to SD size and to a continuous greigite growth in zone 3. SMT = sulfate-methane transition. Modified from (Rowan et al., 2009). _____	51
Figure 37: Marine and terrestrial elements vs. depth. _____	52
Figure 38: Marine-Terrigenous ratio of the proxies Ca/Al and Ca/Fe. Both curves cross each other roughly at Badenian onset (1200-1300 mts) where the influx of sediments is reduced and the carbonates control the lithology. _____	52
Figure 39: Al/Ti ratio and Al/Na ratio indicating high chemical changes in the top and decreasing with depth. 53	
Figure 40: Na/Ti ratio and Al/K ratio calculated indicating chemical weathering strength. Below 1300 mts (Badenian) the intensity decreases. _____	53
Figure 41: The Si/Al and Si/K ratios can be useful proxies for the energy associated with sediment transport. 54	

LIST OF TABLES

Table 1: Summary of factors affecting the magnetic susceptibility signal. P=proportional, IP=inversely proportional,* is explained in the text. _____	12
Table 2: Summary table with the stratigraphic units present in Spannberg-21. _____	20
Table 3: Intervals used for the correlation matrix. Modified from Paulissen (2011). _____	21
Table 4: Zones used for the spectral analysis, indicating depth and time interval as well as sedimentation rates. This zone classification is based on the depth-time correlation defined by Paulissen (2011). _____	27
Table 5: Sedimentation rates and thickness per zone, and the number of orbital cycles that can be expected based on them. _____	28
Table 6: Areas identified in both GR and MS curves along the well section. Normal correlation means high GR-high MS (also low GR-low MS). Anticorrelation means high GR-low MS and vice versa. _____	32
Table 7: Correlation matrix coefficients of the LWD data with the MS data for the six zones. _____	33
Table 8: Distribution of elements by zone according to XRF data. Only representative elements are shown. _	37
Table 9: Summary table with the semiquantitative XRD results for the six samples. _____	39

Chapter 1:

INTRODUCTION

INTRODUCTION

Magnetic susceptibility (MS) represents a very important rock property to be measured. This can be done not only in the laboratory using rocks samples, but also on outcrops or with downhole tools in wells. This property is basically controlled by the type and concentration of magnetic minerals contained in the rock. It can be dominated by minerals that are paramagnetic (clays), diamagnetic (calcite, quartz), or ferromagnetic (magnetite, greigite). It seems to be highly affected by several environmental factors and complex processes, which control its response in the sediments.

The present study constitutes a MSc. Thesis carried out at the Delft University of Technology within the Petroleum Engineering and Geosciences track. The apparent lack of correlation between the basic petrophysical properties and magnetic susceptibility acquired in Well Spannberg 21 was the igniter for considering this study. It was planned in order to determine the factor(s) responsible for the variations in magnetic susceptibilities measured in the borehole Spannberg-21 in the Vienna Basin (Austria).

The development of this thesis is based on the use of a full data set of LWD and WL logs and drill cuttings available for the whole well interval. The data was acquired back in 2007 by the National Operating Company OMV, together with Schlumberger and Delft University of Technology. Previous researchers have studied the magnetic minerals in the area and some conclusions have been drawn regarding the chronostratigraphy, biostratigraphy, and magnetostratigraphy in this well. However, it was until now when the MS problem was tackled.

This study was considered an open-ended research project from the beginning, since this was the first time that a project with such data and such a research objective was being conducted. Therefore, the result of each task was the basis for the next step. The Vienna Basin is very suitable for high-resolution studies like these because it has been widely described through several decennia. Moreover, the rapid sedimentation which occurred in this basin gave rise to the formation of thick sequences. Furthermore, downhole measurements are helpful because they provide a continuous record of the rock properties in the subsurface.

The aim of this MSc. thesis is to perform a detailed analysis employing all the data available, combined with new measurements, in order to find an explanation on what controls the rocks' MS property, what are the reasons for its behavior, and what possible applications can be given after its interpretation.

For this project, apart from the logging data already available, the literature review was an extremely important part for two reasons:

1. The Vienna Basin is well-known geologically because many studies have been conducted there, and
2. Because only few studies have been performed on magnetic susceptibility in boreholes, and these were mostly done on cores.

This study evaluates first the tectonic settings and provides the required geological background in Chapter 2. Chapter 3 explains the technical aspects concerning magnetic susceptibility. The subsequent chapter 4 describes the methodology applied by mentioning the previous studies, and the integration of results along with newly obtained measurements. The results and their discussion are found in Chapter 5. The last two chapters, 6 and 7, contain the conclusions of this work and some recommendations for the future.

Chapter 2:

GEOLOGICAL SETTING

REGIONAL GEOLOGY

The geology of Austria has been widely studied for several centuries and is generally subdivided into the following units: Bohemian Massif, Molasse Zone, Helvetic Zone, Penninic Zone (Flysch Penninic Windows), Austro-Alpine Unit (Central Zone of the Eastern Alps and Northern Calcareous Alps), Southern-Alpine Unit.

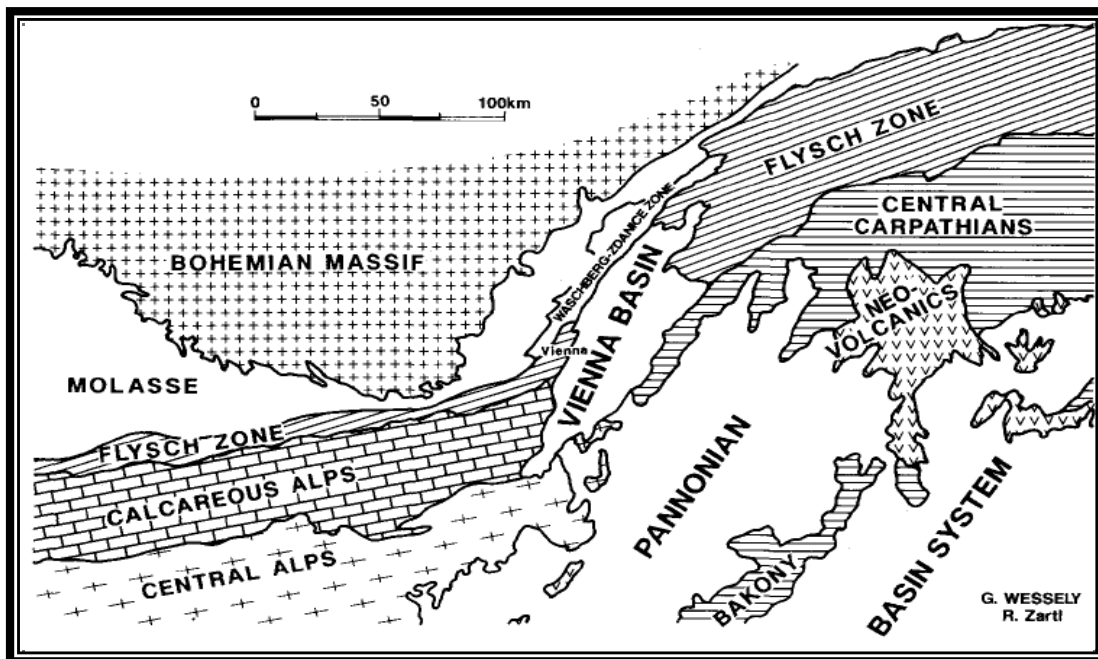


Figure 1: Situation of the Vienna Basin within the Alpine-Carpathian thrust belt (from OMV, 1992)

The northern part of Austria is occupied by the southern margin of the Bohemian Massif including the metamorphic rocks of the Moldanubian Zone and the Moravian Zone. The Molasse Zone comprises a sequence of much younger detrital sediments deposited under marine and brackish conditions. The Helvetic Zone represents a series of mostly Cretaceous limestones, marls and rare sandstones. The Flysch Zone consists predominantly of marls and sandstones deposited in the foreland of the Alpine orogeny. The Austro-Alpine Unit and the Calcareous Alps units represent complex tectonic sequences that were thrust during the Alpine orogeny and are responsible for much of the sediment supply in the younger basins.

VIENNA BASIN

TECTONIC EVOLUTION

The Vienna Basin is of rhombohedral shape with a SW-NE direction and extends from Austria to the Czech Republic and Slovakia. Its development shows a very complex tectonic evolution and is summarized by Kovac et al. (2004) as follows:

1. Formation of a piggy-back basin (Lower Miocene)
2. Formation of a pull-apart basin (Middle to Upper Miocene)
3. E-W compression and basin inversion (Upper Miocene)
4. E-W extension (Pleistocene-Recent)

Time of Tops (Ma)	Epoche	Classical Stages	Central Paratethys Stages	Regional stress field	
7.8	Upper Miocene	Tortonian	Pannonian	Upper Pannonian	Compressive (Peresson & Decker, 1997)
10				Middle Pannonian	
10.5				Lower Pannonian	
11.6	Middle Miocene	Serravallian	Sarmatian	Upper Sarmatian	Pull-Apart (Decker, 1996)
12.2				Lower Sarmatian	
12.7		Langhian	Badenian	Bulimina-Rotalia Zone	
13.6				Spiroplectamina Zone	
14.2				Upper Lagenidae Zone	
14.5				Lower Lagenidae Zone	
16.1		Burdigalian	Karpatian	Aderklaa Conglomerate	
16.3				Upper Karpatian	
16.9				Lower Karpatian	
17.2					
(17.2) 17.5	Lower Miocene	Aquitanian	Ottmangian	Wedge Top System (Piggy-Back)	
18.3			Eggenburgian		

Figure 2: Stratigraphic overview of the Vienna Basin fill. Time axis not to scale. From (Holzel et al., 2010)

Piggy-back basin (Lower Miocene)

Starting in the Early Miocene, subsidence increased abruptly in this area and an incipient basin was created. At this time the Vienna Basin was a piggy-back basin on tectonic nappes transported northward. Weissenböck (1996) mentions that during the very last phase of the Karpatian, tectonic inversion caused uplifting and most of the basin emerged.

Pull-apart basin (Middle to Upper Miocene)

During the late Karpatian, tectonic events caused a change from a piggyback basin into a rhombic pull-apart basin. This change in tectonic regime is documented as a major

regressive event at the Karpatian/Badenian boundary. During Badenian time the main phase of subsidence began and the basin increased its extension. This lasted well into Sarmatian times.

E-W compression and basin inversion (Upper Miocene-Pliocene)

The Pannonian period began with a transgression covering most of the Sarmatian deposits. Primarily clay and sand were deposited in a lacustrine environment during the Early and Middle Pannonian.

SW-NE extension (Pleistocene-Recent?)

Subsidence controlled by fault displacements in a transtensional regime has been determined along the eastern limit of the basin.

DEPOSITIONAL SYSTEMS AND BASIN FILLING

According to the structural history of the basin, two sedimentary cycles can be distinguished: one part controlled by siliciclastic influx and another part dominated by a carbonate/detrital mix. The significant stratigraphic units covered in this study are described here:

BADENIAN (16.4. -13 Ma)

In the central Vienna Basin, the Badenian sediments are divided into proximal deltaic and distal basinal deposits characterized by sandy marls and clay. The conditions for carbonate sedimentation and growth of coral buildups were favorable only during the Badenian stage and developed in two facies: the first facies is the Leitha Limestone with reduced terrigenous input, and the other facies type comprises fine-grained clays and marls. In the uppermost Badenian the sea started to become more brackish, which continued during the Sarmatian. The deposition of sandy sediments increased at this time.

The boundary between the Early Badenian and the Middle Badenian corresponds to the sequence boundary proposed by Weissenböck (1996) within the "Upper Lagenidae Zone" of the southern Vienna Basin. Several small-sized deltaic bodies developed during that phase and they might be related to weakly developed lowstand systems tracts (LST). The mostly freshwater and brackish deposits consist of calcareous clays. In general, the western border of the southern Vienna Basin is strongly influenced by clastic sediment influx from the Northern Alps.

SARMATIAN (13 -11.5 Ma)

The depositional environment turned from fully marine during the Badenian into brackish in the Sarmatian because of the slow but continuous separation of the Pannonian Basin, to which the Vienna Basin was linked in the Southeast, from the Tethys. Salinity decreased and reflects the isolation of the Paratethys from the world oceans. The reduced salinity of the Sarmatian sea caused an intense decrease of the fauna. During the regression at

the Badenian/Sarmatian boundary, the marine settings became restricted to basinal areas of the central and southern Vienna Basin.

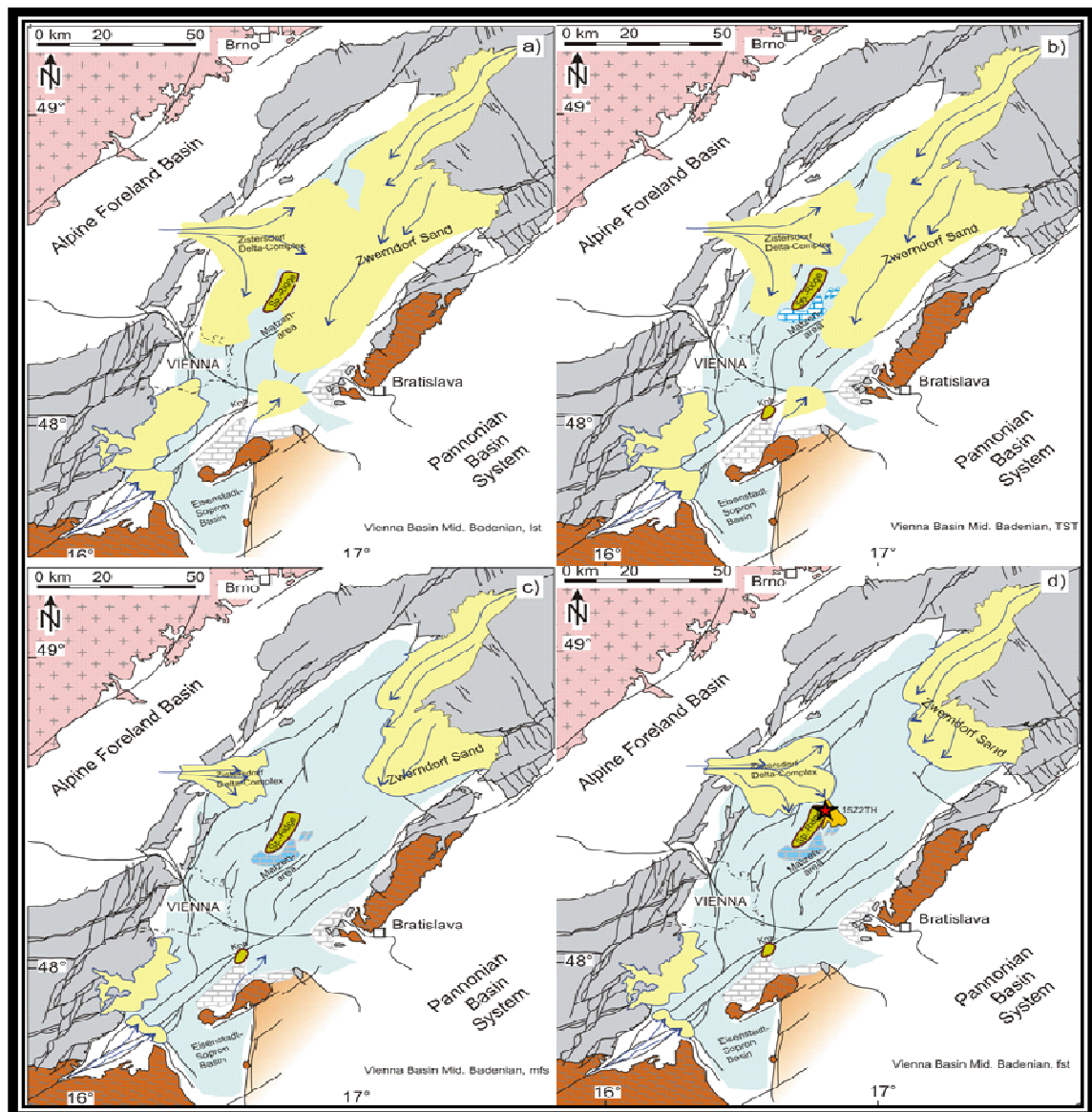


Figure 3: Evolution of the Vienna Basin through the Mid-Badenian times. a) sea level low stand, erosion of Lower Badenian strata. Build up of large low stand delta complexes: Zwerndorf, Zistersdorf and Andlersdorf. b) transgression, retreat of deltas, transgressive 16TH, carbonate platforms. c) highstand, shale and *Matzen Haupt Marker*. Deltas are pushed back to basin limit. d) FSST, Progradation of Zistersdorf delta complex (15 and 14 TH). Deposition of 1522TH basin floor fan (from OMV, 2007). Red star indicates the location of the well.

PANNONIAN (11.5 - 7.1 Ma)

After the sea level drop registered at the Sarmatian/Pannonian boundary, the Pannonian Basin became finally isolated from the Eastern Paratethys. The salinity decreased even more causing a further decrease in fauna diversity compared to the Sarmatian.

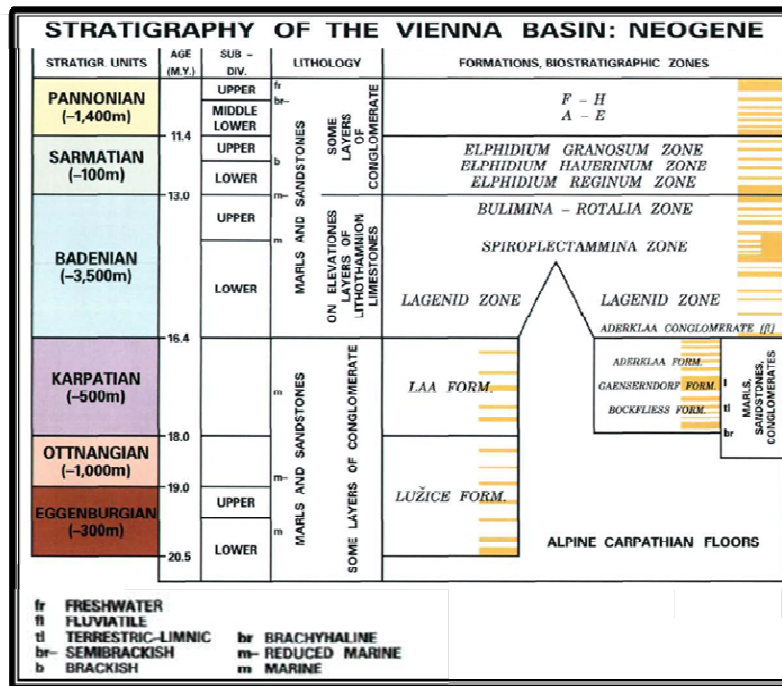


Figure 4: Stratigraphy of the Vienna Basin. From (Hamilton et al., 1999).

STUDY AREA

SPANNBERG-21

The well Spannberg-21 studied here was drilled in 2007 by the Austrian oil and gas company OMV in the central part of the Vienna Basin. The proposed appraisal well Spannberg-21 had the 15Z2TH reservoir level as a target, which is a Middle Badenian basin floor fan (see Figure 5). The well is located northeast on the Matzen-Spannberg ridge and reached a depth of approximately 2000 mts. that covers the Middle to Upper Miocene.

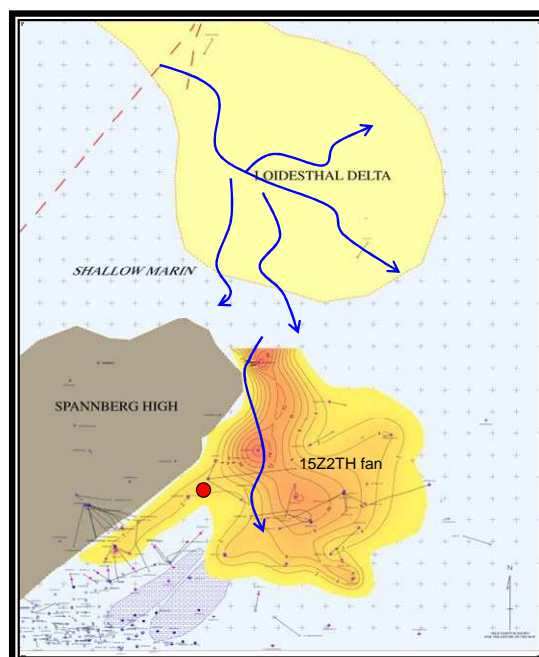


Figure 5: Location of the well Spannberg-21. Red circle indicates the location of the well in the 15Z2TH fan (modified from OMV, 2007). Schematic representation of the basin floor fan and the sediments supply source.

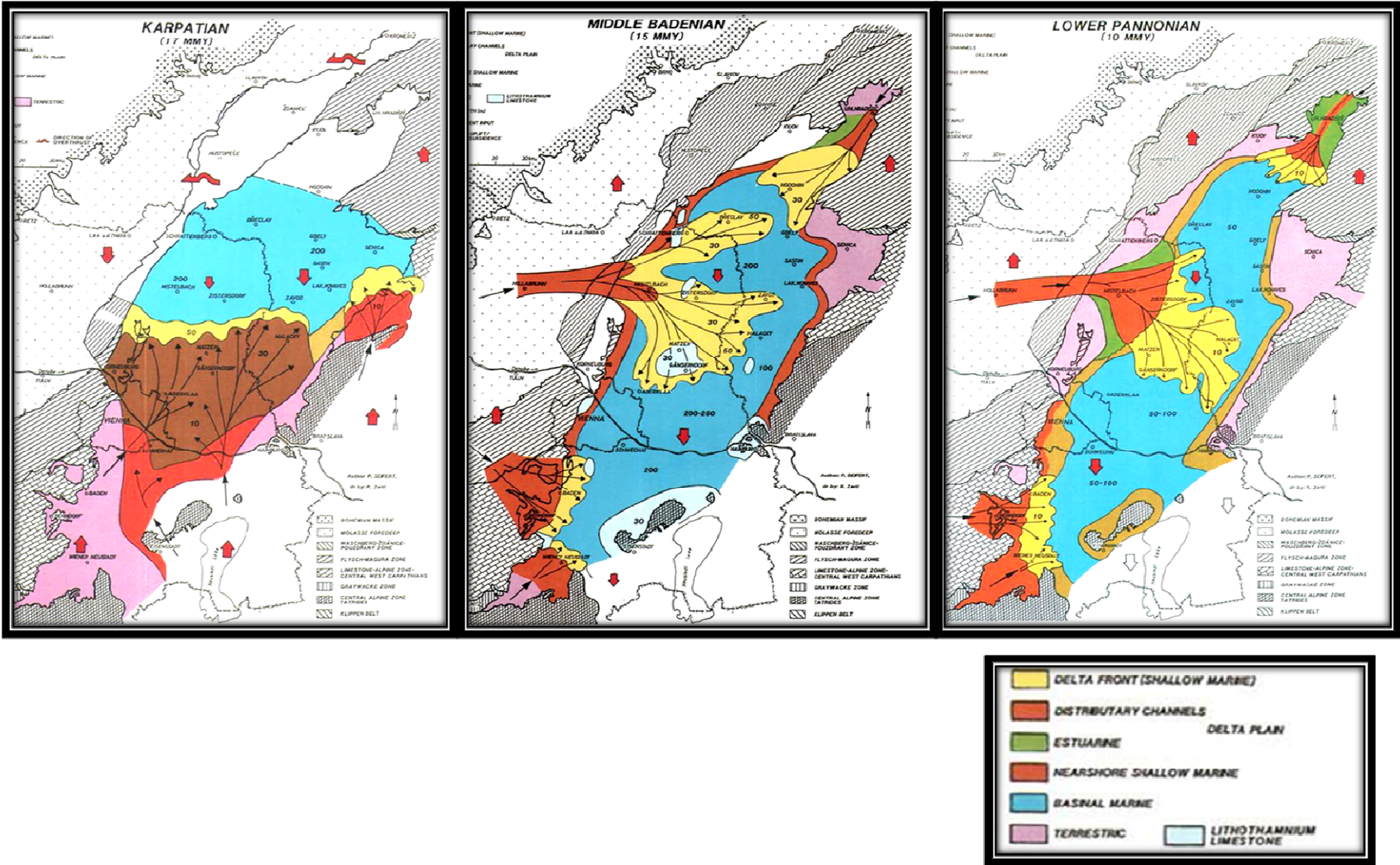


Figure 6: Palaeogeography and Facies distribution during the Karpatian, Badenian, and Pannonian times in the Vienna Basin. Straight red arrows mean uplift/subsidence. Bent red arrows mean directions of overthrust. Black arrows indicate direction of main sediment transport (from OMV, 1992).

Chapter 3:

MAGNETIC SUSCEPTIBILITY

DEFINITION

In the broadest sense, magnetic susceptibility is a measure of the magnetic response of a particular material/rock when a magnetic field is applied. This measurement can tell how much magnetic mineral content is present in a rock. Different laboratory experiments allow the identification of the minerals present and can be used to make a match with the total magnetic susceptibility signal.

Magnetic susceptibility, according to Nelson (1993), can be expressed either as a volume susceptibility (κ) or as a mass susceptibility (χ). Volume susceptibility is defined as the ratio of the volume magnetization produced in a material when a weak magnetic field is applied. This is a dimensionless quantity. Nelson (1993) mentions that mass susceptibility is equal to the volume susceptibility divided by density, and its units are $\text{m}^3/\text{kilogram}$ in the SI system. Thus volume magnetic susceptibility is defined as follows:

$$\chi = H/M \quad (1)$$

where χ is the magnetic susceptibility, H is the magnetic field intensity and M is the magnetization. Schon (2011) describes that based on the magnetic structure, materials can be divided into three basic groups: diamagnetic, paramagnetic, and ferromagnetic materials.

DIAMAGNETIC MATERIALS

This group is characterized for having a negative susceptibility. Generally, the values are very small and the response is independent of the magnetizing field.

PARAMAGNETIC MINERALS

This group is characterized by positive susceptibility. The response is in general higher than the diamagnetic response, but is still weak. It is also independent of the magnetizing magnetic field.

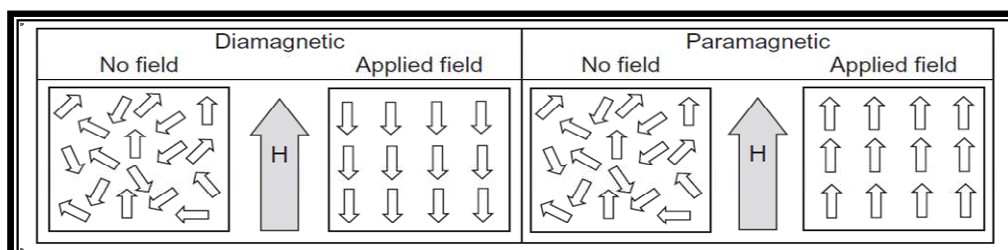


Figure 7: Diamagnetic and paramagnetic material without magnetic field (A) and with magnetic field (B).

FERROMAGNETIC MINERALS

This is the most important group and these materials are characterized by the existence of magnetic domains even in the absence of a magnetic field. MS values caused by this group have a wide range of values and are always positive. These materials are subdivided into three groups: ferromagnetic, where all the atomic magnetic moments are parallel; antiferromagnetic, causing a weak magnetism; and ferrimagnetic materials producing a strong magnetism.

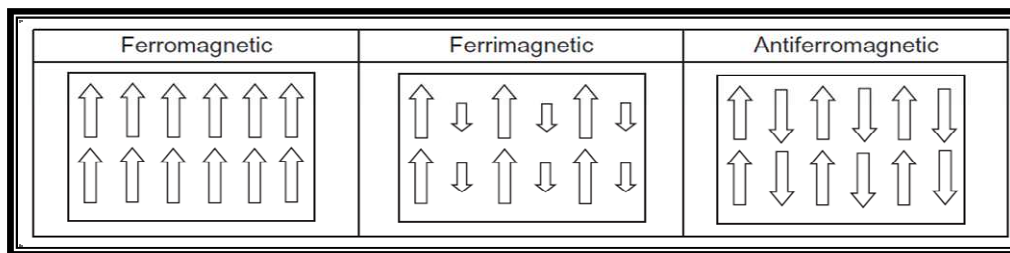


Figure 8: Ferromagnetic, ferrimagnetic, and antiferromagnetic material.

Although the magnetic rock properties are controlled by the ferrimagnetic minerals, their concentration is typically very low in rocks. On the other hand, the most abundant minerals in common rocks are paramagnetic and/or diamagnetic. The importance of concentration of magnetic minerals on MS can be seen schematically in the Figure 10.

Mineral	κ_g [$10^{-8} \text{ kg}^{-1} \text{ m}^3$]
Anhydrite	-2.11
	-0.5 to -2.0
Calcite	-0.48
	-0.3 to -1.4
Dolomite	
Quartz	-0.58
	-0.5 to -0.6
Fluorite	-0.79
Halite	-0.48
	-0.48 to -0.75
Orthoclase	-0.58
	-0.49 to -0.67
Ice	-1

Mineral	κ_g [$10^{-8} \text{ kg}^{-1} \text{ m}^3$]
Olivine	5–130, mean 29
	36
	1–130
Amphibole	16–100, mean 49
	16–69
Pyroxene	4–94
Hornblende	6–100
Smectite	2.7–5
Biotite	52
	52–98
	5–95
Muscovite	
	0–26, mean 8
Illite	15
	15
Montmorillonite	13–14
Chlorite	
Bentonite	5.8
Siderite	100
Dolomite	1.1

Mineral	κ_g [$10^{-8} \text{ kg}^{-1} \text{ m}^3$]
Magnetite	
	20,000–110,000
Maghemite	40,000–50,000
Haematite	
	10–760
Ilmenite	
	46–80,000
Titanomagnetite	2,500–12,000
Titanomaghemite	57,000
Goethite	26–280
Ulvöspinel	100
Pyrrhotite	10–30,000

Figure 9: Mass Susceptibility of some diamagnetic minerals (left), paramagnetic minerals (center), ferrimagnetic, and ferromagnetic minerals (right). From Schon (2011).

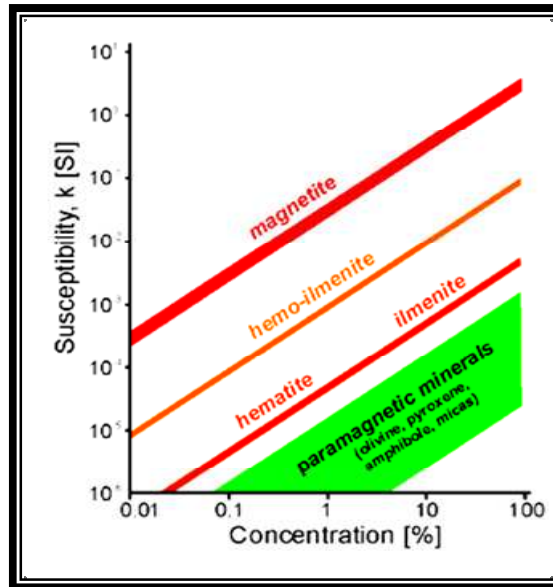


Figure 10: Mineral contributions to rock susceptibility, note that 100 % of mafic silicates contribute less than 1% of magnetite. From (Hrouda et al., 2009).

ORIGIN OF MAGNETIC SUSCEPTIBILITY IN ROCKS

Various studies indicate that magnetic minerals are mainly related to lithogenic sediment inputs, and that, therefore, MS is directly proportional to detrital inputs (Ellwood, 2006; Ellwood et al., 2000; Crick et al., 2000). However, these lithogenic inputs may be caused by climatic, sea level or tectonic changes, which provides one of the main drivers of this study. On the other hand, magnetic susceptibility is inversely correlated with carbonate content (Prof. Ellwood, personal communication).

If the detrital theory is valid, then it has to be influenced by environmental parameters such as water energy, sedimentation rate and perhaps diagenesis. Moreover, MS readings are commonly higher when the sediments are proximal to the source, characterized by coarser grains. There is also evidence showing that during regression events, the MS signal increases since there is a higher input of detrital sediments.

FACTORS CONTROLLING MS

Since magnetic susceptibility is environmentally controlled, it is strongly affected by several factors and these various influences lead to different responses along the depositional profiles. The first factor is the magnetic minerals content or its concentration. However, MS is not only controlled by this and Table 1 lists most of these factors and their relationships with MS. This information is collected in the course of this study with the intention to provide an overview of the controls on the MS signal.

There is a relationship between depositional environments and grain size distribution. There are, however, two opposing ideas with respect to their effect on the magnetic susceptibility signal. The first one supports the idea that fine grains generate higher magnetic susceptibility than coarse grains, while the second one posits that coarse grains produce higher MS readings. The first group is based on the fact that Superparamagnetic domains of

magnetic minerals, responsible for high magnetic susceptibility responses, are immersed in very fine sediments particles. However, such grains are not very stable and might decompose very easily. The second hypothesis relies on the principal fact that MS is directly proportional to detrital input and, since coarse grains are found closer to the sediment source, there should be higher amounts of magnetic minerals there. Actually Waythomas (1991) mentions that even if the magnetic minerals are relatively fine-grained, they will be transported with coarser-grained sediments because of their relatively high specific gravities.

Several studies have been performed on the effect that the magnetic grain size has over the total susceptibility response. The results indicate that this factor plays an important role in the MS signal. The magnetic grain sizes are given by Hatfield (2014) as superparamagnetic (SP < 0.03 μm), single domain (SD, 0.03–0.1 μm), pseudo single domain (PSD*, 0.1–20 μm) and multi-domain (MD > 20 μm). This classification is important because it points out that when the grain size diminishes from MD* to SD* size, the susceptibility decreases, but if the grain diminishes further to the smallest SP* size, then the susceptibility increases again abruptly.

Factor	Relationship
TOC	IP
Salinity	IP
Bioturbation	P
Clay content	P
Diagenesis	IP
Dissolution	IP
Coarse sediments	P
Fine sediments	IP
Porosity	IP
Iron presence	P
Sedimentation rate	P
Detrital input	P
Carbonates	IP
Regression	P
Transgression	IP
pH	P
Sulphur	IP
Pyritization	IP
Distal environment	IP
Concentration of Magnetic Minerals	P
Magnetic Minerals domains	*

Table 1: Summary of factors affecting the magnetic susceptibility signal. P=proportional, IP=inversely proportional,* is explained in the text.

In shallow marine sediments (here represented by the Badenian deposits) where the carbonates form an important percentage and the sedimentation rates are high, the deposition of magnetic minerals is typically reduced. The weak MS signal preserved in these rocks is related to the clastic sources, the carbonate productivity, and probably diagenesis.

*. See the Glossary

An important diagenetic process is post-depositional dissolution, which acts during and after burial. This dissolution process, however, is a function of the environment. Canfield and Berner (1987) explain that this complicated process depends on the availability and reactivity of both organic matter and reductants, and that the chemical reactions that takes place typically yield new minerals, some of which may have different magnetic susceptibilities than their precursors.

GREIGITE AND MAGNETITE

The iron sulphide mineral greigite (Fe_3S_4) has the same crystal structure as magnetite (Fe_3O_4) and is strongly ferrimagnetic. Greigite is the main precursor of pyrite and it is typically formed in anoxic environments. According to Vasiliev et al. (2008), greigite can be divided into magnetosomal and authigenic types, depending on how it is formed. Magnetosomal greigite is formed inside bacteria preferably in anaerobic conditions. Authigenic greigite is formed as an intermediate mineral in the pyrite formation. Pyrite is extremely common in anoxic marine sediments where abundant supply of sulphate is present and iron is available.

Magnetite is the most common magnetic mineral on Earth and is usually found in detrital sediments. In many cases magnetite and greigite behave in a similar way, and laboratory measurements must be conducted in order to properly identify them.

MAGNETIC PROPERTIES OF SEDIMENTS

MARINE SEDIMENTS

The magnetic properties of marine sediments depend not only on the magnetic minerals deposited from detrital sources, but also on the diagenetic processes acting on these sediments after deposition. Sediments acquire what is called a detrital remanent magnetization (DRM) when the magnetite grains are exposed to the geomagnetic field. Opdyke and Channel (1996) have found that the most important magnetic remanence carrier minerals are magnetite, titanomagnetite, hematite, maghemite, goethite, and iron sulfides such as greigite. Opdyke and Channel (1996) also found that magnetite, titanomagnetite, greigite, and goethite can be primary carriers, whereas hematite, pyrrhotite, and greigite are considered authigenic secondary minerals formed during diagenesis. Although greigite is typically formed in the early diagenetic stage, it can be considered a primary carrier in case no other minerals are present since its magnetization is very strong.

TERRESTRIAL SEDIMENTS

The magnetic properties in terrestrial sediments indicate that the dominant carrier is fine-grained magnetite. Greigite is also here an important remanence carrier based on its similarity to magnetite.

Figure 11 below shows the magnetic susceptibility values for some of the most important minerals present in rock in a visual way.

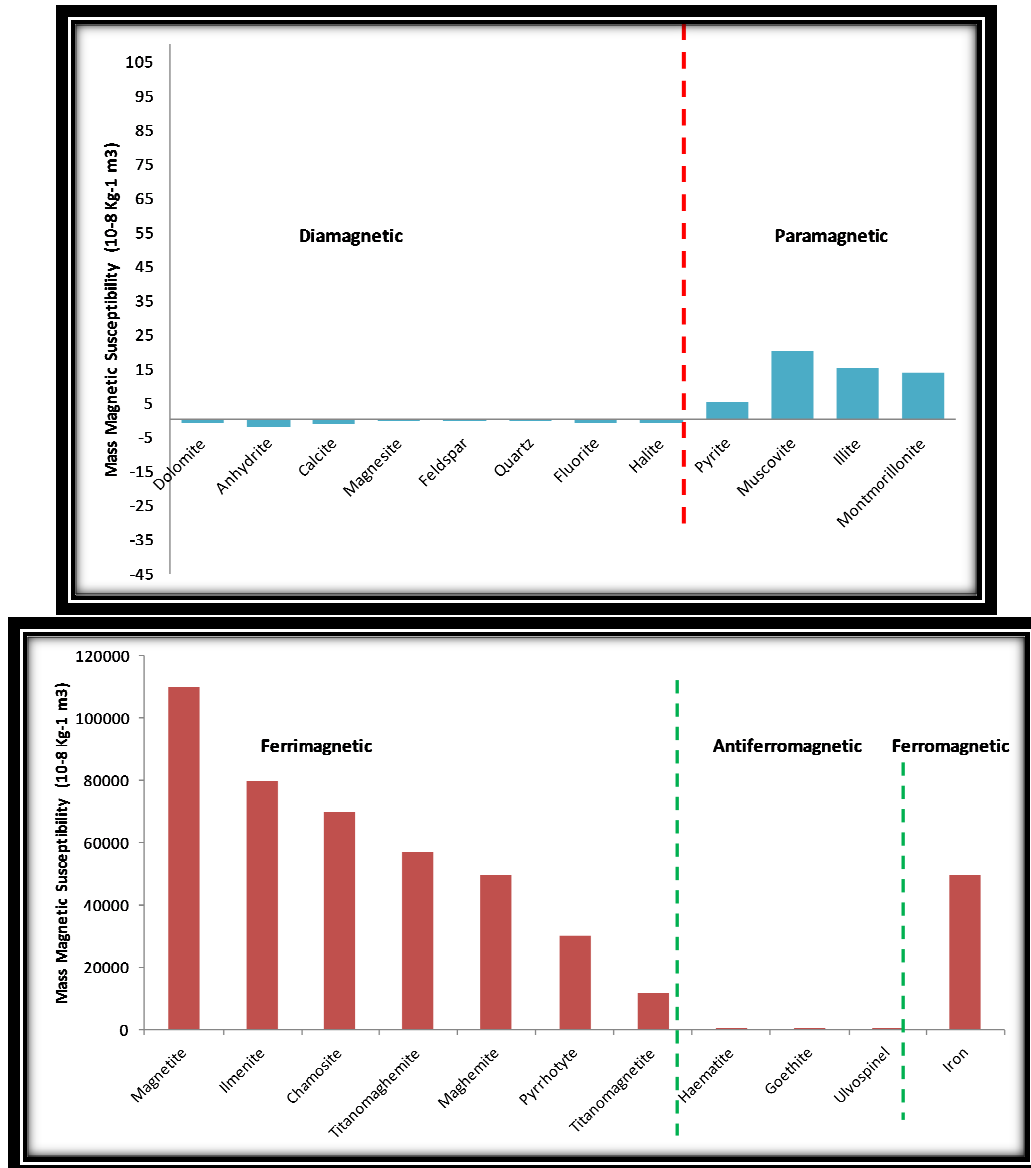


Figure 11: Graphic visualization of magnetic susceptibility values for the most common (*top*) paramagnetic, diamagnetic, and (*bottom*) ferrimagnetic, ferromagnetic, and antiferromagnetic minerals. Compilation from (Schon, 2011) and (Opdyke and Channel, 1996). Values may vary depending on the sources.

CYCLOSTRATIGRAPHY

The core of this discipline is based on using astronomical cycles of known periodicities to date and interpret sedimentary records. The most important of these cycles are the Earth's orbital cycles of precession, obliquity, and eccentricity, known as the Milankovitch cycles, which result from perturbations of the Earth's rotations. These cycles are expressed via climatic or sedimentary changes into the sedimentary sequences.

THE ORIGIN OF THE CYCLES

The sedimentary cycles basically reflect changes in the environment, with some sedimentary rock types being more susceptible to them than others. In general, clastic sediments are good indicators of fluctuations in water energy, whereas carbonates often record changes in chemistry.

A major controlling factor on sedimentary systems is the eustatic sea level, which to some degree is controlled by the climate, which, in turn, may be controlled by the orbital cycles. This, together with subsidence controls the sediment accommodation. Numerous case studies have demonstrated that a detailed analysis of the sedimentary record enables the identification of these cycles with a good level of confidence.

MILANKOVITCH CYCLES

Milankovitch cycles are driven by Earth's natural orbital oscillations. These oscillations may be reflected in many different types of climate proxy data that may include magnetic susceptibility. These prominent cycles have been shown to persist through long geological records.

There are three major periodicities of Milankovitch cycles and they are related to the eccentricity (E) of the Earth's orbit, the obliquity (O) in the Earth's axial tilt, and the precession (P) of the seasons. The eccentricity cycle completes one cycle every 95 to 123 kyr. The obliquity corresponds to a 41 kyr cycle. Finally, the precession cycle oscillates between 19-23 kyr.

WAVELET ANALYSIS

Wavelet analysis is possibly the best way of studying cyclicities in stratigraphic records. Theoretically, power spectra allow the analysis of complex cycles consisting of several oscillations. The data used for this type of studies vary from gamma ray logs, spontaneous potential logs, carbonate content and resistivity data, among others.

The success of this analysis depends on the continuity of the data (quantity) and obviously its quality. There are different methods typically used, all with different mathematical backgrounds and justifications, but they do not always succeed in detecting periodicities. The reason is because most stratigraphic data are subject to more influential factors, for example fluctuations in sedimentation rates from one sedimentary unit to another, which may distort the cyclicities. In the present study very accurate sedimentation rates were determined by Paulissen et al. (2011a; 2011b) improving the reliability of the results to be obtained.

Chapter 4:

METHODOLOGY

The aim of this chapter is to explain the procedures followed during the project. It starts with a brief background about paleomagnetism. Then the origin of the paleomagnetic tool used for this dataset is described and briefly its principles of operation and data acquisition are mentioned. The logging data available, the well location, and characteristics will be presented next. New measurements performed in this study such as XRD/XRF analysis will then be explained. Finally, a wavelet analysis is performed on the magnetic susceptibility data to analyze the possibility of obtaining any Milankovitch cycles (O, P, E).

PREVIOUS WORKS

BASICS OF PALEOMAGNETISM

Paleomagnetism is possible basically because minerals containing iron, such as magnetite or greigite and present in sediments, record the history of the Earth's magnetic field polarities. Paleomagnetic studies are commonly used in constraining ages for rocks and processes. In order to do this, often supplementary chronostratigraphic information is required to validate the paleomagnetic interpretation.

ORIGIN OF THE DOWNHOLE MAGNETIC TOOL (GHMT*)

The idea of this tool started with the collaboration of the major oil and gas operating company TOTAL, together with the CNRS¹ and LETI². They designed a high-precision total magnetic induction and susceptibility tool for borehole applications. These two measurements were combined later on by the major services company Schlumberger into one tool to be used for commercial purposes. The name of the tool is Geological High-Resolution Magnetic Tool (GHMT*).

PALEOMAGNETIC LOGGING TOOL

The paleomagnetic logging tool consists of two sondes: a total induction magnetometer tool (nuclear resonance magnetometer tool, or NRMT) and a magnetic susceptibility tool (susceptibility magnetic tool, or SUMT). These two sondes were combined by Schlumberger in the GHMT. Paulissen (2011) specifies that the precision of the susceptibility signal (χ) is 0.3E-06, which is required for the determination of rock susceptibilities that typically range from 10^{-6} to 10^{-2} .

DATA ACQUISITION

The data was acquired with two different logging suites in two well sections. The shallow 12^{1/4"} section only has WL data. The lower 8^{1/2"} section reached the depth of 1966

1. Centre National de la Recherche Scientifique

2. Laboratoire d'Electronique de Technologie et d'Instrumentation

*. Mark of Schlumberger

mts. TVD. This section was logged with logging while drilling (LWD¹) tools. LWD acquired density, gamma ray, porosity, resistivity, and photoelectric factor logs. The high-resolution electrical borehole images (Formation Microscanner Imager, FMI*) and GHMT were obtained in two runs over the entire well length.

The borehole image measurements acquired in the Spannberg-21 well are not directly used in this study. However, it was an important data set for defining stratigraphic units boundaries and especially for identifying carbonate layers in the Badenian section.

For LQC (log quality control) main and repeat logs were run with the paleomagnetic logging tool over selected intervals. The repeat section indicated that the tool was properly operating and the values were within expected small tolerances (Paulissen, 2011).

LABORATORY DATA

During earlier studies, Koolen (2010) and Paulissen (2011) conducted laboratory measurements in order to identify the magnetic minerals responsible for the recorded signals. These included magnetic susceptibility measurements, IRM, and ARM. Samples were taken from the cuttings acquired by OMV in the 8^{1/2}" section. In total 32 samples were used for these studies. Figure 13 summarizes the results obtained by Koolen (2010) and Paulissen (2011).

Since greigite has coercivity values very similar to magnetite, it is typically very difficult to distinguish between them. Koolen (2010) mentions that sometimes the values for $B_{1/2}^*$ and DP^* were overlapping for magnetite and greigite. For this reason, a Curie temperature test was performed. In the end, Koolen (2010) explains that a small difference in DP values made the difference between choosing greigite or magnetite in several cases.

The results showed that magnetite, greigite, and a combination of both were identified as the main magnetic minerals in the analyzed samples. Koolen (2010) and Paulissen (2011) decided to subdivide greigite into detrital and authigenic based on the work of Vasiliev et al. (2008). Figure 12 shows a plot of MS vs. depth with the magnetic minerals determined during these measurements. This is a helpful tool for visualizing the MS distribution along the well.

LOGGING DATA

The most important curve to analyze in this data set is the magnetic susceptibility (MS). The main idea of this log interpretation is to establish, if any, a correlation or pattern between the magnetic susceptibility curve and the other properties acquired (density RHOB, gamma ray GR, porosity TNPH, photoelectric factor PEF, and resistivity RES_BM* and RES_BS*).

1. For abbreviations see the Glossary at the end of the report.

*. See the Glossary

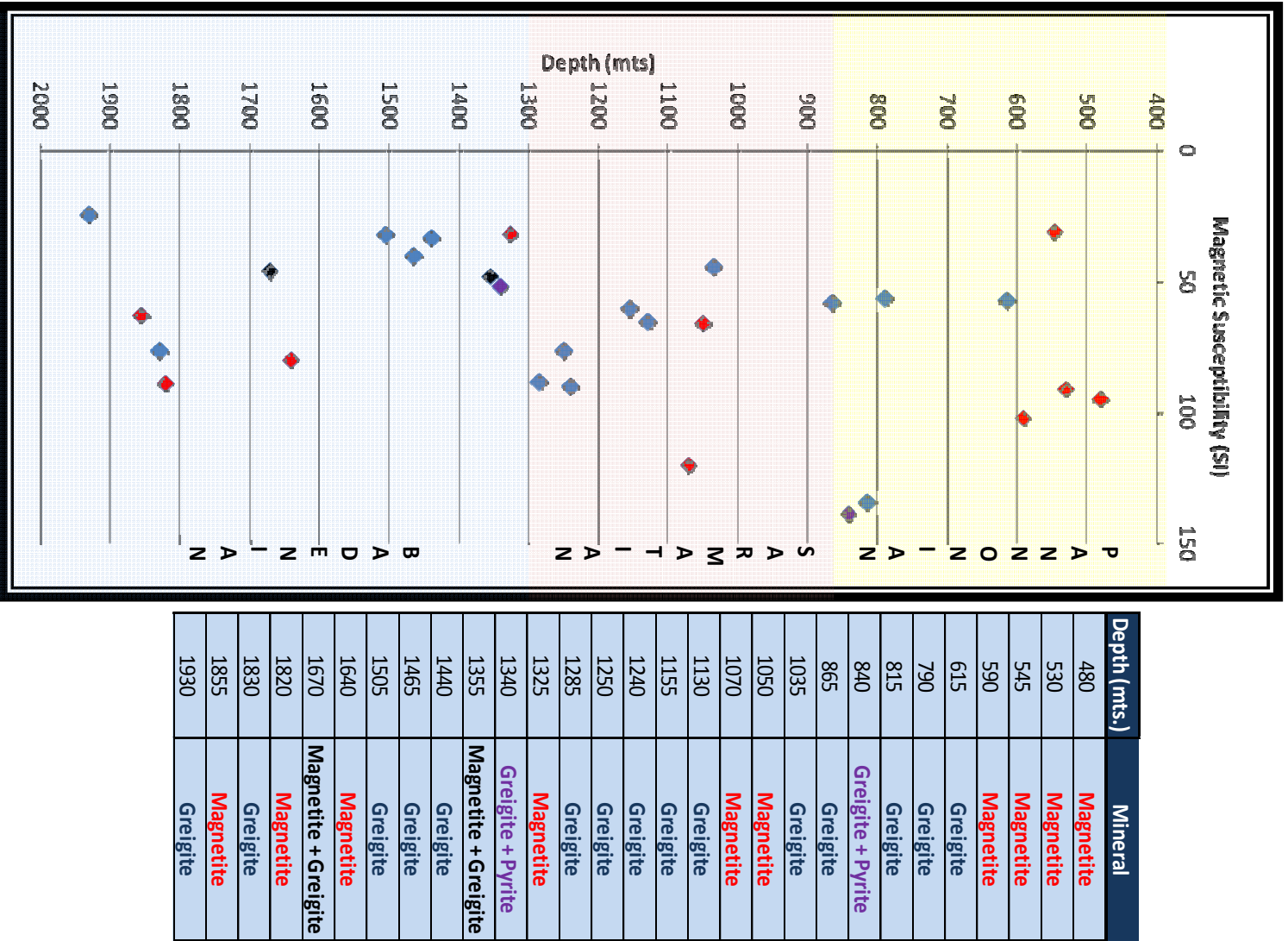


Figure 12: Distribution of magnetic minerals found by Koolen (2010) vs. Depth.

<i>Depth (m)</i>	<i>Lithology</i>	<i>Main component(s)</i>	<i>B_(1/2) 1st component (mT)</i>	<i>DP (mT)</i>	<i>SIRM/total SIRM (%)</i>	<i>total SIRM/kg (*10⁻⁹ Am² /kg)</i>
480	siltstone	magnetite	39,8	0,36	94	1,20
530	sst, very silty	magnetite	31,6	0,38	44	2,47
545	sst, very silty	magnetite	60,3	0,28	59	0,73
590	claystone	magnetite	39,8	0,37	96	2,43
615	siltstone	greigite (M)	75,9	0,22	78	0,29
790	siltstone	greigite (M)	70,8	0,24	67	0,57
815	siltstone	greigite (M)	79,4	0,18	76	0,60
840	siltstone	greigite (M)	75,9	0,19	86	7,49
865	siltstone	greigite (M)	79,4	0,19	74	1,72
1035	sst, silty	greigite (M)	72,4	0,25	83	0,51
1050	sst	magnetite	47,9	0,37	59	2,11
1070	siltstone	magnetite	33,1	0,35	45	2,94
1130	siltstone	greigite (M)	77,6	0,19	67	0,98
1155	silty claystone	greigite (M)	74,1	0,19	78	1,29
1240	siltstone	greigite (M)	70,8	0,17	81	3,87
1250	Siltstone	greigite (M)	70,8	0,17	93	4,77
1285	siltstone, very sandy	greigite (M)	83,2	0,17	64	2,36
1325	sandy clay	magnetite	56,2	0,31	85	0,43
1340	sandy clay	greigite (M)	70,8	0,21	53	1,66
1355	siltstone	magnetite & greigite (A)	39,8/67,6	0,24	49/42	3,52
1440	siltstone	greigite (A)	70,8	0,26	42	1,39
1465	siltstone	greigite (A)	67,6	0,21	60	1,20
1505	siltstone	greigite (A)	61,7	0,26	70	0,65
1640	sst	magnetite	56,2	0,28	79	0,38
1670	sst/siltstone	magnetite & greigite (A)	31,8/89,1	0,24	46/46	0,39
1820	siltstone/calc sst	magnetite	50,1	0,35	53	0,76
1830	siltstone/shaly sst	greigite (A)	67,6	0,30	81	0,20
1855	siltstone/shaly sst	magnetite	50,1	0,35	79	0,52
1930	calc. sst	greigite (A)	64,6	0,30	70	0,28
1987,5	calc sst	magnetite	36,3	0,35	90	1,99

Figure 13: Summary table with results of the 32 samples analyzed by Koolen (2010).

The log was divided into the three stratigraphic units present in the well. These units constitute the core of this study in the Miocene, particularly the Middle to Upper Miocene Badenian, Sarmatian, and Pannonian (see Table 2).

In the well Spannberg-21, from top to bottom, we distinguish first from the surface down to 300 mts. deposits which belong to the Upper Pannonian. From this depth until 500 mts. the sediments correspond to the Middle Pannonian, and until approximately 860 mts. to the Lower Pannonian. Deposits from the Lower Pannonian and the Upper Sarmatian have more shales. From there until 1100 mts., the Upper Sarmatian sediments are found and down to the range of 1283-1300 mts., the Lower Sarmatian. The Sarmatian-Badenian boundary is interpreted within this range based on FMI and MS data. The reason why it is not specified at a particular depth is because by looking the resistivity microimages, a sharp contact is found at 1283 mts. However, the MS curve shows this sharp contact at 1300 mts. and it is characterized by a significant drop in the readings.

		Unit	Depth (mts)
MIOCENE	LATE	PANNONIAN	Upper 0-300
			Middle 300-500
			Lower 500-860
	MIDDLE	SARMATIAN	Upper 860-1100
			Lower 1100-(1283-1300)
		BADENIAN	Upper (1283-1300)-1590
			Middle 1590-1966 (TD)
			Lower not reached

Table 2: Summary table with the stratigraphic units present in Spannberg-21.

The bottom part of the log shows Upper Badenian sediments from the 1283-1300 mts. range until 1590 mts., and finally the Middle Badenian down to the total depth of the well at 1966 mts.

CURRENT WORKS

CROSS-PLOTS

After doing a quick-look interpretation and identifying the trends described above, the next step was to analyze the magnetic susceptibility curve. The idea was to find a matching pattern or correspondence between this curve and the others. The first aspect noticeable was the apparent poor match between MS and GR. However, this was difficult to conclude at first sight since the magnetic susceptibility has a wide range of values. Due to this, the log was divided and different scales were defined. As a result, a good match was present between these curves in the Badenian interval, but in the Pannonian and Sarmatian the match was not so good. This will be developed further in Chapter 5.

In order to establish a correlation between MS and the other curves, a correlation matrix was built. The six different zones are taken from (Paulissen, 2011) where these intervals were chosen for the determination of the sedimentation rates. In this case, these intervals were modified a bit based on the MS and also the FMI data. Particularly for the Sarmatian-Badenian boundary, it has been narrowed down because the proposed boundary was located between 1290-1350 mts. Table 3 shows the intervals defined as MS_i.

MS1	MS2	MS3	MS4	MS5	MS6
455-500 mts	500-860 mts	860-1100 mts	1100-1300 mts	1300-1590 mts	1590-TD

Table 3: Intervals used for the correlation matrix. Modified from Paulissen (2011).

The interval MS1 is the shortest since there are no logging data available in the first 450 meters of this zone (density, porosity, resistivity, and photoelectric factor). For this correlation matrix, all values were normalized. The porosity TNPH is inversely correlated with MS and for the purpose of this exercise, it is only used as a reference. The full plots can be found in Appendix C.

These results were the starting point for investigating the origin of the magnetic susceptibility. The very peculiar and interesting patterns and trends observed are an obvious invitation to figure out what could be the factors involved in the process, what makes a sediment more or less magnetic, which minerals control the magnetic susceptibility curve, etc., among other important questions.

ACID TEST

As part of the study an acid test was performed on some samples in order to assess the amount of carbonate. The cuttings are available for the whole log interval and after checking the type of lithology in the well, this basic test was performed with HCl at 10% concentration. The selection criteria was based on taking enough samples for each stratigraphic unit and especially at the boundaries. In total, 92 samples were analyzed. All samples showed fizz, in some cases stronger or faster. This demonstrated that calcite is ubiquitous throughout the well, albeit in different concentrations. Appendix D shows the table with the samples and depths selected for this exercise.

XRD/XRF ANALYSIS

The objective of these two analyses, X-ray powder diffraction and X-ray fluorescence, was to determine the clay mineralogy and the geochemistry of the rocks of each zone. The plots generated for the correlation matrix showed what is called here "the hockey stick" pattern. As can be seen in the Chapter 5 and in Appendix C1-C4, the first four zones (MS1-MS4) were showing this specific shape but that it was absent in the bottom two zones (MS5 and MS6), corresponding to the Badenian.

By combining these plots with the magnetic mineral identification results from Koolen (2010), the following conclusions were reached: There are apparently two different types of shales, i.e. Pannonian and Sarmatian vs. Badenian, and there must be an important source of iron in the top units allowing the formation of greigite.

For the XRD/XRF analysis, six samples in total were selected. The criteria was to choose two samples in the Pannonian, two samples in the Sarmatian, and two samples in the Badenian. Since the cuttings available are sampled every five meters, and keeping in mind that the idea was to determine the clay mineralogy of the shales, the samples were picked up at every extreme side of the plots (refer to Figure 14). This was done to secure a pure shale sample, but also the highest MS values.

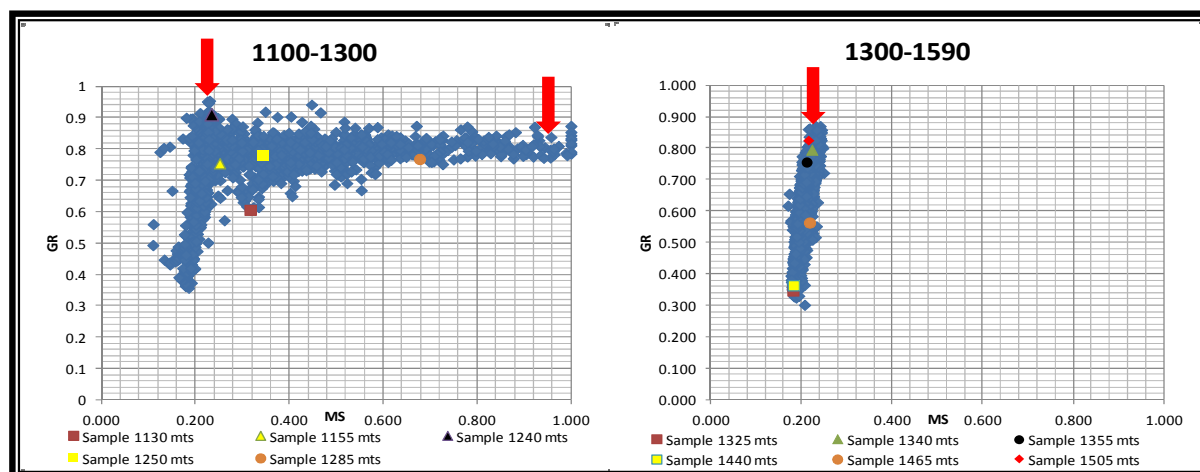


Figure 14: Criteria used for choosing the samples for semiquantitative analysis. *Left: Sarmatian unit, Right: Badenian unit.*

As a part of the selection process, the 32 samples analyzed by Koolen (2010) were plotted on the same graphs generated for the correlation matrix. This is first observed in Figure 15 showing the whole data and Figure 16 per zone. The main graph used was GR vs. MS to evaluate not only the trend, but also the high/low values of GR and MS. It is important to mention that since the cuttings were sampled every 5 meters and the idea was to have a pure shale, only those samples with the whole interval of five meters meeting the criteria were selected. This was not an easy task because as observed in Figure 17, the readings in the Pannonian and the Sarmatian were not confined to a particular zone only, but rather they were spread out.

Once the samples were chosen, a small portion of about 50 gr. of each was put in the oven. All the samples were dried for 72 hrs at 70 degC to remove all the water. Then, using a mortar and pestle the samples were ground and a fine powder was produced. The grinding was performed by hand for about 10 minutes at a constant force. The procedure was executed very carefully avoiding contamination and misidentification of samples. Finally, the fine powder of the six samples were given to the XRD/XRF technician for laboratory analysis.

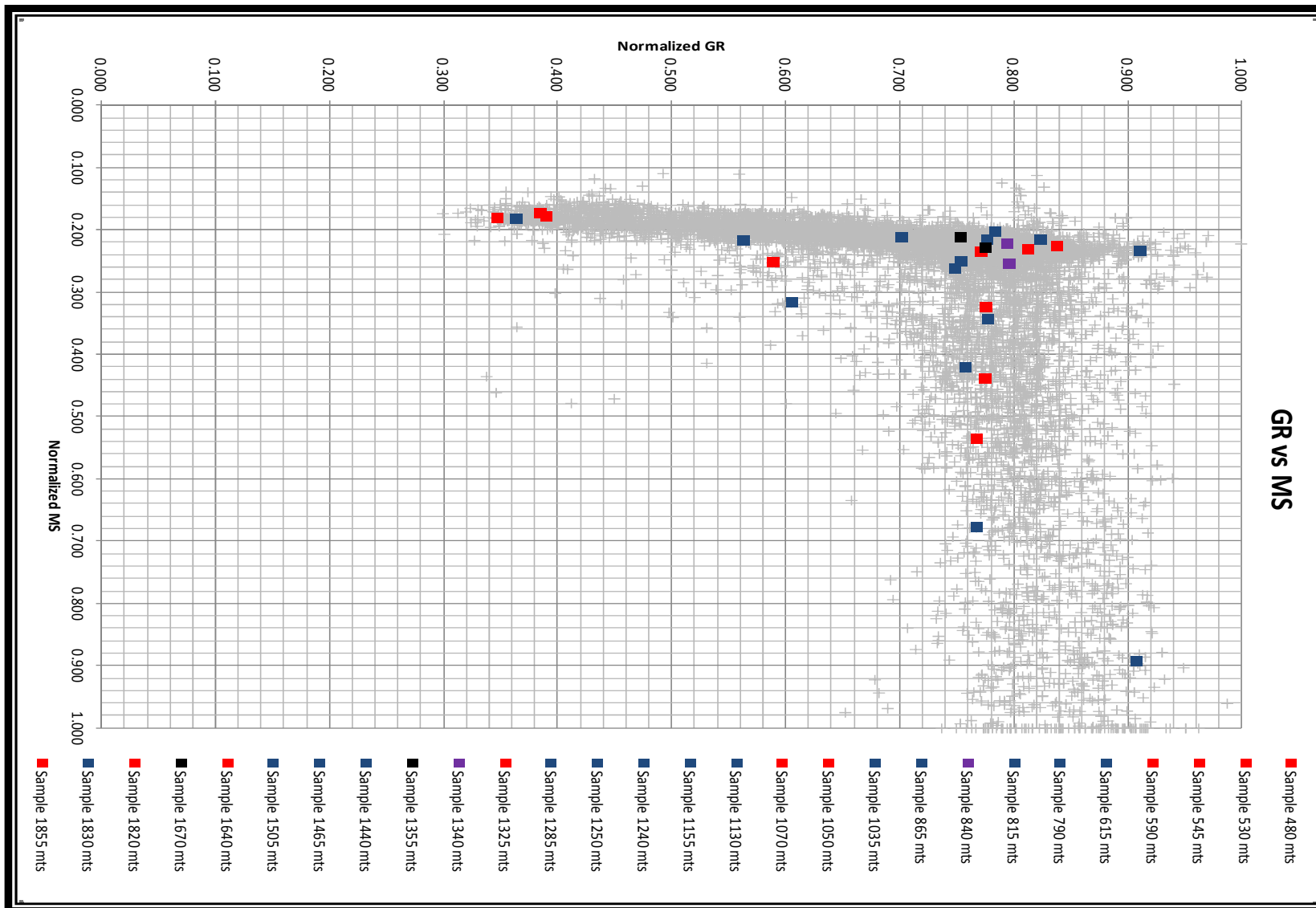


Figure 15: Superposition of the 32 samples analyzed by Koolen (2010) in the GR vs. MS plot used for the correlation matrix. This shows the wide distribution of magnetic minerals with depth. Purple: greigite + pyrite found. Black: magnetite + greigite found. Red: magnetite. Blue: greigite.

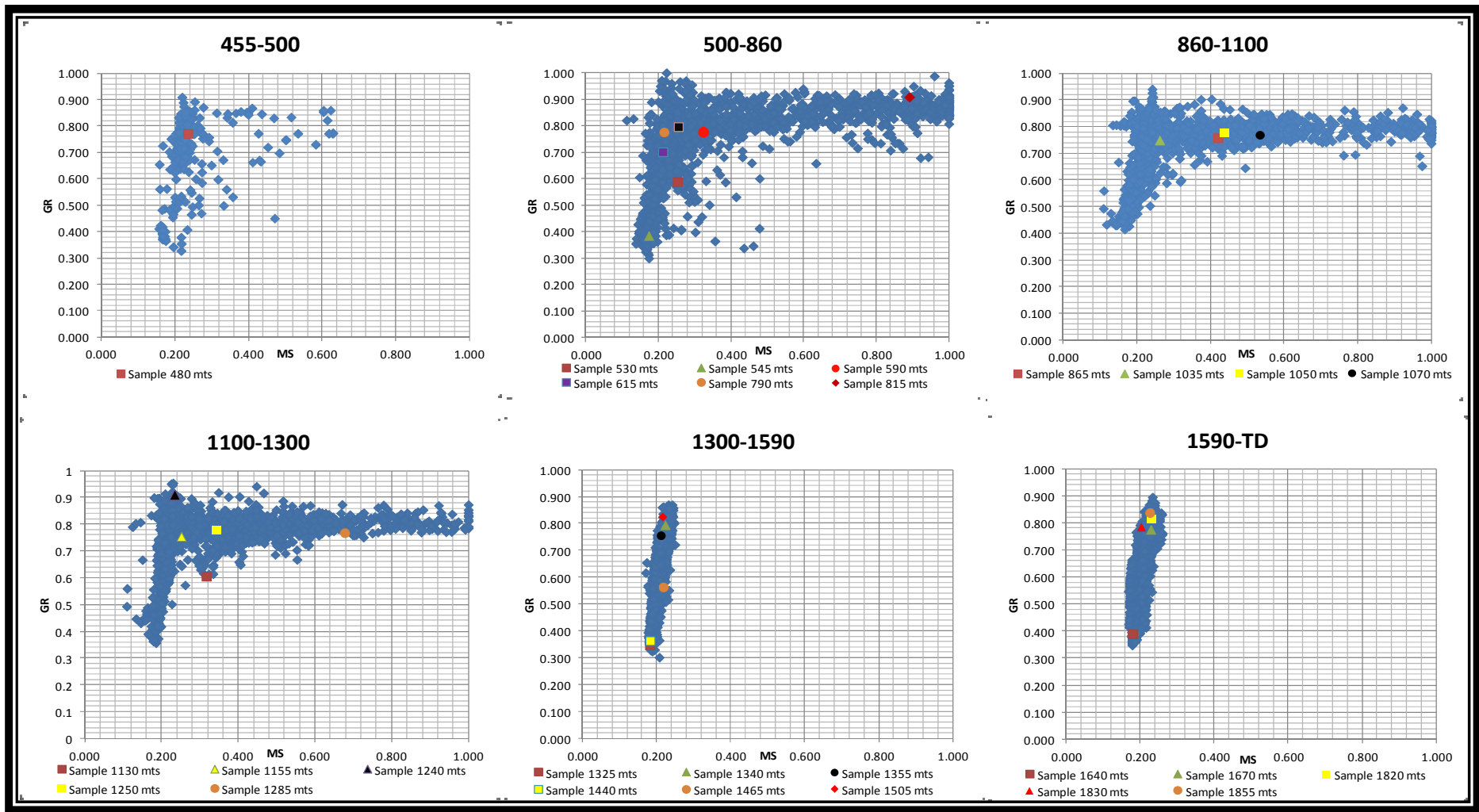


Figure 16: Superposition of the 32 samples chosen by Koolen (2010) in the GR vs. MS plot used for the correlation matrix. These plots were helpful for the further samples selection.

The XRD/XRF analysis was performed initially by the X-ray diffraction facilities at the Materials Science and Engineering of the TU Delft, Faculty of 3mE. After the results were obtained, a further semiquantitative analysis was proposed in order to determine the chemistry and percentage of each sample. The idea of this was to check in more detail the weight of each component and to look for specific phases such as magnetite and iron, which are very important for the study.

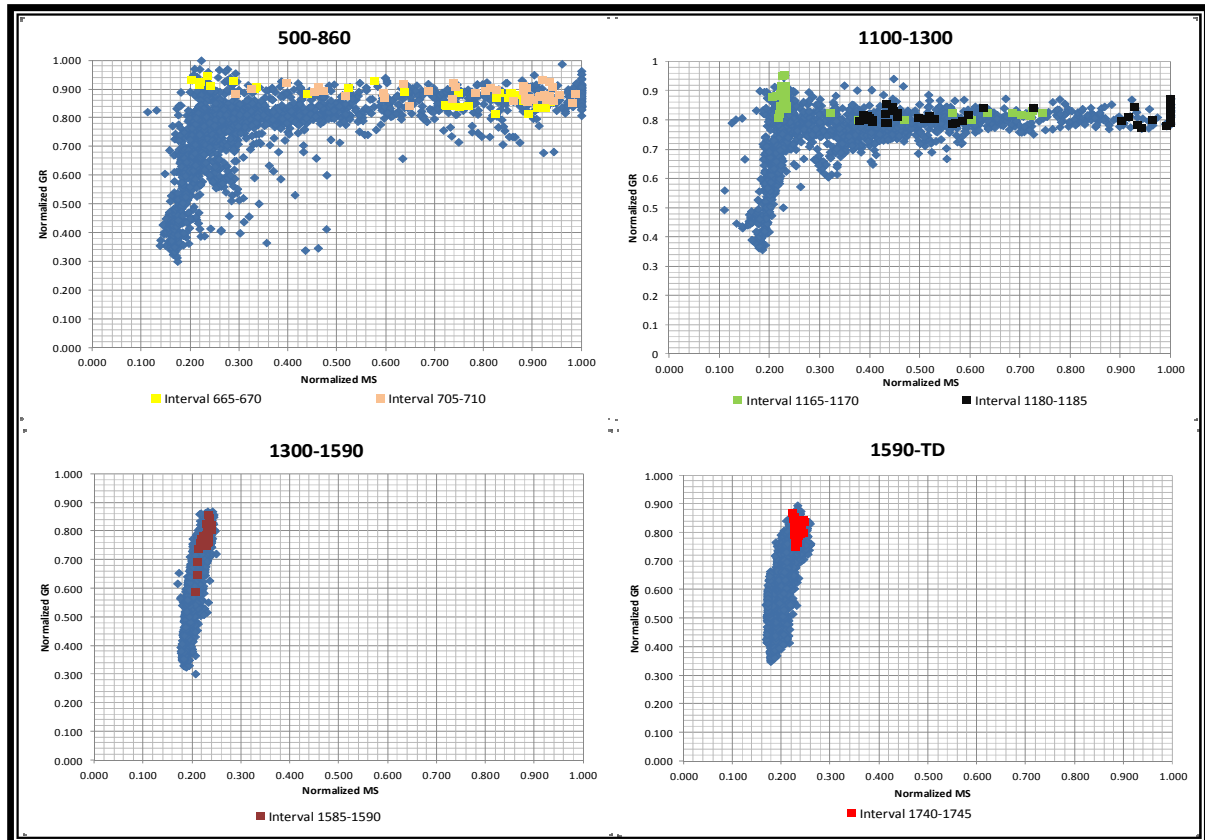


Figure 17: Samples chosen for the analysis. In total 6 samples. The criteria is fully explained in the text.

For a semiquantitative analysis to be correct, the samples must be prepared following a very strict procedure. This was not done here during the first time. This was noticed while using a computer program for this purpose called RockJock (RJ), developed by Dennis Eberl in 2003 while working for the USGS.



Figure 18: Mortar and samples analyzed. This was the methodology applied in the first XRD/XRF preparation.

According to Eberl (personal communication) there are two ways to perform this analysis, either using the Rietveld method or whole pattern fitting, which is what RJ does. Rietveld calculates the pattern from first principles, but is not so good for minerals or mineraloids which have poorly defined structures and compositions. RJ uses a library of standard patterns of known intensities that are fitted to the diffraction pattern by a solver in Excel. The spectrum calculated and the resulting phases identified showed that effectively the samples were not prepared accurately enough for this purpose. The phases were not showing a proper match and not all phases were identified.

Dennis Eberl mentions (personal communication) that the degree of fit must be <0.1 , however this data had on average only a degree of fit of around 0.25. Therefore, the results can only be used as a reference. Also, all interesting components such as magnetite, iron, pyrrhotite, pyrite, maghemite could not be detected. Only the common components mentioned in the XRD/XRF report were detected.

Because of the lacking quality of this first test, a second XRD was performed personally by Dennis Eberl in his facilities in the USA following his standard procedure for subsequent semiquantitative analysis. This procedure can be found in Eberl (2003). The results turned out to be much more accurate because all the peaks are fitted by the calculation with a degree of fit for all samples of <0.1 , and with the total close to 100% (Figure 19).

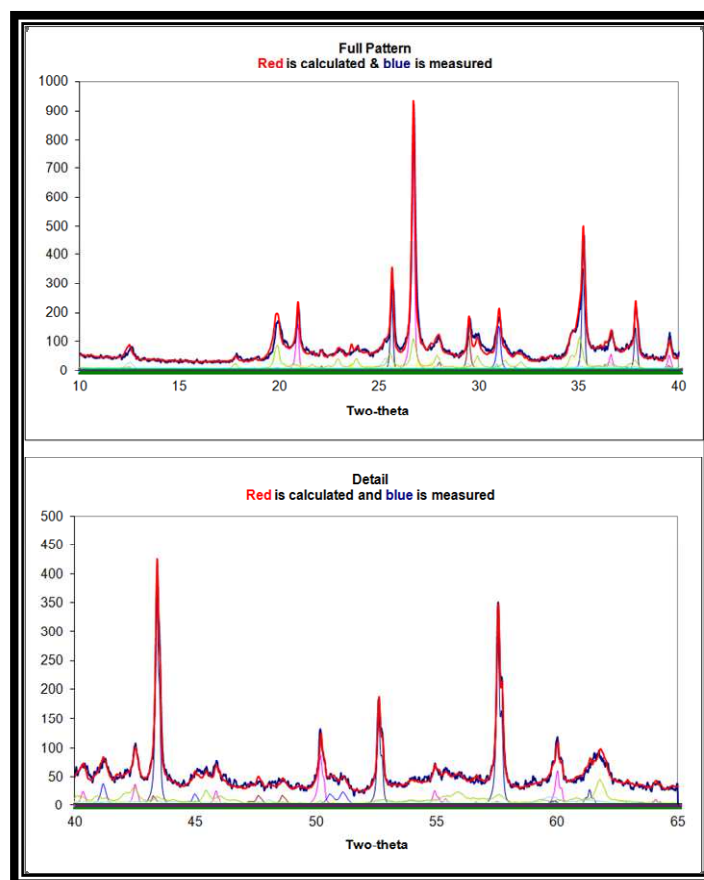


Figure 19: Matching patterns performed by Rock Jock Excel program.

TIME-SERIES ANALYSIS

The spectral analysis performed in this study used the magnetic susceptibility log. Previous workers in the area (Paulissen, 2011; Paulissen et al. 2011b) have used gamma ray logs and high resolution logs (electrical borehole images). The methodology described here does not assume beforehand that any of the Milankovitch cycles are preserved and/or present in the sedimentary record observed in the study area.

According to Torrence and Compo (1997), the wavelet analysis is more efficient than standard Fourier spectral-method because it gives information both in the time and frequency domains as a time-frequency representation of the signal. The wavelet transform can be used to analyze time series that contain non-stationary power at many different frequencies. This feature is very suitable for the type of data used here.

The wavelet transform was applied using the open source code provided by Torrence and Compo (1997). The mother wavelet was set to the Morlet wavelet ($\omega_0 = 6$). Since the present data was initially per meter distributed and then yearly distributed (kyr), the key parameter " δt " for the wavelet analysis was set as 0.2, 0.5, and 0.8. Finally, the plots were generated with the 0.5 value. The other parameters were $N =$ variable for each zone, $\delta t = 0.2, 0.5, 0.8$ yr, $s_0 = 2 * \delta t$, $\delta j = 0.2$. Torrence and Compo (1997) explain that this value of δj is commonly used since it appears adequate for providing a smooth picture of the wavelet power.

A critical aspect of time-series analysis is the conversion of the signal from the depth domain into the time domain. In this case this task was performed using the sedimentation rates determined by Paulissen (2011) in the Pannonian and Sarmatian interval. In the Badenian interval no sedimentation rates could be determined because the magnetic signal was too weak to perform a magnetostratigraphic analysis. This depth-to-time conversion is considered to be very accurate since the sedimentation rates were determined using a combination of biostratigraphy, magnetostratigraphy, seismic stratigraphy and lithostratigraphy. Only six short intervals were selected in that study. In the present study a continuous interval of nearly 1300 mts. will be used for it.

Table 4 below lists the zone subdivision with their respective depth and time interval and the corresponding sedimentation rates. Zone 1 includes the Upper Pannonian and 160 mts. of the Middle Pannonian. Zone 2 includes the rest of the Pannonian. Zone 3 consists of Upper Sarmatian and Zone 4 of the Lower Sarmatian.

Zone	Depth Interval (mts)	Time Interval (Ma)	Sedimentation rate (mts/kyr)
1	30-460	8.9-10.6	0.3
2	460-860	10.6-11.65	0.36
3	860-1100	11.65-11.92	1.2
4	1100-1250	11.92-12.45	0.43

Table 4: Zones used for the spectral analysis, indicating depth and time interval as well as sedimentation rates. This zone classification is based on the depth-time correlation defined by Paulissen (2011).

Table 5 below shows the number of Milankovitch cycles that can be expected in each interval. The Milankovitch cycles considered here are the long and short eccentricity of 400 kyr and 100 kyr respectively, the obliquity of 41 kyr and the precession of 23 kyr and 19 kyr. However, Zones 3 and 4 are not long enough to show a complete 400 kyr cycle. Therefore, this cycle was not considered for the study.

Zone	Rate (mts/kyr)	Zone Thickness (mts)	Orbital periods (kyr)				
			400	100	41	23	19
1	0.3	430	3.6	14.3	35.0	62.3	75.4
2	0.36	400	2.8	11.1	27.1	48.3	58.5
3	1.2	240	0.5	2.0	4.9	8.7	10.5
4	0.43	150	0.9	3.5	8.5	15.2	18.4

Table 5: Sedimentation rates and thickness per zone, and the number of orbital cycles that can be expected based on them.

Chapter 5:

RESULTS AND DISCUSSION

The aim of this chapter is to show the results combined with a discussion of previous works performed either in the study area or in the field of magnetic susceptibility. A detailed log interpretation is performed. Also, the correlation matrix analysis is explained. The idea is to present an analysis about magnetic susceptibility, its origin, and its controlling factors based on the present data acquired and their interpretation. This is done with careful discussion considering all the key points. Additionally, the wavelet maps are analyzed for any possible Milankovitch cycles. Finally, some answers are given for some of the questions that were initially raised. However, there still remain uncertainties about the magnetic susceptibility signal observed in Spannberg-21.

LOG DESCRIPTION

As mentioned earlier in the Methodology chapter, only LWD data is available from the Lower Pannonian down to TD (the full logs can be found in Appendix A). Therefore, the following log interpretation refers to this interval only. In Table 2 found in Chapter 4 the different units present in Spannberg-21 and their depths can be found. Figure 20 on the next page shows the logs for a quick reference of the following explanations.

There is a slight decreasing trend of GR with depth. The GR values are high for the Pannonian and Sarmatian, but show lower values downwards to the Badenian. The GR shows a fully serrated behavior in the Badenian sediments. The GR readings in this zone is on an average 75 GAPI, with some clean zones of 45 GAPI. In the Pannonian and Sarmatian there are some long intervals that are more constant, with very subtle fluctuations. The GR in these zones is around 90 GAPI with very few clean zones of 45 GAPI.

In terms of the density curve, there is a more noticeable increasing trend with depth. The Pannonian shows density values of around 2.25 gr/cc. The Sarmatian has higher values of about 2.35 gr/cc. The Badenian has the highest values in the section with values on average around 2.45 gr/cc.

Regarding photoelectric factor, the values decrease with depth. The trend is slightly noticeable. The readings start at about 7 in the Pannonian, keeping the same values on average in the Sarmatian, but decrease down to 5.5-6 in the Badenian. This is due to reduction of shales in the sediments, which have a wider range of values.

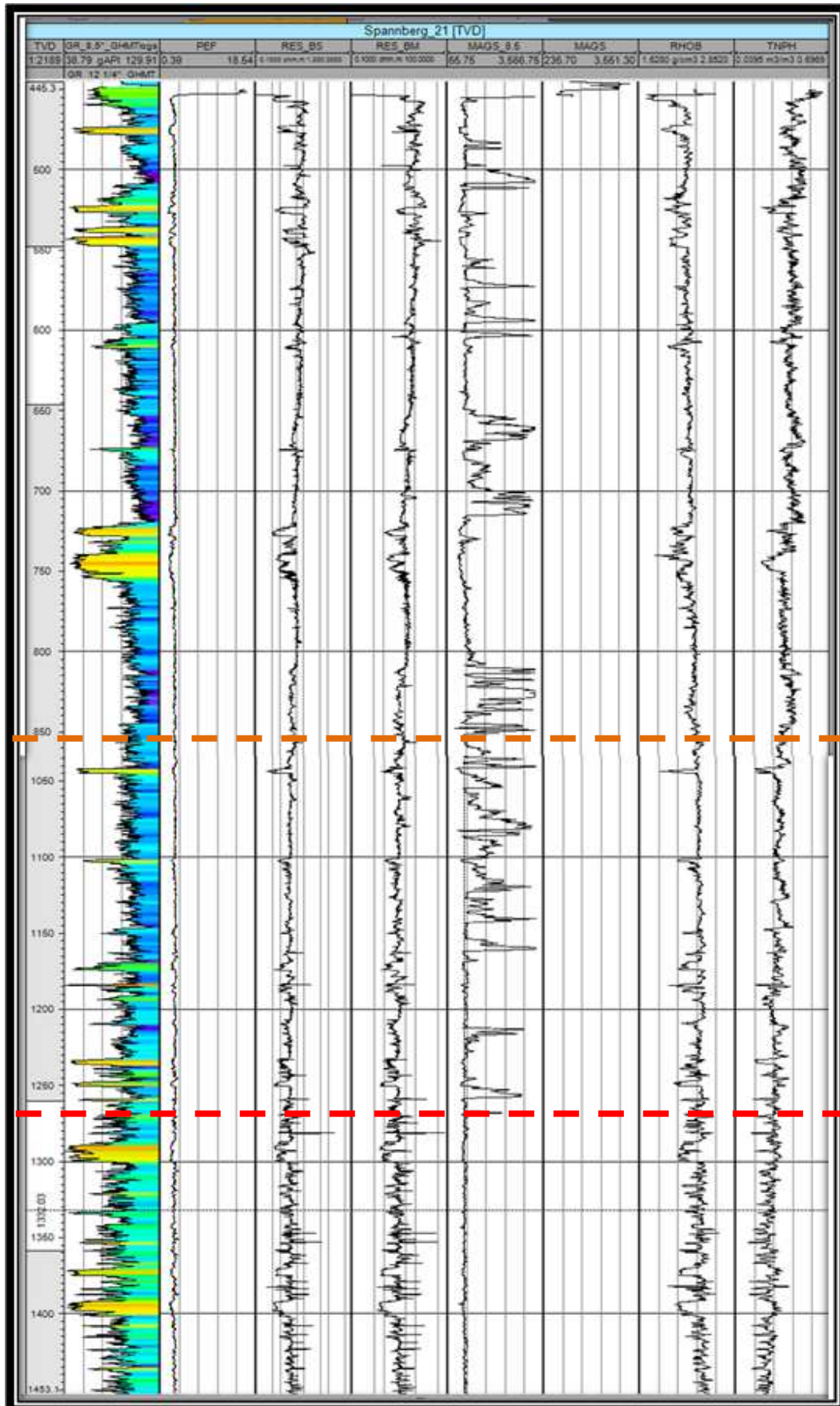


Figure 20: Logging data from Spannberg-21 - 8^{1/2}" section. Orange dashed line marks the Pannonian-Sarmatian transition. Red dashed line marks the Sarmatian-Badenian transition. From left to right: GR, PEF, RES_BS, RES_BM, MS, RHOB, TNPH.

The porosity curve, with a similar principle as density, changes with depth. In this case the values decrease from the Pannonian to the Badenian.

The resistivity curve varies slightly along the well section. It has values above 100 ohm.mts in the Pannonian and then the readings decrease down to 80 ohm. mts on average in the Sarmatian sediments. In the Badenian, the values go up a bit up to about 90 ohm.mts. However, the important feature is not about the values itself but about the spiky behavior observed in this part of the log. Multiple spikes are shown in the resistivity curve of the Badenian sediments while these spikes are completely absent in the sediments above.

The FMI data represent a very valuable source of information especially for a better visualization of the lithologic changes, units boundaries, and confirmation of possible features observed in the LWD curves. In this case, the FMI data allowed the interpretation of the Sarmatian-Badenian boundary at the 1283-1300 mts. range, which was already constrained between 1350 and 1290 mts. by Paulissen (2011).

Considering the resistivity curve, it was mentioned earlier that the Badenian section is characterized by multiple spikes in the readings. These are definitively not related to any malfunction of the logging tool. All the spikes have a match with the gamma ray showing a sharp decrease, with sharply increasing density and sharply decreasing porosity readings. Comparing these matches with the images from the FMI, it is found that every spike coincides with highly resistive layers (white in the color scale of this log). These highly resistive layers are the carbonates present in the Badenian deposits and some of them show natural fractures.

The magnetic susceptibility curve (MS) shows a very particular behavior for each of the zones described above, and the values can be divided into low, medium, and high. Since this data was acquired in the 8^{1/2}" section with wireline, the data covers all the stratigraphic units. Appendix B shows the magnetic susceptibility distribution along the well.

Starting in the Upper Pannonian, the first 140 mts are very low in magnetic susceptibility with some punctually high values. Unfortunately there is no LWD data in this zone to correlate with the MS data. The readings then increase to medium-high values passing from 600 ppm on average to 1000 ppm approximately, with some peaks of higher values. The Middle Pannonian readings continue with the same average values of the Upper Pannonian until 390 mts, after that the values increase and this trend is kept along the Lower Pannonian and the whole Sarmatian where the highest values are reached. Almost the entire unit is characterized by very high readings having peaks above 3000 ppm. At the Sarmatian-Badenian boundary, specifically at 1300 mts. a sharp decrease occurs and the curve shows the lowest output in the entire log. An almost flat curve of 250 ppm on average is observed from 1300 mts. until TD at 1966 mts. corresponding to the Upper and Middle Badenian.

The very few clean zones found in the Pannonian and Sarmatian show a good correlation between all the curves, similar to what is observed in the Badenian section. This is

indicative of the relationship between clean lithologies (less clay) and magnetic susceptibility.

In the correlation between magnetic susceptibility curve and gamma ray four areas can be identified. Some hypotheses are raised for each area based on the GR and MS values and the magnetic behavior of some minerals (Table 6). The analysis was performed with these two curves because it was here where the patterns could be best recognized. The density and photoelectric factor curves show a very similar behavior as the gamma ray (Table 7).

High GR - High MS = normal correlation, deposition probably dominated by clay minerals. MS can be caused by the paramagnetic behavior of the clay minerals and also some ferromagnetic minerals can be present.
High GR - Low MS = deposition probably dominated by clay minerals, probably less ferromagnetic minerals present and the MS can be caused by the paramagnetic behavior of the clay minerals.
Low GR - High MS = anti-correlation observed with low GR but high MS values. The MS can be caused by the presence of ferromagnetic minerals. Less clays present.
Low GR - Low MS = normal correlation, very weak MS signal probably due to the diamagnetic behavior of some minerals. Less clays present and probably less ferromagnetic minerals present.

Table 6: Areas identified in both GR and MS curves along the well section. Normal correlation means high GR-high MS (also low GR-low MS). Anticorrelation means high GR-low MS and vice versa.

CORRELATION MATRIX

The plots generated for the correlation matrix and the characteristic pattern observed in the results allow us to consider several key questions. For example, is this trend a pure magnetic mineral effect? Or is it a combined effect of two different situations. Are there more factors related to this behavior? Why do the high magnetic susceptibility values occur only in the Pannonian and Sarmatian, and how could this be linked to the obtained pattern? What is the main magnetic carrier in the study area? Which magnetic minerals are present? What are the differences between the stratigraphic units capable of producing such a different range of values and curve behavior? And finally, what are the depositional and diagenetic contributions to this response?

To answer all these questions we start by analyzing the cross-plots. The plot of magnetic susceptibility vs. gamma ray shows clearly two different patterns. As seen in Figure 21, the first pattern identified in zone MS1 (and in zones MS2, MS3, and MS4) seems to have a combined effect caused by two superimposed trends. The first trend shows high values for GR and a wide range of MS (horizontal response), while the second trend shows low MS but medium to high GR values (vertical/diagonal response). Together they form something like a hockey stick. The second pattern is also observed in the bottom zones MS5 and MS6 (Figure 21, right, only shown for MS5) but the first pattern is entirely absent in these two Badenian zones.

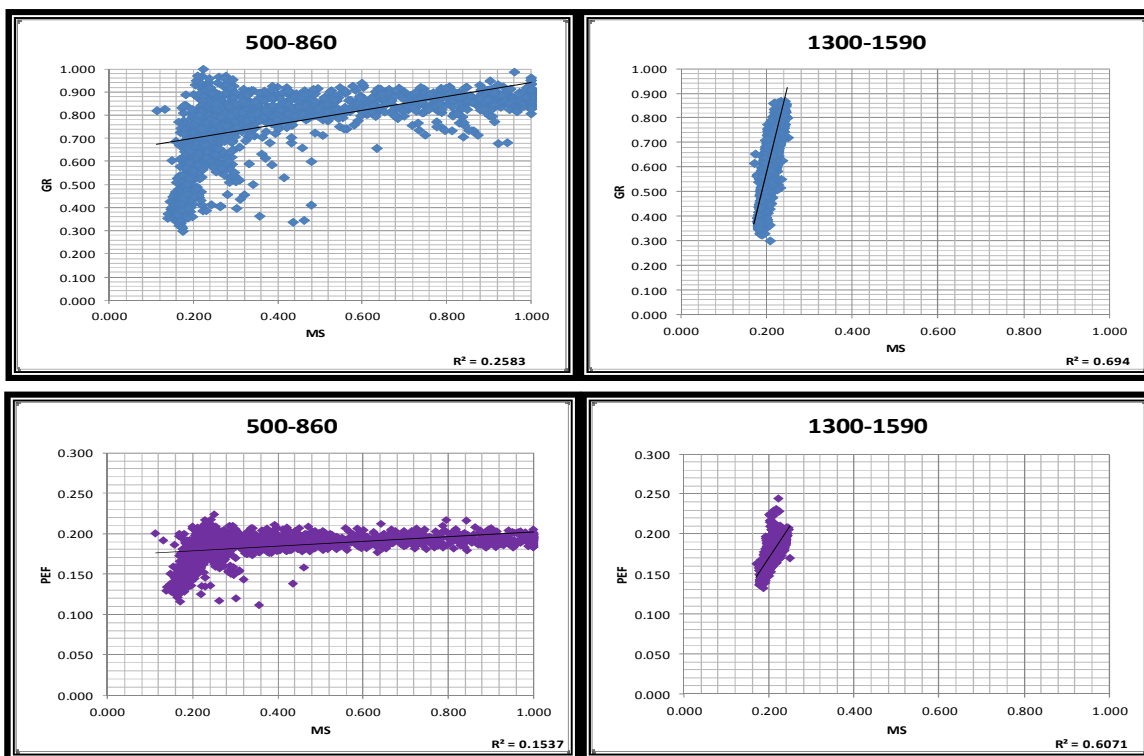


Figure 21: Correlation matrix plots generated. *Top* plots are GR vs. MS. *Bottom* plots are PEF vs. MS. The specific pattern is observed in zone MS2 (500-860 mts) corresponding to Lower Pannonian and the other zone MS5 (1300-1590 mts) corresponding to Badenian.

The other plots, density vs. MS and photoelectric factor vs. MS, show exactly the same patterns from MS1 to MS6 as found with the gamma ray log. Even the plot of porosity vs. MS, which has an inverse relationship, shows the same trend but upside down. All these plots can be found in Appendix C.

The correlation matrix results are shown in Table 7. The red numbers indicate the highest correlation coefficients which are obtained in the Badenian intervals MS5 and MS6. On the other hand, the correlation is very poor in the top intervals corresponding to the Pannonian and Sarmatian.

	MS1	MS2	MS3	MS4	MS5	MS6
GR	0.08	0.26	0.12	0.15	0.69	0.62
RHOB	0.04	0.09	0.07	0.07	0.56	0.61
PEF	0.07	0.15	0.12	0.14	0.61	0.72
TNPH	0.007	0.17	0.06	0.13	0.02	0.02

Table 7: Correlation matrix coefficients of the LWD data with the MS data for the six zones.

Although there was no LWD data available for the first 450 mts., a cross-plot between GR from wireline and MS was generated. The characteristic pattern obtained in the zones from MS1 to MS4 is not easily observed here (Figure 22, top). The correlation coefficient is

only 0.11. However, what is interesting is the general low trend of magnetic susceptibility values as found in the Badenian, but the units are very different.

Even though the magnetic susceptibility values observed in the Upper Pannonian and the Badenian look similar, their behavior is different. The Badenian shows a steady behavior with no sudden fluctuations and an average value of about 650 ppm. On the other hand, the Upper Pannonian shows many fluctuations and in general the MS values increase with depth, starting slightly above 500 ppm and ending almost at 1000 ppm at the Upper-Middle Pannonian boundary. Also some sharp peaks are observed in this interval.

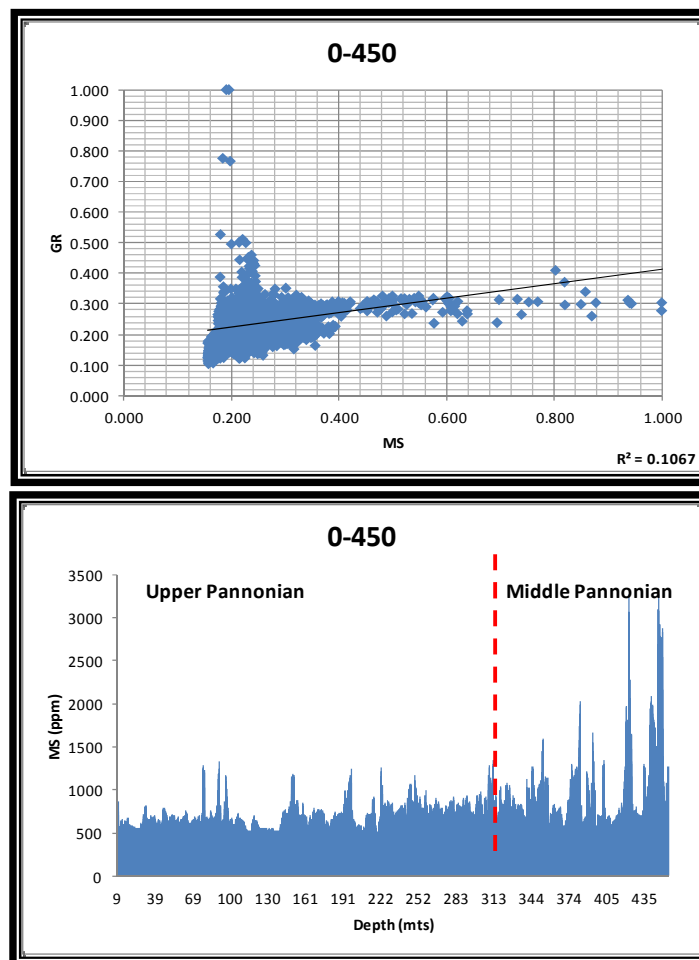


Figure 22: *Top* plot shows GR vs. MS in the top interval. In this zone the pattern observed in the zones from MS1 to MS4 is not evident. *Bottom* plot shows the MS vs. Depth for the same interval. Red line indicates the limit between Upper Pannonian and Middle Pannonian.

The comparison between GR, RHOB, PEF, TNPH and MS in every zone is displayed in Figure 23. There, three short sections from the three stages are shown with the GR and the MS alongside each other.

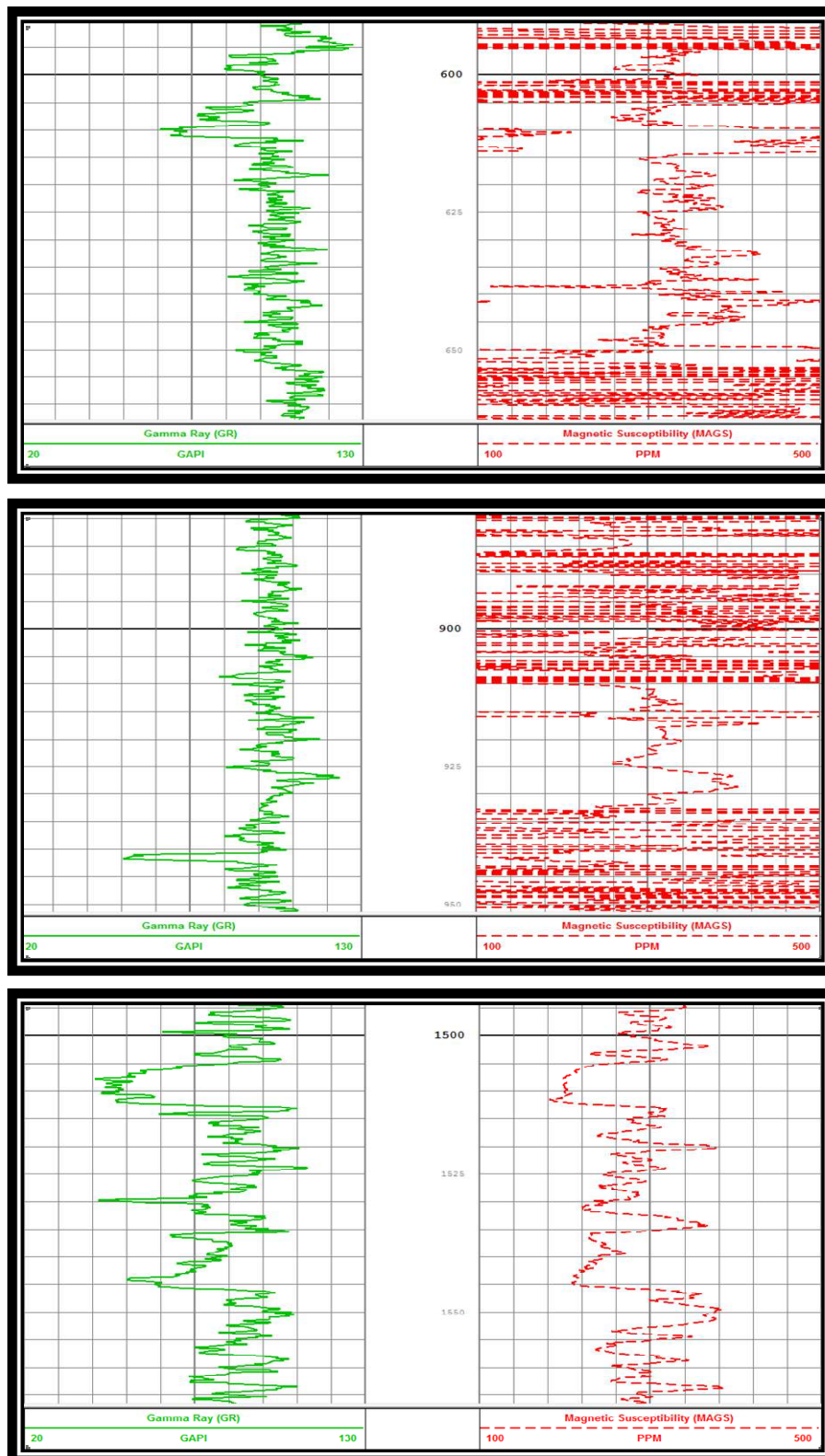


Figure 23: Magnetic susceptibility and GR comparison. The light green curve in the left track is the GR. The middle track is depth in meters. The red curve in the third track is MS. *Top* is Pannonian, *Center* is Sarmatian, and *Bottom* is Badenian.

XRD/XRF

The range of the GR values in the cross-plots shown above confirms the presence of shales in the Pannonian, Sarmatian, and Badenian, but only the Pannonian and Sarmatian show high MS values. The Badenian shales do not show high MS values. The first

impression therefore is that the shales in the Pannonian and the Sarmatian are different from the shales in the Badenian.

Previous work performed by Koolen (2010) and Paulissen (2011) shows that there are zones with mostly greigite, zones with mostly magnetite, and zones with a combination of both. The lowest susceptibility values are found mostly in greigite-bearing intervals, whereas the highest values are found in both mostly magnetite-bearing and mixed zones. However, greigite is much more abundant than magnetite according to Koolen (2010). This is the main reason why greigite has been considered in recent studies as the main magnetic carrier in the area (Vasiliev et al., 2007).

The following were the main two reasons for performing the XRD/XRF analysis: 1. if greigite is considered the main magnetic carrier, there must be then an important source of iron allowing its formation in every unit, and 2. the variable responses of the signal observed indicates the likelihood of having different types of shales.

The results of the first XRD analysis indicated that all the samples contained the same minerals, but in different quantities. The components found were quartz, albite, muscovite, clinocllore, dolomite, and calcite. After reviewing the data, a mineral substitution was proposed for checking other fitting options. Appendix F shows the XRD results for all the samples. It was proposed to check for illite, smectite, and kaolinite instead of muscovite, clinocllore, and albite. This was done but the results indicated that although illite and muscovite were both possible, the muscovite fitted somewhat better, and albite fits much better than kaolinite. The smectites like nontronite and montmorillonite did not fit the measured patterns.

The Table 8 shows the XRF values organized into three categories: main mineral components, feldspar and clay components, and ferromagnetic mineral components. Based on these results, it makes more sense to perform a semiquantitative analysis because these percentages represent the total compound, but each element can be present in more than one phase (e.g. some SiO_2 is in quartz and some in muscovite).

665-670		Total %	705-710		Total %	1165-1170		Total %
SiO ₂	54.021	77.902	SiO ₂	53.93	77.784	SiO ₂	54.737	80.162
CaO	6.181		CaO	5.856		CaO	9.972	
Al ₂ O ₃	17.7		Al ₂ O ₃	17.998		Al ₂ O ₃	15.453	
Na ₂ O	0.898	11.788	Na ₂ O	0.943	12.337	Na ₂ O	0.932	11.082
K ₂ O	6.643		K ₂ O	7.137		K ₂ O	5.734	
MgO	4.247		MgO	4.257		MgO	4.416	
Fe ₂ O ₃	7.945	9.585	Fe ₂ O ₃	7.849	9.104	Fe ₂ O ₃	6.229	7.961
TiO ₂	0.917		TiO ₂	0.845		TiO ₂	0.796	
SO ₃	0.723		SO ₃	0.41		SO ₃	0.936	
1180-1185		Total %	1585-1590		Total %	1740-1745		Total %
SiO ₂	55.934	80.538	SiO ₂	54.913	80.776	SiO ₂	54.11	79.866
CaO	9.808		CaO	13.143		CaO	10.744	
Al ₂ O ₃	14.796		Al ₂ O ₃	12.72		Al ₂ O ₃	15.012	
Na ₂ O	0.933	11.749	Na ₂ O	0.998	12.405	Na ₂ O	0.894	11.932
K ₂ O	6.554		K ₂ O	5.976		K ₂ O	6.509	
MgO	4.262		MgO	5.431		MgO	4.529	
Fe ₂ O ₃	5.839	7.114	Fe ₂ O ₃	4.522	6.224	Fe ₂ O ₃	5.558	7.463
TiO ₂	0.723		TiO ₂	0.718		TiO ₂	0.749	
SO ₃	0.552		SO ₃	0.984		SO ₃	1.156	

SiO ₂	Al ₂ O ₃	CaO	K ₂ O	MgO	Na ₂ O	Fe ₂ O ₃	TiO ₂	SO ₃
main minerals components			feldspars/clays			ferromagnetic minerals		

Table 8: Distribution of elements by zone according to XRF data. Only representative elements are shown.

The Pannonian and Sarmatian sediments have the highest percentage of clays as mentioned in the log interpretation with a slight decreasing trend with depth. This is better noticed with the semiquantitative analysis results (see Table 9 and Figure 24). The clay percentage is about 64% in the Pannonian (Middle and Lower), on average 53% in the Sarmatian, and on average 38% in the Badenian, where the lowest value of 32% is found. Table 9 summarizes the main minerals present in every sample analyzed.

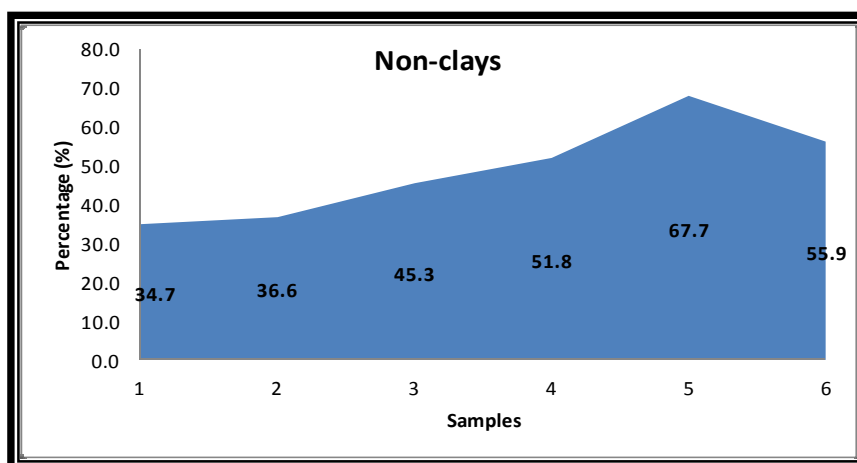


Figure 24: Non-clays content in every sample according to the semiquantitative analysis. The clear increasing trend with depth is observed.

The second XRD analysis was able to identify and therefore to confirm the presence of two different shales in the well. A very accurate semiquantitative analysis was performed this time. According to Mr. Eberl (personal communication), apparently a variable slit system was used in the first experiment because the intensities increase with two-theta. Randomly oriented patterns of the samples were also run to be able to identify different types of clays. This is how smectite and illite were recognized for the six samples chosen (Figure 25).

Smectites, which are much more iron prone than illite, decreases from 10.5% in the Pannonian to 2.7% and 3.9% for the two samples in the Badenian.

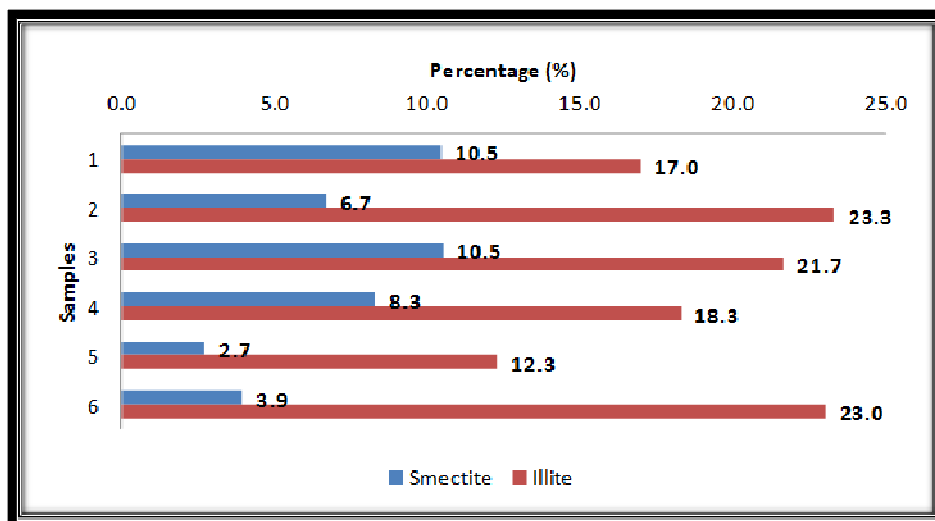


Figure 25: Smectite vs Illite content expressed in weight percentage in the samples according to the semiquantitative XRD analysis. For sample locations see Table 8.

The patterns shown in Table 9 below are reflected in the XRF results. As seen in Figure 26, diamagnetic minerals such as quartz, calcite, and dolomite increase with depth. Combined they contribute about 25% in the Pannonian whereas for the Badenian their contribution is 55%. Only one ferromagnetic mineral could directly be identified: Maghemite was found at 1.5% in the first sample corresponding to the Pannonian and at 0.2% in both samples of the Sarmatian. Goethite is present in the first two units, but at very low percentages.

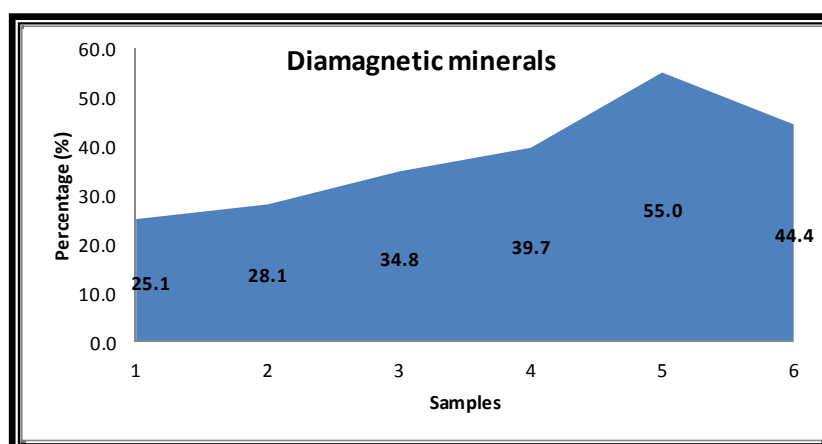


Figure 26: Plot showing the content of diamagnetic minerals present in every sample. A clear increasing trend with depth is observed. Sample 5 shows the highest value.

Sample number:	1	2	3	4	5	6
Sample name:	665 to 670	705 to 710	1165 to 1170	1180 to 1185	1585 to 1590	1740 to 1745
Full pattern degree of fit:	0.094	0.099	0.088	0.095	0.100	0.095
Mineral	Weight %					
NON-CLAYS						
Quartz	14.3	17.3	20.1	24.2	34.0	28.5
Kspar (sanidine)	3.1	1.6	2.2	3.1	2.9	2.1
Kspar (anorthoclase)	0.9	4.4	2.1	3.8	2.1	3.8
Plagioclase (albite, var. cleavelandite)	2.1	1.4	2.7	2.7	4.5	2.9
Calcite	3.6	3.2	8.2	7.5	7.2	7.7
Calcite (Mg-rich)	1.4	1.5	1.2	0.9	0.4	0.5
Dolomite (Fe-rich)	5.8	6.1	5.3	7.1	13.4	7.8
Ankerite	0.9	0.4	2.5	1.6	2.2	2.4
Amphibole (ferrotschermakite)	1.0	0.6	0.5	0.5	0.9	0.3
Magnetite	0.0	0.0	0.0	0.0	0.0	0.0
Goethite	0.2	0.1	0.3	0.3	0.0	0.0
Maghemite	1.5	0.0	0.2	0.2	0.1	0.0
Total non-clays	34.7	36.6	45.3	51.8	67.7	55.9
CLAYS						
Dickite	1.2	2.6	1.5	1.5	0.4	0.8
Smectite (ferruginous)	10.5	6.7	10.5	8.3	2.7	3.9
Illite (1Md)	17.0	23.3	21.7	18.3	12.3	23.0
Chlorite (Fe-rich; Tusc)	11.5	11.1	7.6	6.3	6.7	7.4
Chlorite (Mg; Luzenac)	1.0	0.8	0.1	0.5	0.6	0.2
Muscovite (2M1)	24.1	18.9	13.3	13.3	9.6	8.7
Total clays	65.3	63.4	54.7	48.2	32.3	44.1
TOTAL	100.0	100.0	100.0	100.0	100.0	100.0

Table 9: Summary table with the semiquantitative XRD results for the six samples.

Minerals with paramagnetic behavior such as muscovite decreases with depth. Its content varies from 24% in Pannonian to almost 9% in Badenian. Iron rich chlorite with a high ferromagnetic behavior decreases with depth as well. The distribution and percentages of all minerals identified with the semiquantitative analysis are listed in the Figure 27.

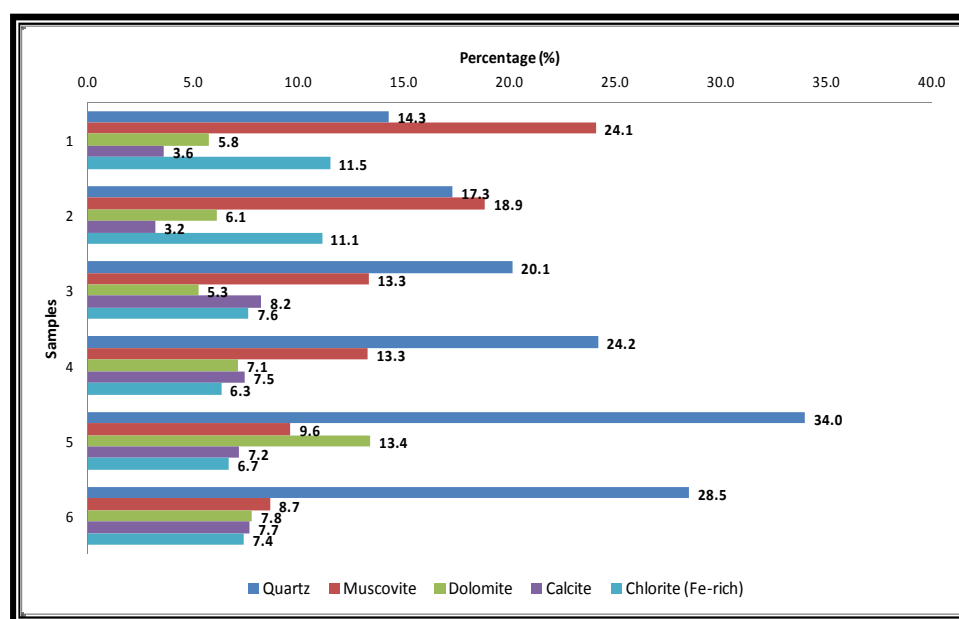


Figure 27: Diamagnetic and paramagnetic minerals vs. depth.

A clear trend of minerals is observed. Quartz (diamagnetic) increases with depth, starting at 14.3% at the top unit and ending up with 28.5% at the bottom unit reaching the maximum value of 34% in the second last sample.

SPECTRAL ANALYSIS

The wavelet analysis can produce a high intensity response where the data correlates with the shape of the wavelet. Hence it is important to use a wavelet that resembles the shape of the feature being investigated. Torrence and Compo (1997) explain that while using a Morlet wavelet with $\omega_0 = 6$, the Fourier period $\lambda = 1.03s$ and the wavelet scale is almost equal to the Fourier period. This is very helpful for interpretation.

Since our data are both in the time and depth domain, the spectrum is also obtained in depth and time, allowing to distinguish periodicities in both domains easily. The spectral analysis of the Sarmatian and Pannonian shows various cycles that are significant. The Badenian unit is not part of this analysis since sedimentation rate data was not available and also because the MS signal is weak with little movement.

The global wavelet spectrums generated show in general three major peaks: 93 kyr in Zone 1 and Zone 4, another peak at 65 kyr in Zone 2 and Zone 3, and another cycle at about 30 kyr, which is strong in Zone 3 and Zone 4. These peaks are all above the 95% confidence level. There are other weaker peaks below the confidence level in Zone 1, Zone 2, and Zone 4. The 93 kyr cycle closely matches the short eccentricity cycle of 95 kyr comparable to the cycle value defined by Laskar et. al. (2004). This cycle was also part of the results obtained by Paulissen and Luthi (2011).

The global wavelet spectrum and the power spectra obtained from the wavelet analysis of the four intervals selected are shown in Figures 28 (a, b) and 29 (c, d). Each interval displays its magnetic susceptibility curve, the wavelet spectra vs. time and depth, and the global wavelet spectrum. At the border of the wavelet power spectra there is a zone called the cone of influence. Below this cone of influence the data is considered doubtful. However, nearly the entire spectrum is found inside or above the cone. Since we are dealing with finite-length time series, errors are expected to occur at the beginning and end of the wavelet power spectrum. The plots are generated over zones that exclude unconformities (Paulissen et al., 2011a).

The contour maps generated with the wavelet analysis are found in Figures 28 and 29. The first cycle with a periodicity of 93 kyr is observed between the Middle to Lower Pannonian. Additionally, some short cycles are found in the Upper Sarmatian and a strong cycle in the Lower Sarmatian. The thick contour encloses regions with confidences higher than 95%.

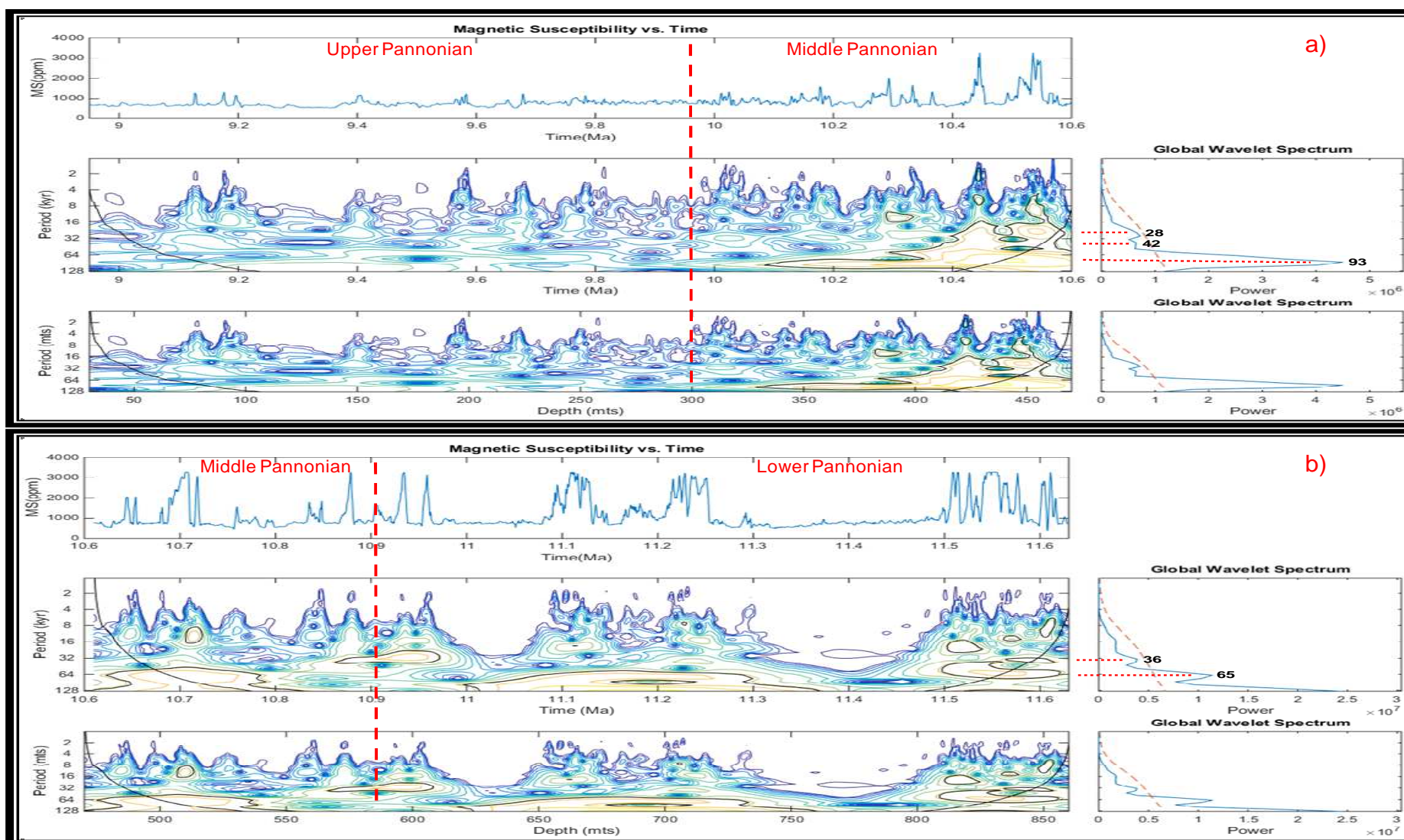


Figure 28: Wavelet analysis contour maps and global wavelet spectra indicating the periodicities in each interval. Dashed orange line indicates the 95% confidence level. Both time and depth domains along the magnetic susceptibility response are shown. *a)* Upper and Middle Pannonian; *b)* Middle and Lower Pannonian. Modified MATLAB code from (Torrence and Compo, 1997)

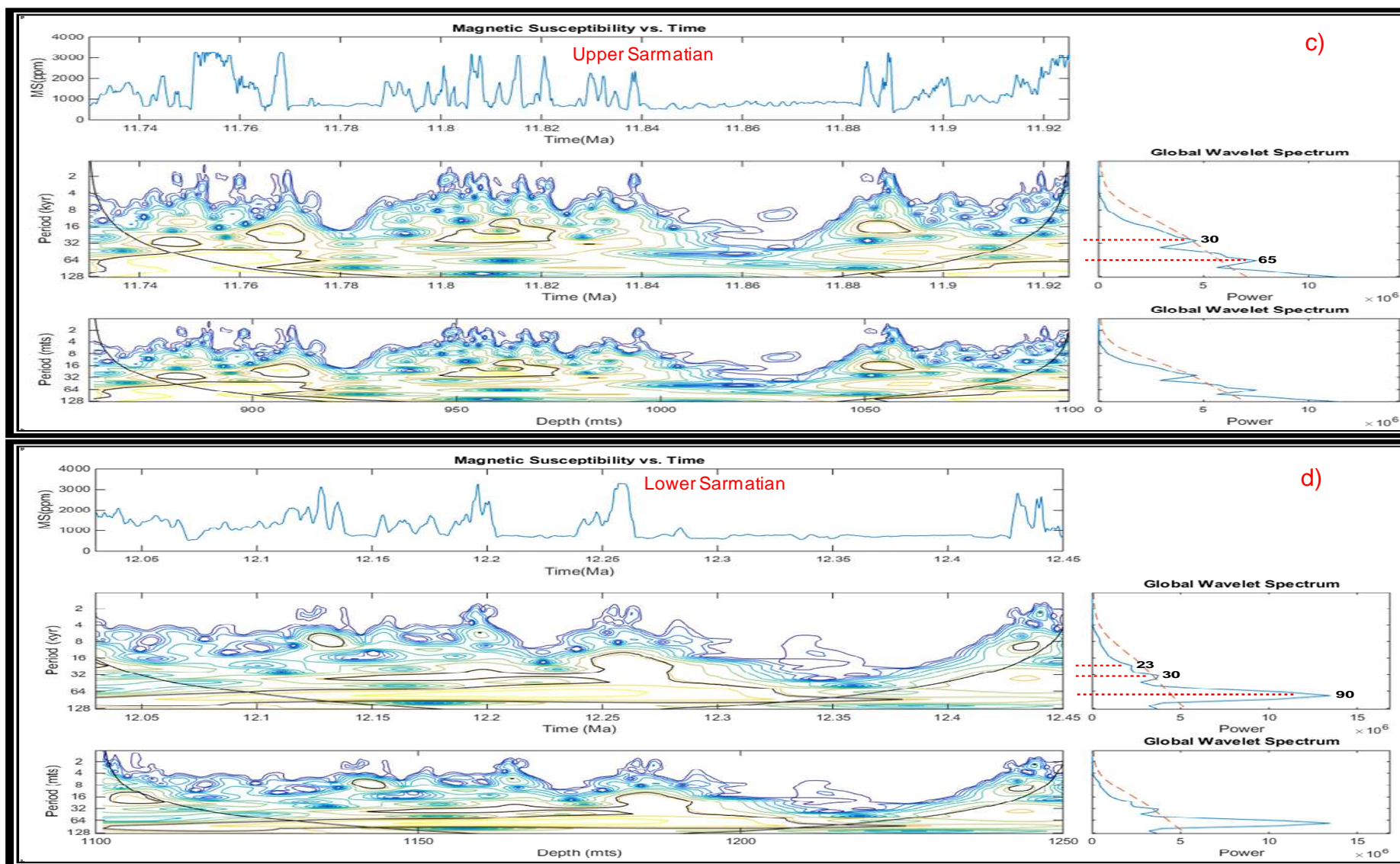


Figure 29: Wavelet analysis contour maps and global wavelet spectra indicating the periodicities in each interval. Dashed orange line indicates the 95% confidence level. Both time and depth domains along the magnetic susceptibility response are shown. c) Upper Sarmatian; d) Lower Sarmatian. Modified MATLAB code from (Torrence and Compo, 1997)

DISCUSSION OF RESULTS

ORIGIN OF THE MAGNETIC SUSCEPTIBILITY SIGNAL

Our data indicate that there is clearly a correlative relationship of the MS signal with the detrital content and an inverse relationship with the carbonate content (Figure 30).

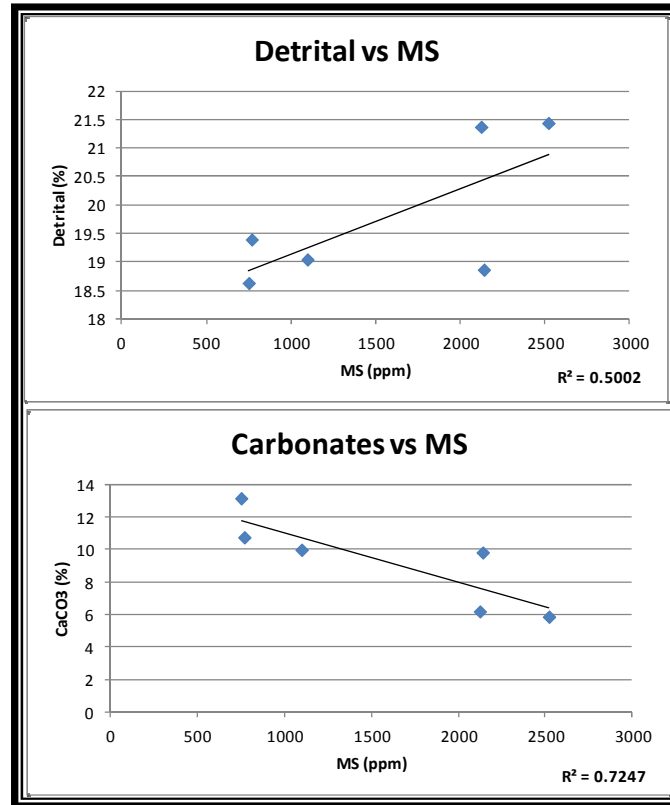


Figure 30: *Top* plot indicates the direct relationship between MS and detrital input. Detrital data are obtained from the XRF analysis. *Bottom* plot indicates the inverse relationship between MS and carbonate content. Data are also obtained from XRF.

In Figure 31 the Ti content is used as a terrigenous proxy, while Ca is used as a marine proxy. The aforementioned relationship between MS and carbonate/detrital input can be clearly observed on these plots. Additionally, the marine-terrestrial ratio represented by these elements is also shown. This ratio strongly correlates with lithology and thereby also with carbonate content. In other words, these plots provide information on when the carbonate production slowed down because of detrital input caused by the sea level change at the Badenian-Sarmatian boundary. These plots are based on the XRF data of the six samples analyzed.

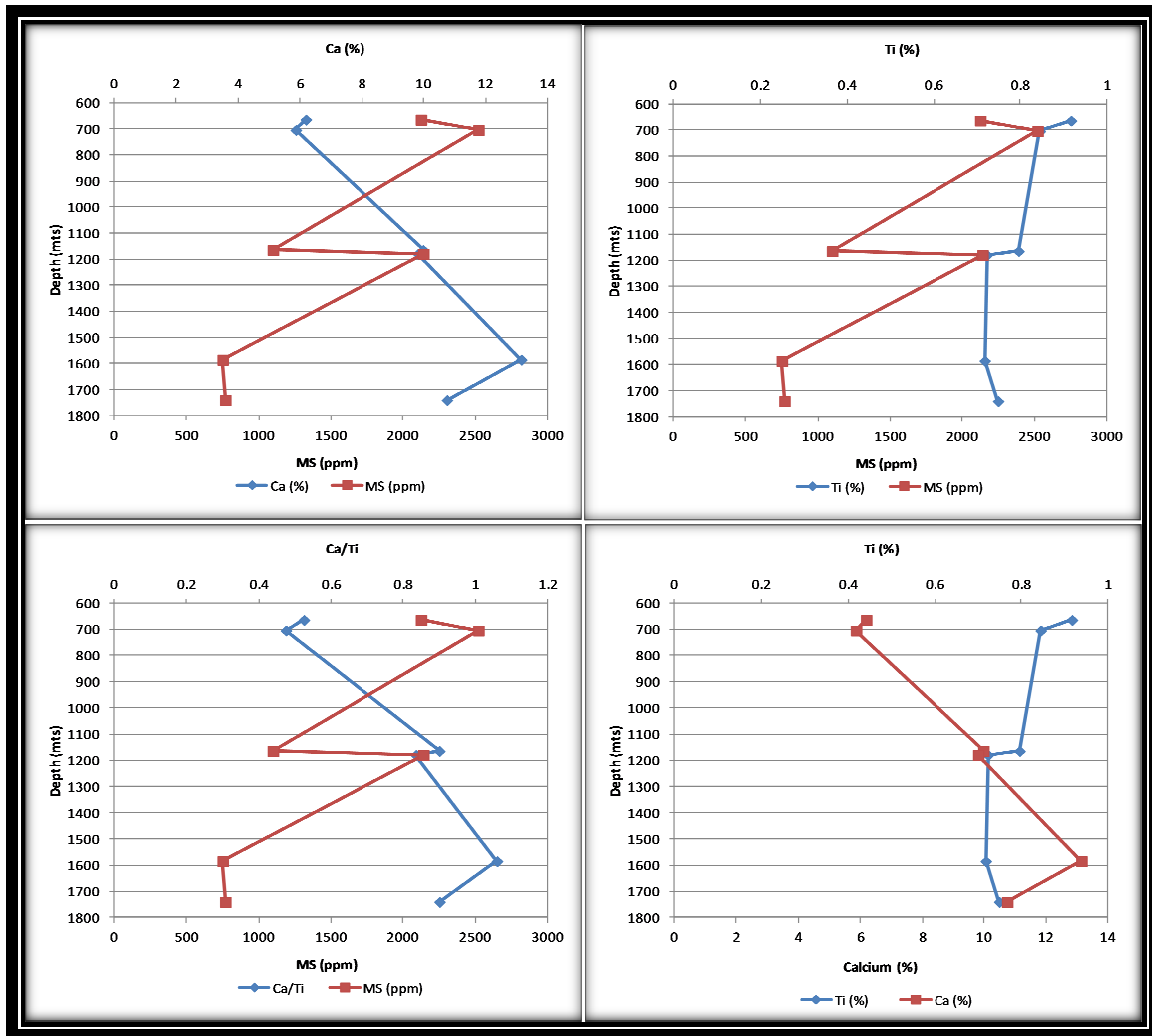


Figure 31: *Top left* shows carbonate content and MS response. *Top right* shows titanium content and MS response. *Bottom left* indicates marine -terrestrial ratio (Ca/Ti) and MS response vs. depth. *Bottom right* shows titanium vs. calcium vs. depth. This helps to visualize the relationship between high/low MS values and the calcium/terrigenous content.

The information obtained from the plots above along with the relationship established between MS and detrital/carbonate content, serves as evidence for the high MS values found in the Pannonian and the Sarmatian, showing the highest contents of terrigenous elements. Similarly, it shows how MS decreases in the Badenian as the carbonate content rises. In general terms, the highest concentration of magnetic minerals matches the highest amounts of Fe, Ti and Al, while the lowest concentrations in these elements coincide with zones of reduced magnetic minerals.

Ca/Ti and Ca/Al essentially represent carbonate productivity over terrigenous input. The analysis of the elemental ratios indicate that the Pannonian and Sarmatian were more susceptible to siliciclastic sediments, whereas the Badenian was more susceptible to carbonates, confirming the ideas of Piller (1999). According to a chemical weathering indicator, mobile elements (Na, Ca) dominate the geochemistry of the sediments in the bottom part of the well represented by the last two samples. This correlates with the decrease of the magnetic susceptibility profile observed on the logging data.

DEPOSITIONAL ENVIRONMENTS

It is important to recall that the Pannonian interval corresponds to a delta front and pro delta environment with some distributary channels. The Sarmatian is similar to the Pannonian environment and the Badenian is characterized by the presence of mouth bars and distributary channels with some delta front areas (Paulissen, 2011). Besides the high influence of clays, the peak of the carbonate production is reached only during the Badenian (Piller et al., 2007). The target of the Spannberg-21 well was the 15THZ2 basin floor fan deposited during the middle Badenian.

The XRD results indicate that the Pannonian sediments look more immature than the Badenian deposits. This, at least, in terms of the composition. The Pannonian and the Sarmatian are more compositionally diverse than the Badenian (Figure 27). Therefore, effectively the Badenian sediments are interpreted to correspond to a more distal environment than both the Pannonian and the Sarmatian. The presence of mostly quartz (hard mineral) and less muscovite (soft mineral) in the Badenian supports this idea. The opposite trend is found in the Pannonian and the Sarmatian.

The high magnetic susceptibility are found in the coarser sediments located in the Pannonian (Middle and Lower) and the Sarmatian, and the lowest values in the Badenian. Figure 32 shows the MS trends for the Sarmatian (right) and the Pannonian (left).

GRAIN SIZE

Koolen (2010) documented the presence of magnetosomal greigite in the Sarmatian and Pannonian intervals and authigenic greigite in the Badenian. He also mentions that the abundance and distribution of magnetotactic bacteria are dependent on organic matter, iron content, oxygen, and sulphide. These magnetosomal minerals are in the SD domain and they are very stable. However, these SD grains have magnetic susceptibilities that are significantly lower than those produced by SP or MD structures.

Authigenic greigite, a precursor of pyrite, is formed under anoxic conditions. Of the three stratigraphic units, this condition is probably best met in the Badenian marine sediments. In this case, organic matter and a high sedimentation rate may enable the sulfate reduction to stop before all FeS is converted into pyrite, as explained by Berner et. al. (1979). However, there is more greigite in the Sarmatian and the Middle/Lower Pannonian than in the Badenian. Koolen (2010) hypothesizes that the greigite in the Sarmatian and Pannonian has most likely a magnetosomal origin, while the one in Badenian is authigenic. Roberts and Turner (1993) mention that the low permeability caused by clays prevents the penetration of sulfate resulting in the consumption of the H₂S available before the full reaction to pyrite can occur. In the case of the Upper Pannonian, where more magnetite than greigite is observed, the fresh water conditions combined with the lower sedimentation rates may have prevented the formation of greigite.

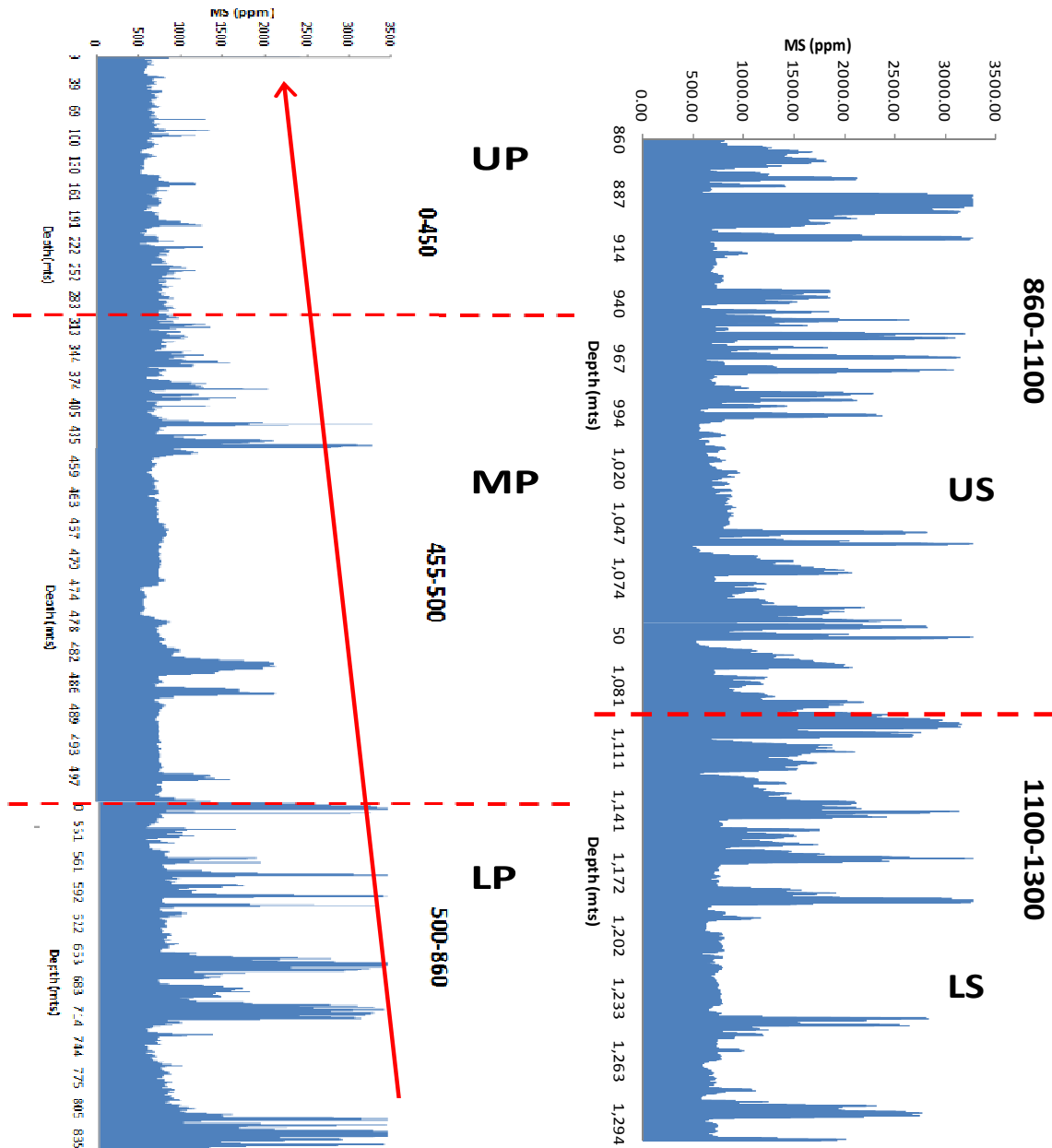


Figure 32: *Left*: MS vs. Depth along the Pannonian unit showing the decreasing trend of MS values towards the top. The trend is discussed in the text. *Right*: It is also a MS vs. Depth plot, but the MS values does not show any increase or decrease trend. UP stands for Upper Pannonian, MP Middle Pannonian, LP Lower Pannonian, US Upper Sarmatian, LS Lower Sarmatian.

One of the reasons why the magnetic susceptibility in the Lower/Middle Pannonian and the Sarmatian is significantly higher than in the Badenian although the magnetic minerals are mostly SD greigite, is because the effect produced by the concentration of magnetic minerals is much higher than the effect produced by grain size. Actually Clark (1997) has found that the microstructure and size of the grains does not greatly affect the susceptibility.

High ARM in case of magnetosomal minerals present are a good indicator of high interaction between the particles. On the other hand, the low values can be attributed to some authigenic greigite present. Also, the SIRM/MS ratio displays high values where smaller SD grains are present. The conclusion here is that the high MS signal in both Sarmatian and

Pannonian are attributed to the abundant SD magnetosomal greigite and some PSD-MD authigenic greigite. Still some detrital magnetite could be present.

It seems clear that the high MS intensity observed in the Pannonian and the Sarmatian is the combined effect of magnetite and greigite. However, the response cannot be attributed to any of the two magnetic minerals present. On the other hand, the low response in the Badenian is most likely generated solely by authigenic greigite. Hence, one could postulate that high MS values are proportional to magnetite presence, whereas greigite presence is not a direct indicator of high MS. The response in the Badenian allowed to make this distinction because greigite should give high values as well, but apparently it suffered abrupt geochemical changes after deposition causing a reduction of its magnetic intensity.

IRON EFFECT

By combining the results into the categories mentioned in the XRF analysis, it was possible to highlight some important aspects. The iron content itself is obviously important, but its abundance is not proportional to the MS response observed. Even in zones with low iron content, greigite still occurs and the MS is very low. The Sarmatian and Pannonian intervals, with the highest MS readings recorded, have on average very similar iron content as the Badenian which has the lowest MS signal. However, the Pannonian and Sarmatian show much more greigite than magnetite. The behavior of the curve confirms that the ferromagnetic minerals present are not the same (magnetite and greigite).

The small amounts of pyrite found in the samples occurred always together with greigite. This is an indication that the pyritization process took place, but most likely due to an iron shortage, the process was interrupted and the intermediate product greigite dominated the content. Pyrite is not able to carry any remanent magnetization, and therefore was not further investigated here.

Figure 33 shows the XRF results with a conspicuous pattern namely that at low ferromagnetic contents a high feldspars/clay content is observed and vice versa. Moreover, there is a slight decreasing trend of ferromagnetic minerals with depth. This trend initially makes sense in the Pannonian and the Badenian, but not in the Sarmatian (in terms of MS vs. ferromagnetic minerals).

As for the necessary iron for the greigite formation, the relative high presence of smectite in the top two intervals and its low presence in the Badenian might be the answer. In this case, the illitization of smectite occurring at shallow depths and lower temperatures liberates the required iron for the formation of greigite. The iron content together with the high sedimentation rate suggests that not only magnetosomal greigite is present in the Pannonian and the Sarmatian, but also some authigenic greigite is formed here as well. The insufficiently dissolved sulfate could have avoided a more significant formation of these minerals. This option cannot be ruled out. In general, the same greigite abundance is observed either at low or high iron content percentage. Nevertheless, and as shown in Table 8, the iron content in the Pannonian and the Sarmatian is slightly higher than in the Badenian

and this helps in explaining the greigite dominance in these units. During the Badenian, the amount of iron was not enough for completing the pyrite formation, resulting in authigenic greigite.

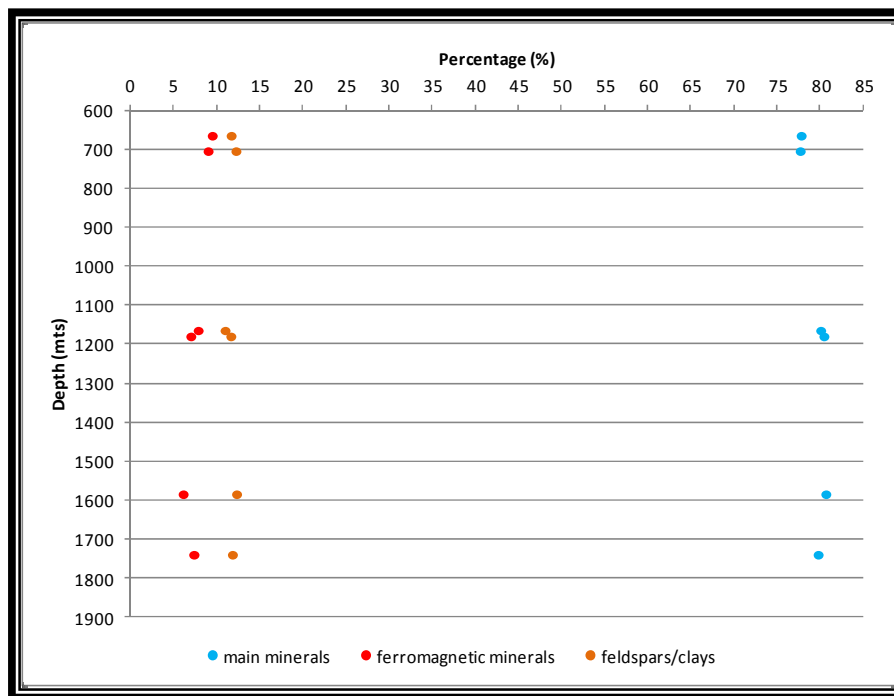


Figure 33: A plot of three mineral groups versus depth, based on the XRF results.

BADENIAN LOW RESPONSE

The Badenian has so far been interpreted to be dominated by authigenic greigite formed in the pyritization process. However, the reason for the low magnetic content and the low response in this interval remains unclear. It is unlikely that the MS can be explained by the effect of one single factor/process, and it is more likely to be a combination of several factors, many of them very complex, some still unclear and the combined effect produces what is on the log. In this particular question, the situation can be explained either by changes in the provenance of the sediments, or by a decrease in detrital magnetic minerals input, or even by post-depositional processes acting on the sediments. This is explain as follows:

PROVENANCE OF THE SEDIMENTS

Some elements such as Na, Ca, K, and Sr are very mobile and are easily removed from parent rocks. Among the common terrigenous elements found in the XRF results, Si, Fe, and K are not necessarily good indicators of terrigenous influences. By contrast, Al and Ti are very resistant to weathering or diagenetic processes and are well conserved elements. For this, they are generally used to estimate the abundance of terrigenous materials in sedimentary sequences. Wei et. al. (2006) found that Ti is the best proxy for terrestrial materials. Figure 34 shows correlations of these two elements and their positive relationship indicates that there was not a big change in the provenance of sediments. Additionally, Rb and Fe are also shown and they are also seen to correlate with these elements and thus could be seen as additional terrigenous input indicators. On the other hand, Ca often represents the carbonate fraction of the sediment.

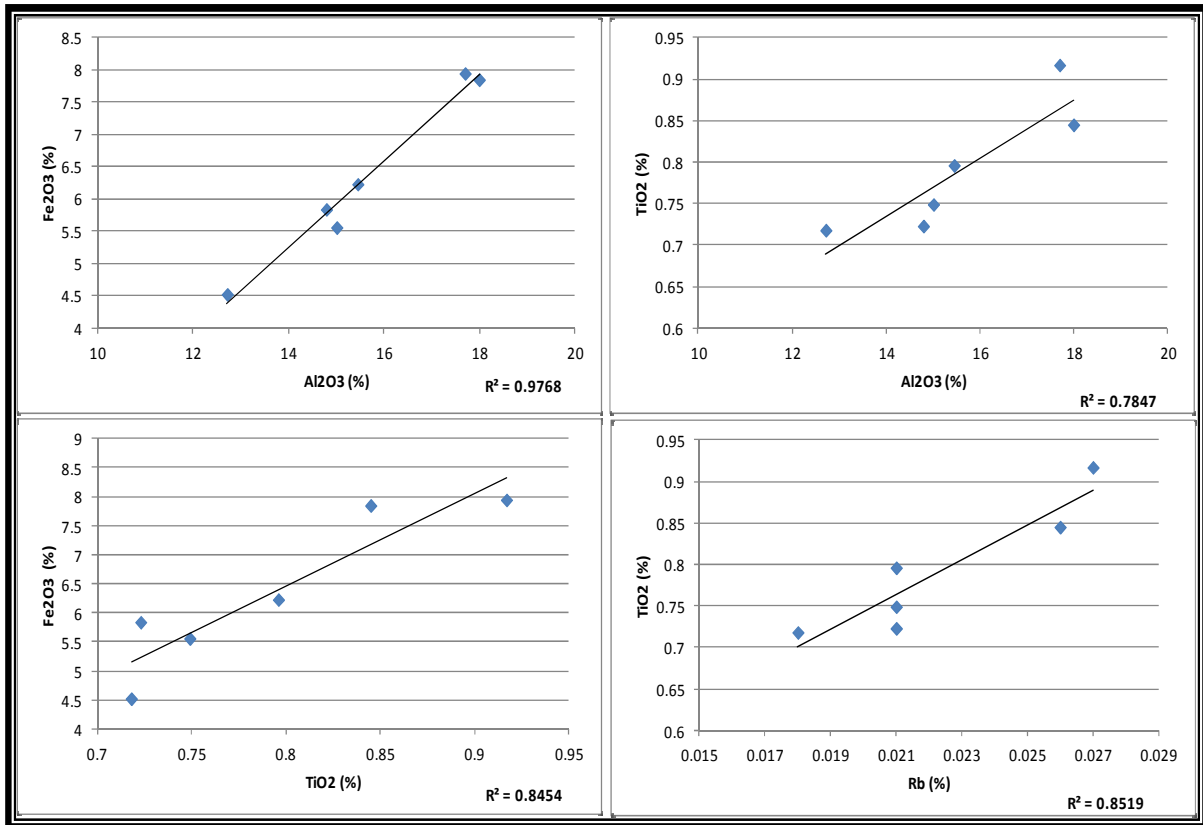


Figure 34: Detrital elements correlation.

DETRITAL INPUT

During Badenian times, where the conditions were more suitable for carbonate deposition, the terrestrial input was still quite high. This indicates that the only possible explanation for the low MS response in the Badenian lies on the post depositional processes that acted on the sediments (dissolution).

DISSOLUTION

There is some evidence for significant dissolution in the study area: 1) the magnetic susceptibility values in the low readings zones are as low as typical diamagnetic / paramagnetic values, which suggests that most magnetite and greigite particles have been removed or reduced in size. 2) Low magnetic units were deposited under anoxic conditions, either marine or with high sedimentation rates, characterized by high organic carbon contents. 3) Pyrite has been identified in some samples with low MS zones but was not detected in high MS zones.

If there was significant dissolution in the Badenian, the first grains that disappear were probably SD and SP. If the process continued, PSD and finally MD disappeared as well. If mostly authigenic greigite is present with particles in the PSD-MD range, then the dissolution effectively was strong, reducing the concentration of the magnetic minerals and thus producing a decrease in its MS signal. This is shown with the positive relationship in the ARM vs. MS plot and also the low ARM (indicating fining of grains) (Figure 35, right) (Koolen, 2010). The low ARM response is also caused by the absence of magnetic minerals.

Figure 35 (left) shows that exactly at the start of the Badenian, there is an increase in the ARM/MS ratio indicating fine magnetic grains coinciding with the decrease of the MS readings. Further evidence of this loss can be seen by normalizing the ARM (sensitive to grain size and concentration) to SIRM (sensitive to concentration), to get a parameter sensitive to grain size.

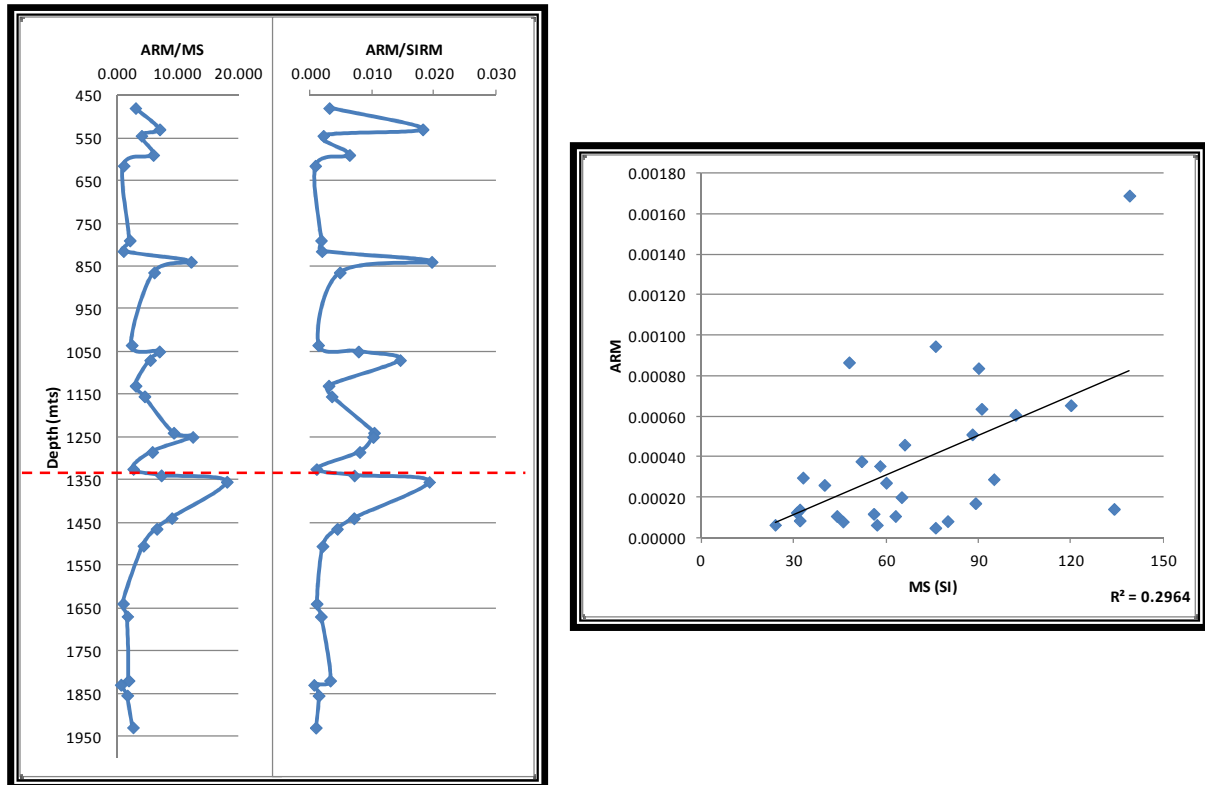


Figure 35: *Left* plot (modified from Koolen, 2010) shows ARM/MS and ARM/SIRM vs. depth. Red dashed line marks the start of the Badenian. *Right* plot shows MS vs. ARM with a positive correlation coefficient indicating a change of the magnetic grains with depth. ARM and SIRM show a clear indicative of the low concentration of magnetic minerals in the Badenian. Plots generated using the data acquired by Koolen (2010). ARM/SIRM is expressed in A/mts. MS is expressed in $\cdot 10^{-6}$ SI.

Organic matter and the sedimentation rate are the key elements for the dissolution process. The Badenian sediments had the conditions for this to happen with high sedimentations rates and high organic input, causing the progressive dissolution and/or transformation of the magnetic minerals into greigite. Even in some cases the formation of magnetite is interrupted in these conditions.

Since dissolution has been proposed here as a major factor for the magnetic susceptibility response in the Badenian, the geochemistry of the sediments linked to chemical weathering is also studied. It is important to point out that the chemical weathering mentioned here is referred to the sediments during and after deposition. It can be seen as either a diagenetic or a paleoclimate indicator.

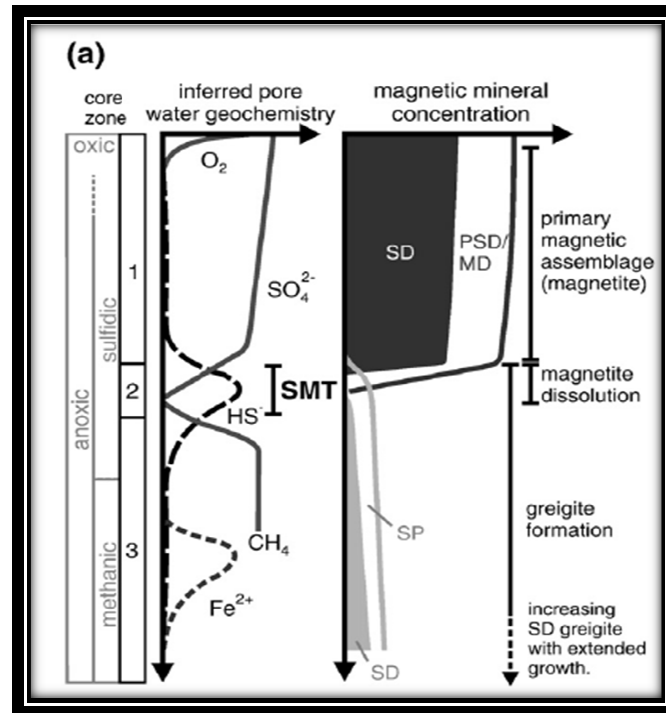


Figure 36: Simplified model illustrating the progressive dissolution of SD and PSD magnetite (dark/grey area/line) and the formation of SP/SD greigite (light grey line/area), followed by the delay before greigite grows to SD size and to a continuous greigite growth in zone 3. SMT = sulfate-methane transition. Modified from (Rowan et al., 2009).

ELEMENTAL RATIOS ANALYSIS

Elemental ratios are more useful than single elements because they are typically insensitive to dilution effects (Govin et al., 2012). Among existing ratios, calcium/titanium (Ca/Ti), titanium/aluminum (Ti/Al), calcium/iron (Ca/Fe), aluminum/silicon (Al/Si) and calcium/aluminum (Ca/Al) are the most commonly used for paleoclimate and source studies. Elements with different mobilities are differentiated during chemical weathering, and the degree of chemical differentiation is determined by the intensity of chemical weathering. Element ratios of detrital materials such as Al/Ti, Al/K, Al/Na, Ca/Ti, K/Ti, Na/Ti, Ca/Fe, Rb/Sr and, Si/K in mixed carbonate and detrital sediments have been used here to decipher this intensity. Additionally, Ti/Al, Mg/Al, Si/Al, and Rb/Al for mixed carbonate and detrital sediments also have been used to trace the intensity of chemical changes.

In Figure 37, the top left plot shows the increase of calcium with depth. Similarly, the Ca/Ti and Ca/Fe ratios also indicate an increasing trend with depth. Therefore, titanium is decreasing with depth. Figure 38 shows how the increasing Ca/Fe ratio with depth matches with the decreasing MS signal. These results demonstrate that the MS readings are proportional to the amount of terrigenous input and inversely proportional to the carbonate content.

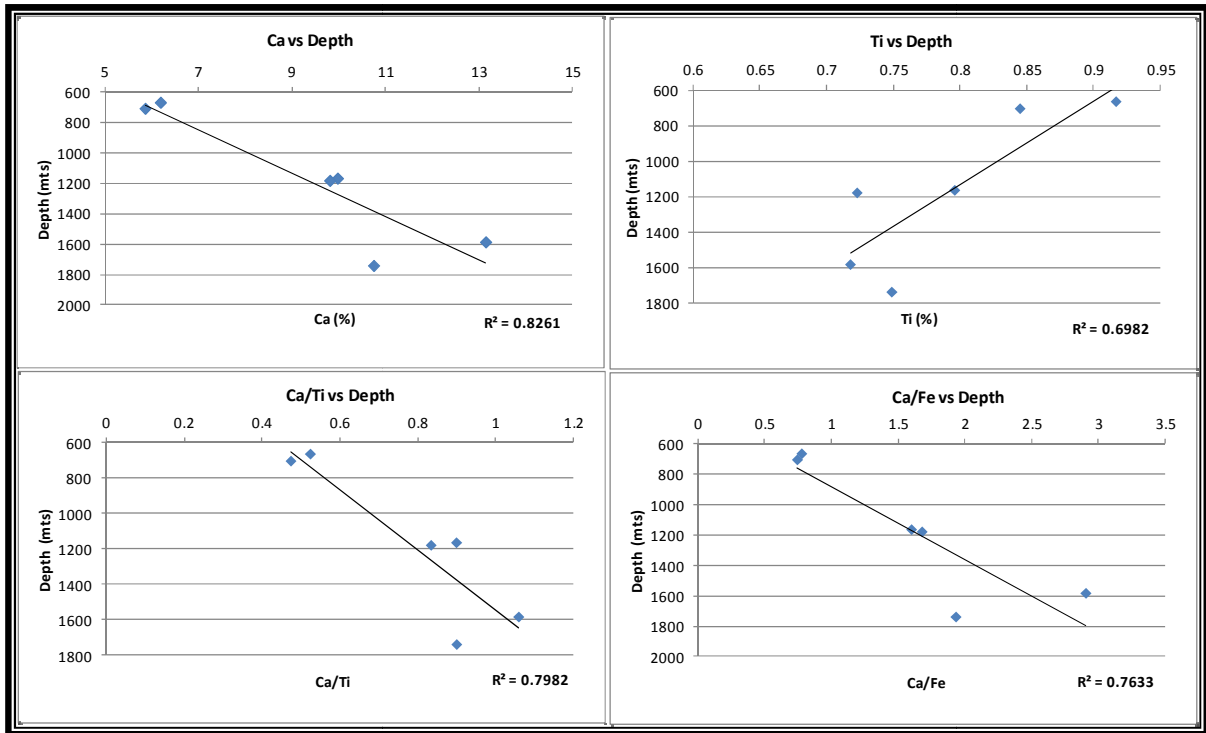


Figure 37: Marine and terrestrial elements vs. depth.

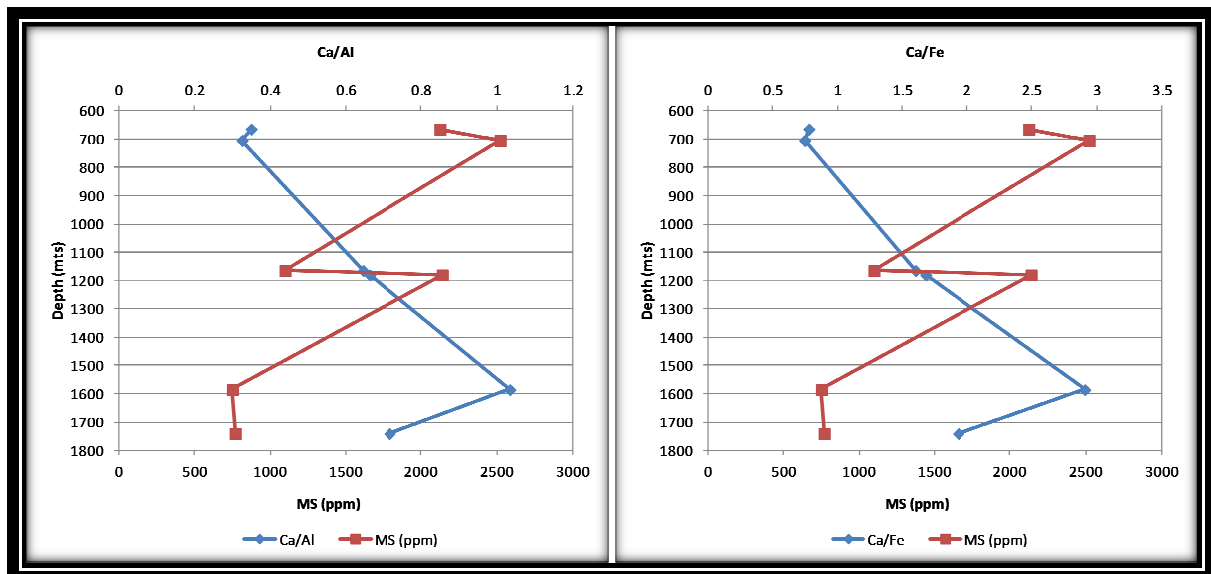


Figure 38: Marine-Terrigenous ratio of the proxies Ca/Al and Ca/Fe. Both curves cross each other roughly at Badenian onset (1200-1300 mts) where the influx of sediments is reduced and the carbonates control the lithology.

An increase of the chemical weathering may result in higher Al/Ti and Al/Na ratios. Actually the general trend seems to indicate that chemical weathering is decreasing with depth as shown by Figure 39.

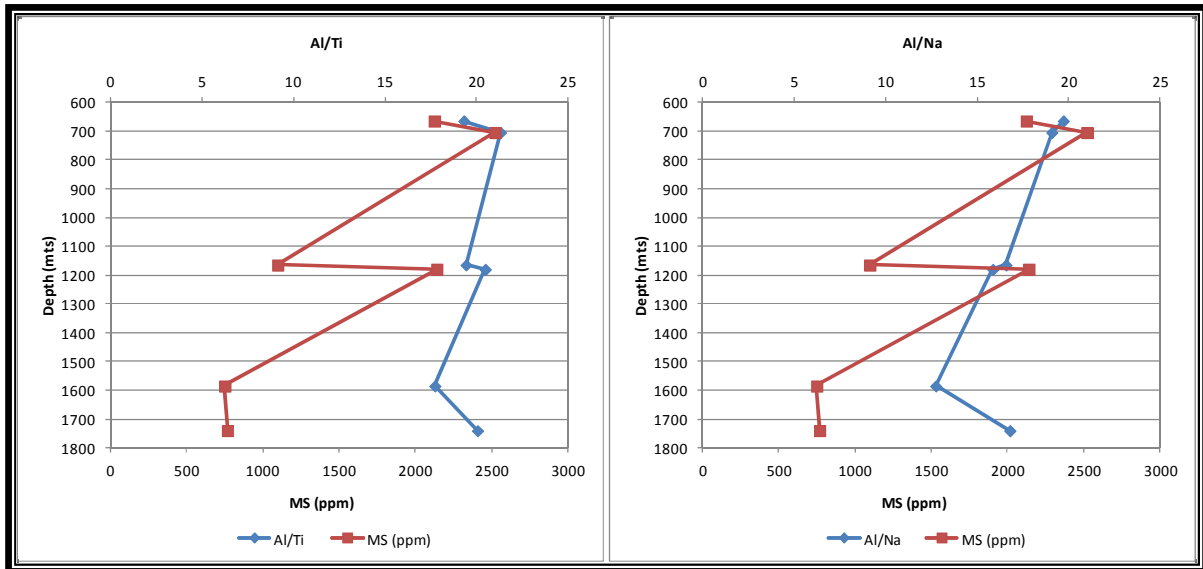


Figure 39: Al/Ti ratio and Al/Na ratio indicating high chemical changes in the top and decreasing with depth.

Ca/Ti, Na/Ti, Ti/Al, Mg/Al, and Si/Al ratios show increasing trends with depth accompanied with a decreasing trend of Al/Na, Al/K, Al/Ti (Figures 40 and 41). Even Rb/Sr and Al/Ca shows the highest values for the top samples, suggesting a higher degree of weathering. All this seems to suggest a decrease of chemical weathering intensity with depth. The Chemical Index of Alteration (CIA) was also calculated here and the values present in both Sarmatian and Pannonian sediments reflect that these units were subjected to strong chemical weathering. The CIA values of the sediments range from 38.7 to 56.3. This and the rest of the elemental plots can be found in Appendix G.

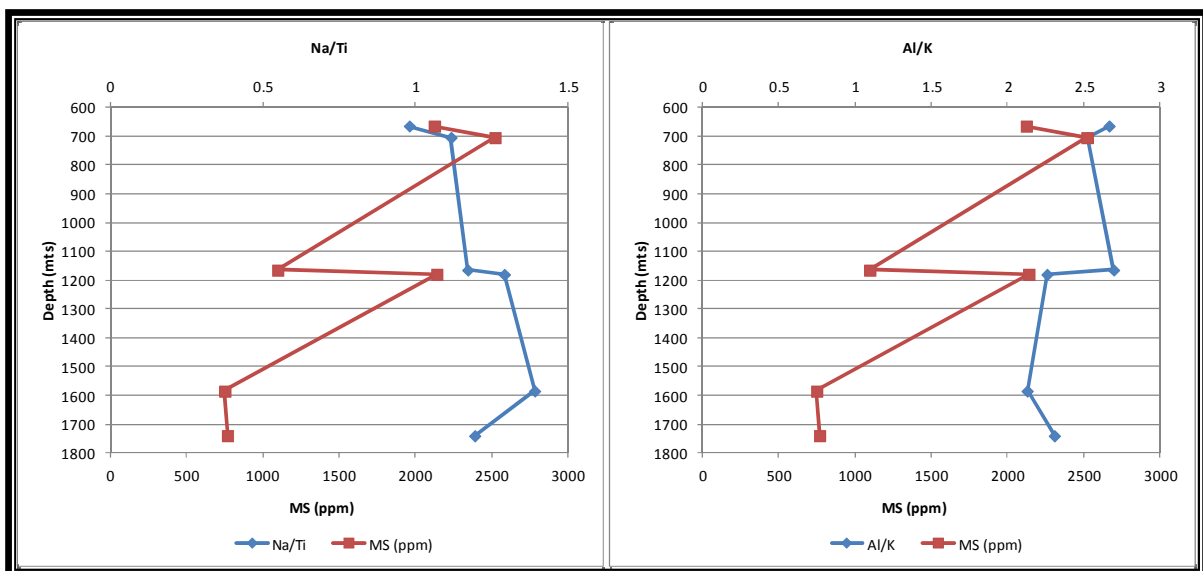


Figure 40: Na/Ti ratio and Al/K ratio calculated indicating chemical weathering strength. Below 1300 mts (Badenian) the intensity decreases.

An increase in Si/Al and Si/K may be related to an enhanced input of quartz, which in turn may be due to a higher transport energy. In agreement with this, the higher values of Si/Al and Si/K observed in the bottom interval may be explained as consequence of this. This is observed in the XRD results that show predominantly quartz for the distal sediments (the

Badenian) whereas less quartz and other phases are found in proximal sediments interpreted as the Sarmatian and Pannonian.

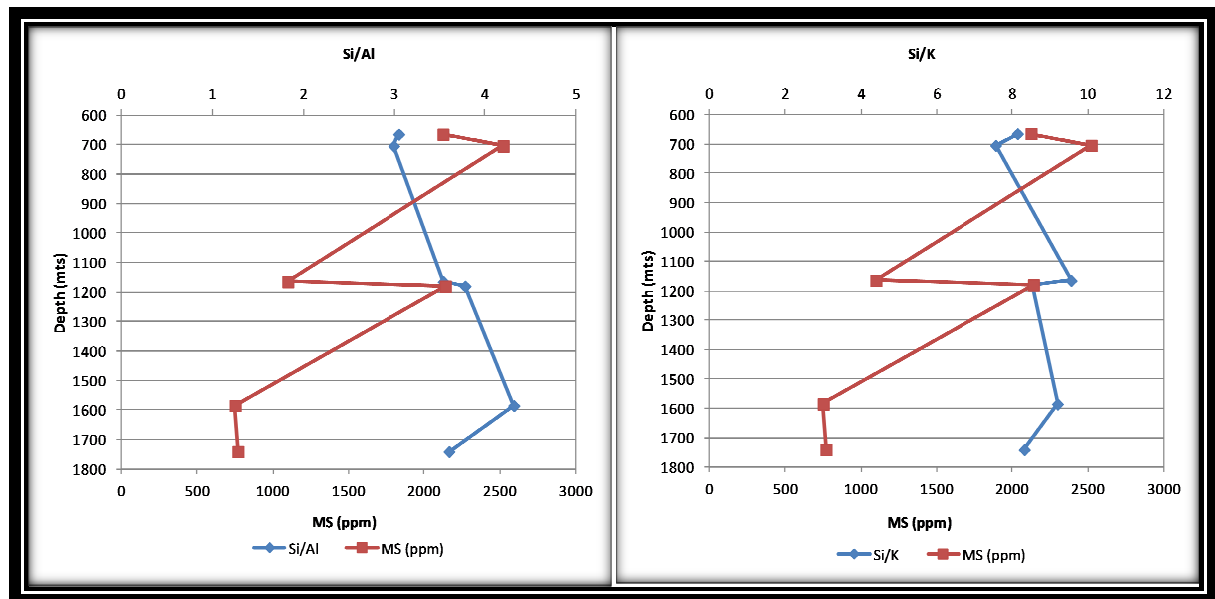


Figure 41: The Si/Al and Si/K ratios can be useful proxies for the energy associated with sediment transport.

To sum up, the combination of the effect caused by the depositional environment, the detrital/carbonate influence, the increasing trend with depth of diamagnetic minerals, the decreasing trend with depth as well of paramagnetic/ferromagnetic minerals, the high concentration of magnetic minerals in the top two units, and the dissolution/dilution effect seem to explain the behavior of the magnetic susceptibility signal recorded.

WAVELET ANALYSIS

Sedimentary cycles are caused either by eustatic sea level changes or tectonic events. In this case, the 95 kyr cycle may be linked to the global sea level drop that occurred at the Badenian-Sarmatian boundary and to orbital forces. However, from the Middle to Upper Miocene, the sedimentation was governed by combination of pull-apart tectonics and multiple sea-level changes associated with them. Therefore, the smaller cycle of 65 kyr is very likely to have a tectonic origin and does not record an orbital influence.

Two types of lithological cycles were predominant in the Vienna Basin and even in the other basins in the vicinity. The first type is characterized by siliciclastics cyclicity, while the second one is predominated by carbonate-clay cycles. Due to the different sedimentary regimes, strong differences in the expression of periodicities are shown in the lithological cycles. Van Vugt et al. (2001) concluded that carbonate-dominated basins are susceptible to precession whereas siliciclastic basins are more sensitive to eccentricity. In our analysis no carbonates sections were considered (Badenian) and that could be a reason why no precession cycles were identified.

The presence of these multiple sand/clay cycles is very typical in the Sarmatian-Pannonian sedimentary record in the Vienna Basin. These major trends in the sedimentary fill

observed on the well logs indicate changes caused by orbital forces based on the results shown in the wavelet analysis. The smaller periodicities observed are generally difficult to define accurately in this type of environments (shallow marine) because the record is often discontinuous. The discontinuity of the cycles in the Sarmatian is originated by the multiple sea level changes caused in turn by the tectonic events that took place during this time. For this reason, and considering the zonal classification defined by (Paulissen, 2011), it was convenient to divide this interval into two. This division allows us to notice the discontinuity in the cycles very clearly. On the other hand, since this typical sedimentary pattern is not only present in the Vienna Basin, but in the Styrian and Transylvanian Basin as well as pointed out by Harzhauser et al. (2004), the changes of depositional environments can be correlated throughout the whole Paratethys zone. All this indicates that effectively some of the cycles are not caused only by local tectonic movements, but by major oscillations in the relative sea level in the whole area.

Chapter 6:

CONCLUSIONS

CONCLUSIONS

Significant changes in magnetic properties are observed above and below the Badenian-Sarmatian boundary. This major event definitively marked the end of one cycle and the onset of a very different one, and it had probably created different conditions suitable for the formation and/or preservation of magnetic minerals. Therefore, magnetic susceptibility can be seen as a powerful but complicated proxy for interpreting changes in climate and depositional environments.

Authigenic greigite is considered the main precursor of pyrite and its formation is related to the shortage of either iron minerals, dissolved sulphate or organic matter during the pyritization process. The high sedimentation rate was the main factor capable of generating the anoxic conditions needed for greigite formation in the Sarmatian and Badenian. The dissolution of the detrital magnetite in the Badenian seems to be the best explanation for the negligible MS response observed in that unit. The results show that magnetic susceptibility is dominated and controlled by the mineral magnetite and therefore, it is the main magnetic carrier.

It is concluded during this study that the magnetic susceptibility property cannot be explained by the single effect of one process. In fact, multiple processes at different times are responsible for the evolution of this signal. The combination of these processes during deposition and post-deposition produces remarkable changes in the magnetic properties of the sediments.

This thesis offers a compilation of data on the relationship between magnetic susceptibility (MS), environmental parameters (proximal-distal, mineralogy, grain size distribution, sedimentation rates) and depositional environments (shallow marine and terrigenous) during different Miocene stages. In general, the magnetic susceptibility signal depends on the presence of ferromagnetic minerals. However, the susceptibility response observed in the Badenian seems to be carried not by ferromagnets but by diamagnets. The susceptibility in the top units is determined by both the presence of magnetic minerals and the abundance of terrigenous Fe-rich clays.

The excellent negative correlation between magnetic susceptibility and carbonate content verifies that the susceptibility signal reflects the concentration of the non-carbonate fraction.

Since the MS is related mostly to lithogenic inputs, the decreasing trend of values with distance observed in the three units is confirmed with the semiquantitative analysis results. According to these results, the Badenian sediments were deposited far from the source or at a higher relative sea level. Moreover, this interval is affected strongly by carbonate production that prevented the deposition of magnetic minerals.

Another major factor has to do with eustatic sea level changes because it controls the detrital influx, influencing therefore the magnetic susceptibility behavior. This is what it is observed in the Sarmatian and Pannonian after the respective sea level drops.

The reduced detrital input documented in the Badenian does not look strong enough to be the only responsible agent for the low MS response. Here we propose a prolonged dissolution affecting all magnetic mineral domains leaving the MS response to be solely produced by diamagnetic minerals as supported by the semiquantitative analysis results.

In terms of cyclostratigraphy, one can conclude primarily by saying that the combination of a fully environmentally controlled property such as magnetic susceptibility with the analysis of sedimentary cycles, which also reflects changes in environmental conditions, represent a powerful method for reconstructing climate conditions.

The wavelet analysis provided evidence that not only Milankovitch cycles are present in the Sarmatian and Pannonian. Definitively orbital forces affected the central part of the Vienna Basin during the Miocene and these forces are related to the sedimentary 93 kyr cycle observed. The short eccentricity cycle of 95 kyr is related to the major sea level fall which occurred at both Sarmatian-Pannonian and Badenian-Sarmatian boundaries. It looks continuous throughout the record and it is represented by a strong peak in the power spectra. There are, however, other prominent cycles present having a more discontinuous behavior easily observed during Sarmatian. The 65 kyr cycle is very strong, but represents more of a tectonically originated cycle than a eustatic cycle.

The data quality and quantity was definitively a positive feature of the magnetic susceptibility signal. The unconformities did not play any role in the interpretation of the results as they could be eliminated by the integrated study of Paulissen et al. (2011). This accuracy of the sedimentation rates was also important for guaranteeing the quality of the results. The prominent cycle of 95 kyr is observed mostly in shaly environments, hence the record seems to be reliable. The presence of the cycles and their distribution are consistent with the fact that sea level fluctuations and tectonic events occurred at these times.

Chapter 7:

RECOMMENDATIONS

RECOMMENDATIONS

The idea of this chapter is to mention some points that can be helpful in the understanding of some ideas still unclear after this work. The purpose is to propose further studies if more knowledge is desired about magnetic susceptibility in order to be able to minimize doubts as expressed in this thesis.

The recommendations are as follows:

- ❖ Thin sections would be useful for samples in the Pannonian, Sarmatian, and especially Badenian for confirming the theory about dissolution, but also to verify the magnetic grain size of the magnetosomal greigite present in the top two units. Looking for SP domains would be also interesting.

- ❖ The low MS values in the Badenian characterized mainly by greigite, which is supposed to have also high readings, represent an interesting problem. For this reason, DTA or TGA experiments are proposed to see if the peaks there also show greigite.

- ❖ SEM analysis might be helpful for a more convincing identification of the magnetic minerals present.

- ❖ Despite an improving understanding of magnetic susceptibility and the effect that diagenesis has on this property, a better identification and even quantification of this effect should remain a priority for future research.

BIBLIOGRAPHY

REFERENCES

- Ahrens, T.J.** (1995). *Rock Physics and Phase Relations. A Handbook of Physical Constants.* Washington D.C.: AGU Books Board.
- Ali Imhmed, S.** (2012). Thesis: Application of magnetic susceptibility measurements to oilfield scale management. Edinburgh, Scotland.
- Ao, H., Deng, C., Dekkers, M., and Liu, Q.** (2010). Magnetic mineral dissolution in Pleistocene fluvio-lacustrine sediments, Nihewan Basin (North China). *Earth and Planetary Science Letters*, vol. 292, p. 191-200.
- Babek, O., Kalvoda, J., Aretz, M., Cossey, P., Devuyst, F., and Gerbig, H.** (2010). The correlation potential of magnetic susceptibility and outcrop gamma-ray logs at Tournaisian-Viséan boundary sections in western Europe. *Geologica Belgica*, vol. 13 (4), p. 291-308.
- Baldi, K.** (2006). Paleooceanography and climate of the Badenian (Middle Miocene, 16.4–13.0 Ma) in the Central Paratethys based on foraminifera and stable isotope ($\delta^{18}O$ and $\delta^{13}C$) evidence. *Int. Journal Earth Sci (Geol Rundsch)*, vol. 95, p. 119-142.
- Baldi, K., Benkovics, L., and Sztano, O.** (2002). Badenian (Middle Miocene) basin development in SW Hungary: subsidence history based on quantitative paleobathymetry of foraminifera. *Int. Journal Earth Sci (Geol Rundsch)*, vol. 91, p. 490-504.
- Balla Ondo, A., Ngos III, S., Ndjeng, E., Abolo, A., and N’Nanga, A.** (2014). Contribution of the Magnetic Susceptibility to the Characterization of the Babouri-Figuil Cretaceous Basin. *Open Journal of Soil Science. Published Online August 2014 in SciRes.* <http://www.scirp.org/journal/ojss>, vol. 4, p. 272-283.
- Berner, R.** (1981). A new geochemical classification of sedimentary environments. *Journal of sedimentary petrology*, vol. 51 (2), p. 359-365.
- Berner, R.** (1984). Sedimentary pyrite formation: An update. *Geochimica et Cosmochimica*, vol. 48, p. 605-615.
- Berner, R., Baldwin, T., Holdren, G. R.** (1979). Authigenic iron sulfides as paleosalinity indicators. *Journal of sedimentary petrology*, vol. 49 (4), p. 1345-1350.
- Blanchet, C., Thouveny, N., and Vidal, L.** (2009). Formation and preservation of greigite (Fe_3S_4) in sediments from the Santa Barbara Basin: Implications for paleoenvironmental changes during the past 35 ka. *PALEOCEANOGRAPHY*, vol. 24, p. 1-15.
- Booth, C., Walden, J., Neal, A., and Smith, J.** (2005). Use of mineral magnetic concentration data as a particle size proxy: a case study using marine, estuarine and fluvial sediments in the Carmarthen Bay Area, South Wales, U.K. *Sci. Total Environ*, vol. 347, p. 241-253.
- Brachfield, S., Barletta, F., St-Onge, G., Darby, D., and Ortiz, J.** (2009). Impact of diagenesis on the environmental magnetic record from a Holocene sedimentary sequence from the Chukchi–Alaskan margin, Arctic Ocean. *Global and Planetary Change*, vol. 68, p. 100-114.
- Canfield, D., and Berner, R.** (1987). Dissolution and pyritization of magnetite in anoxic marine sediments. *Geochimica et Cosmochimica Acta*, vol. 51, p. 645-659.

- Clark, D.** (1997). Magnetic petrophysics and magnetic petrology: aids to geological interpretation of magnetic surveys. *AGSO Journal of Australian Geology and Geophysics*, vol. 17 (2), p. 83-103.
- Crick, R.E., Ellwood, B., El Hassani, A., and Feist, R.** (2000). Proposed magnetostratigraphy susceptibility magnetostratotype for the Eifelian–Givetian GSSP (Anti-Atlas, Morocco). *Episodes*, vol. 23, no. 2, p. 93-101.
- da Silva, A. C., and Boulvain, F.** (2010). Magnetic susceptibility, correlations and Palaeozoic environments: foreword. *Geologica Belgica*, vol. 13 (4), p. 287-290.
- da Silva, A. C., Mabilie, C., and Boulvain, F.** (2009). Influence of sedimentary setting on the use of magnetic susceptibility: examples from the Devonian of Belgium. *Sedimentology*, vol. 56, p. 1292-1306.
- da Silva, A. C., Potma, K., Weissenberger, J., Whalen, M., Boulvain, F., and Mabilie, C.** (2009). Magnetic susceptibility evolution and sedimentary environments on carbonate platform sediments and atolls, comparison of the Frasnian from Belgium and Alberta, Canada. *Sedimentary Geology*, 214, p. 3-18.
- da Silva, A. C., Yans, J., and Boulvain, F.** (2010). Early-Middle Frasnian (Early Late Devonian) sedimentology and magnetic susceptibility of the Ardennes Area (Belgium): identification of severe and rapid sea level fluctuations. *Geologica Belgica*, vol. 13 (4), p. 319-332.
- de Leeuw, A., Bukowski, K., Krijgsman, W., and Kuiper, K.** (2010). Age of the Badenian salinity crisis; impact of Miocene climate variability on the circum-Mediterranean region. *Geology*, 38, 715-718.
- de Leeuw, A., Filipescu, S., Matenco, L., Krijgsman, W., Kuiper, K., and Stoica, M.** (2013). Paleomagnetic and chronostratigraphic constraints on the Middle to Late Miocene evolution of the Transylvanian Basin (Romania): Implications for Central Paratethys stratigraphy and emplacement of the Tisza–Dacia plate. *Global and Planetary Change*, vol. 103, p. 82-98.
- Dearing, J.** (1999). Environmental Magnetic Susceptibility. Using the Bartington MS2 System. British Library.
- Decker, K., Peresson, H., and Hirsch, R.** (2005). Active tectonics and quaternary basin formation along the Vienna Basin Transform Fault. *Quaternary Science Review* (24), p. 305-320.
- Dewangan, P., Basavaiah, N., Badesab, F., and Usapkar, A.** (2013). Diagenesis of magnetic minerals in a gas hydrate/cold seep environment off the Krishna–Godavari basin, Bay of Bengal. *Marine Geology*, vol. 340, p. 57-70.
- Dubuisson, G., Thibal, J., Barthes, V., Pocachard, J., and Pozzi, J.** (1995). Downhole magnetic logging in sediments during LEG 145: usefulness and magnetostratigraphic interpretation of the logs at site 884. *Proceedings of the Ocean Drilling Program, Scientific Results*, vol. 145.
- Dunoyer de Segonzac, G.** (1970). The transformation of clay minerals during diagenesis and low-grade metamorphism: A review. *Sedimentology*, vol. 15, p. 281-346.
- Eberl, D.** (2003). User's guide to RockJock: A program for determining quantitative mineralogy from powder X-ray diffraction data. Colorado: USGS.
- Ellwood, B.** (2008). Time series analysis of magnetic susceptibility variations in deep marine sedimentary rocks: A test using the upper Danian–Lower Selandian proposed GSSP, Spain. *Palaeogeography, Palaeoclimatology, Palaeoecology*.
- Ellwood, B.** (n.d.) Magnetic Susceptibility as an important tool in stratigraphy: instruments, methods, problem areas, previous work, cycles, applications. Department of Geology and Geophysics, Louisiana State University, USA.

- Ellwood, B., and Ledbetter, M.** (1977). Antarctic bottom water fluctuations in the Vema Channel: effects of velocity changes on particle alignment and size. *Earth and Planetary Science Letters*, vol. 35, p. 189-198.
- Ellwood, B., Balsam, W., and Roberts, H.** (2006). Gulf of Mexico sediment sources and sediment transport trends from magnetic susceptibility measurements of surface samples. *Marine Geology*, vol. 230, p. 237-248.
- Ellwood, B., Crick, R.E., El Hassani, A., Benoist, S.L., Young, R.H.** (2000). Magnetostratigraphy method applied to marine rocks: Detrital input versus carbonate productivity. *Geology*, vol. 28 (12), p. 1135-1138.
- Elmore, R., Muxworthy, A., Aldana, M., and Mena, M.** (2012). Remagnetization and chemical alteration of sedimentary rocks. *Geological Society Special Publication*, vol. 371, p. 25-53, 229-251.
- Fodor, L., Jelen, B., Marton, E., Rifelj, H., Kraljic, M., and Kevric, R.** (2002). Miocene to Quaternary deformation in NE Slovenia: complex paleomagnetic and structural study. *Journal of Geodynamics*, vol. 34 (5), p. 627-651.
- Fukuma, K.** (1998). Origin and applications of whole-core magnetic susceptibility of sediments and volcanic rocks from LEG152. *Proceedings of the Ocean Drilling Program, Scientific Results. Saunders, A.D., Larsen, H.C., and Wise, S.W., Jr. (Eds.)*, vol. 152, p. 271-280.
- Garming, J., Bleil, U., and Riedinger, N.** (2005). Alteration of magnetic mineralogy at the sulfate–methane transition: Analysis of sediments from the Argentine continental slope. *Physics of the Earth and Planetary Interiors*, vol. 151, p. 290-308.
- Gier, S., Worden, R., Johns, W., and Kurzweil, H.** (2008). Diagenesis and reservoir quality of Miocene sandstones in the Vienna Basin, Austria. *Marine and Petroleum Geology*, vol. 25, p. 681-695.
- Govin, A., Holzwarth, U., Heslop, D., Ford Keeling, L., Zabel, M., Mulitza, S., Collins, J.A., and Chiessi, C.M.** (2012). Distribution of major elements in Atlantic surface sediments (36°N–49°S): Imprint of terrigenous input and continental weathering, *Geochem. Geophys. Geosyst.*, 13, Q01013, doi:10.1029/2011GC003785.
- Hagstrum, J., Daniels, J., and Scott, J.** (1980). Analysis of the Magnetic Susceptibility Well Log in Drill Hole UE25a-5, Yucca Mountain, Nevada Test Site. USGS.
- Hagstrum, J., Daniels, J., and Scott, J.** (1980). Interpretation of Geophysical Well-Log Measurements in Drill Hole UE25a-1, Nevada Test Site, Radioactive Waste Program. Denver: USGS.
- Hamilton, W., Wagner, L., and Wessely, G.** (1999). Oil and Gas in Austria. *Mitt. Osterr. Geol. Ges.*, vol. 92, p. 235-262.
- Harzhauser, M., and Piller, W.** (2004). Integrated stratigraphy of the Sarmatian (Upper Middle Miocene) in the western Central Paratethys. *Stratigraphy*, vol. 1 (1), p. 65-86.
- Harzhauser, M., Daxner-Hock, G., and Piller, W.** (2004). An integrated stratigraphy of the Pannonian (Late Miocene) in the Vienna Basin. *Austrian Journal of Earth Sciences*, vol. 95/96, p. 6-19.
- Hatfield, R.** (2014). Particle Size-Specific Magnetic Measurements as a Tool for Enhancing Our Understanding of the Bulk Magnetic Properties of Sediments. *Minerals*, vol. 4, p. 758-787.
- Hinsch, R., Decker, K., and Wagneich, M.** (2005). 3-D mapping of segmented active faults in the southern Vienna Basin. *Quaternary Science Reviews*, vol. 24, p. 321-336.
- Hohenegger, J., Coric, S., and Wagneich, M.** (2014). Timing of the Middle Miocene Badenian Stage of the Central Paratethys. *Geological Carpathica*, vol. 65 (1), p. 55-66.
- Holzel, M., Decker, K., Zamolyi, A., Strauss, P., and Wagneich, M.** (2010). Lower Miocene structural evolution of the central Vienna Basin (Austria). *Marine and Petroleum Geology*, vol. 27, p. 666-681.

- Holzel, M., Wagreeich, M., Faber, R., and Strauss, P.** (2008). Regional subsidence analysis in the Vienna Basin (Austria). *Austrian Journal of Earth Sciences*, vol. 101, p. 88-98.
- Horg, C., and Chen, K.** (2006). Complicated Magnetic Mineral Assemblages in Marine Sediments Offshore of Southwestern Taiwan: Possible Influence of Methane Flux on the Early Diagenetic Process. *Terr. Atmos. Ocean. Sci.*, vol. 17 (4), p. 1009-1026.
- Hrouda, F., Chlupacova, M., and Chadima, M.** (2009). The use of magnetic susceptibility of rocks in geological exploration. Brno: TerraPlus.
- Irving, E., and Major, A.** (1964). Post-depositional detrital remanent magnetization in a synthetic sediment. *Sedimentology*, vol. 3, p. 135-143.
- Janoschek, W. M.** (1980). Outline of the Geology of Austria. *Abb. Geol.*, vol. 34, p. 7-98.
- Jelinowska, A., Tucholka, P., Guichard, F., Lefevre, I., Badaut-Trauth, D., Chalie, F.** (1998). Mineral magnetic study of Late Quaternary South Caspian sediments: palaeoenvironmental implications. *Geophys. J. Int.*, vol. 133, p. 499-509.
- Joseph, L., Rea, D., and van der Pluijm, A.** (1998). Use of grain size and magnetic fabric analyses to distinguish among depositional environments. *Paleocoenography*, vol. 13 (5), p. 491-501.
- Jovanne, L., Florindo, F., Bazylinski, D., and Lins, U.** (2012). Prismatic magnetite magnetosomes from cultivated *Magnetovibrio blakemorei* strain MV-1: a magnetic fingerprint in marine sediments? *Environmental Microbiology Reports*.
- Kapounek, J., Koelbl, L., and Weinberger, F.** (1963). Results of new exploration in the basement of the Vienna Basin. p. 206-221.
- Karlin, R., and Levi, S.** (1985). Geochemical and sedimentological control of the magnetic properties of hemipelagic sediments. *Journal of Geophysical Research*, vol. 90 (B12), p. 10373-10392.
- Karlin, R., Lyle, M., and Heath, G.** (1987). Authigenic magnetite formation in suboxic marine sediments. *Nature*, vol. 326, p. 490-493.
- Katari, K., and Tauxe, L.** (2000). Effects of pH and salinity on the intensity of magnetization in redeposited sediments. *Earth and Planetary Science Letters*, vol. 181, p. 489-496.
- Kazmer, M.** (1990). Birth, life and death of the Pannonian Lake. *Palaeogeography, Palaeoclimatology, Palaeoecology*, vol. 79, p. 171-188.
- Keller, W. D.** Diagenesis in clay minerals - A Review. University of Missouri, Columbia, Missouri.
- Kodama, K.** (2012). *Paleomagnetism of Sedimentary Rocks : Process and Interpretation*. John Wiley and Sons, Ltd.
- Kodama, K., and Hinnov, L.** (2014). *Rock Magnetic Cyclostratigraphy*. John Wiley and Sons, Ltd.
- Koolen, G.** (2010). Identification of Ferromagnetic Minerals: Magnetic minerals analysis of Pannonian, Sarmatian and Badenian (10.5-13.7 Ma) sediments from the Spannberg 21 Well (Ebenthal, Austria). Delft.
- Kovac, M., Barath, I., Harzhauser, M., Hlavaty, I., and Hudackoova, N.** (2004). Miocene depositional systems and sequence stratigraphy of the Vienna Basin. *Courier des Forschungs Instituts Senckenberg* (246), p. 187-212.
- Kovac, M., Barath, I., Kovacova-Slamkova, M., Pipik, R., Hlavaty, I., and Hudackova, N.** (1998). Late Miocene paleoenvironments and sequence stratigraphy: Northern Vienna Basin. *Geologica Carpathica*, vol. 49 (6), p. 445-458.
- Krammer, K.** (1990). Magnetic susceptibility log measured in hole 395A, LEG 109. *Proceedings of the Ocean Drilling Program, Scientific Results*, 106/109.
- Ladwein, H.** (1988). Organic Geochemistry of Vienna Basin: Model for Hydrocarbon Generation in Overthrust Belts. *The American Association of Petroleum Geologists Bulletin*, vol. 72 (5), p. 586-599.

- Lankreijer, A., Kovac, M., Cloetingh, S., Pitonak, P., Hloska, M., and Biermann, C.** (1995). Quantitative subsidence analysis and forward modelling of the Vienna and Danube basins: thin-skinned versus thick-skinned extension. *Tectonophysics*, vol. 252 (1-4), p. 433-451.
- Lantos, M., and Elston, D.** (1995). Low- to high-amplitude oscillations and secular variation in a 1.2 km late Miocene inclination record. *Physics of the Earth and Planetary Interiors*, vol. 90, p. 37-53.
- Lapointe, P., Morris, W., and Harding, K.** (1986). Interpretation of magnetic susceptibility: a new approach to geophysical evaluation of the degree of rock alteration. *Can. J. Earth Sci.*, vol. 23, p. 393-401.
- Leslie, B., Lund, S., and Hammond, D.** (1990). Rock Magnetic Evidence for the Dissolution and Authigenic Growth of Magnetic Minerals Within Anoxic Marine Sediments of the California Continental Borderland. *Journal Of Geophysical Research*, vol. 95 (B4), p. 4437-4452.
- Li, Y., and Schoonmaker, J.** (2005). *Sediments, Diagenesis and Sedimentary Rocks* (ed.F.T. Mackenzie). Oxford: Elsevier.
- Lopez, P., Navarro, E., Marce, R., and Caputo, L.** (2006). Elemental ratios in sediments as indicators of ecological processes in Spanish reservoirs. *Limnetica*, p. 499-512.
- Lovlie, R., and Veen, V.** (1995). Magnetic susceptibility of a 180m sediment core: reliability of incremental sampling and evidence for a relationship between susceptibility and gamma activity. *In P. Turner and A. Turner, eds., Paleomagnetic Applications in Hydrocarbon Exploration and Production, Geological Society Special Publication* vol. (98), p. 259-266.
- Lu, R., Banerjee, S., and Marvin, J.** (1990). Effects of Clay Mineralogy and the Electrical Conductivity of Water on the Acquisition of Depositional Remanent Magnetization in Sediments. *Journal of Geophysical Research*, vol. 95 (B4), p. 4531-4538.
- Luthi, S.M.** (2001). *Geological Well Logs: Their use in reservoir modeling*. Berlin: Springer.
- Maher, B., and Hallam, D.** (2005). Magnetic carriers and remanence mechanisms in magnetite-poor sediments of Pleistocene age, southern North Sea margin. *Journal Of Quaternary Science*, vol. 20, p. 79-94.
- Mork, M., and Olesen, O.** (1996). Magnetic susceptibility of sedimentary rocks from shallow cores of Mid Norway and crystalline rocks from adjacent onland areas. Trondheim: IKU Petroleum Research and NGU.
- Muller, H., von Bebeneck, T., and Nehmiz, W.** (2010). Near-surface electromagnetic, rock magnetic, and geochemical fingerprinting of submarine freshwater seepage at Eckernförde Bay (SW Baltic Sea). *Geo-Mar Lett*, vol. 31, p. 123-140.
- Nelson, P.** (1993). Magnetic susceptibility logs from sedimentary and volcanic environments. *SPWLA 34th Annual Logging Symposium*. Colorado.
- Neretin, L., Jorgensen, B., Volkov, I., Hilgenfeldt, K., and Bottcher, M.** (2004). Pyritization processes and greigite formation in the advancing sulfidization front in the Upper Pleistocene sediments of the Black Sea. *Geochimica et Cosmochimica*, vol. 68, p. 2081-2093.
- Neubauer, F., and Hock, V.** (2000). Aspects of Geology in Austria and Adjoining Areas: Introduction. vol. 92, p. 7-14.
- Oldfield, F., Hao, Q., Bloemendal, J., Gibbs-Eggar, Z., Patil, S., and Guo, Z.** (2009). Links between bulk sediment particle size and magnetic grain size: General observations and implications for Chinese loess studies. *Sedimentology*, vol. 56, p. 2091-2106.
- OMV.** (2007). *Intend to Drill: Spannberg 21 Well*. Vienna.
- OMV.** (1992). Outline of Sedimentation, Tectonic Framework and Hydrocarbon Occurrence in eastern Lower Austria. *Mitt. Osterr. Geol. Ges. Guidebook*, vol. 85, p. 5-96.

- Opdyke, N., and Channel, J.** (1996). *Magnetic Stratigraphy*. San Diego, US: Academic Press.
- Paulissen, W.** (2011). Integrated high-resolution stratigraphy: Relative contributions of tectonics, eustasy and climate on basin evolution (Vienna Basin, Austria). *Uitgeverij BOXPress*, Oisterwijk.
- Paulissen, W., and Luthi, S.M.** (2011). High-frequency cyclicity in a Miocene sequence of the Vienna Basin established from high-resolution logs. *Palaeogeography, Palaeoclimatology, Palaeoecology*, vol. 307, p. 313-323.
- Paulissen, W., Luthi, S.M., Grunert, P., Coric, A., and Harzhauser, M.** (2001). Integrated high-resolution stratigraphy of a Middle to Late Miocene sedimentary sequence in the central part of the Vienna Basin. *Geologica Carpathica*, vol. 62 (2), p. 155-169.
- Peresson, M., Coric, S., and Wimmer-Frey, I.** (2005). New stratigraphic and mineralogical data of Neogene sediments from the City of Vienna (Vienna Basin). *12th Congress Patterns and Processes in the Neogene of the Mediterranean Region*. Vienna.
- Piller, W.** (1999). The Neogene of the Vienna Basin. *Foregs - Dachstein-Hallstatt-Salzkammergut Region*, p.11-19.
- Piller, W., Harzhauser, M., and Mandic, O.** (2007). Miocene Central Paratethys stratigraphy – current status and future directions. *Stratigraphy*, vol. 4, nos. (2/3), p. 151-168.
- Porsch, K., Dippon, U., Rija, M., Appel, E., and Kappler, A.** (2010). In-situ magnetic susceptibility measurements as a tool to follow geomicrobiological transformation of Fe minerals. *Environmental Science and Technology*, vol. 10 (44), p. 3846-3852.
- Potter, D.K., Al-Ghamdi, T.M., and Ivakhnenko, O.P.** (2008). Sensitive carbonate reservoir rock characterization from magnetic susceptibility: mineral quantification, correlation with petrophysical properties and anisotropy. Abu Dhabi, UAE.
- Potter, D. K.** (2004). Downhole magnetic susceptibility: potential applications of an environmentally friendly technique. *Geophysical Research Abstracts. European Geosciences Union, 1st General Assembly Nice, France*, vol. 6.
- Potter, D. K.** (2007). Magnetic Susceptibility as a Rapid, Nondestructive Technique for Improved Petrophysical Parameter Prediction. *Petrophysics*, vol. 48 (3), p. 191-201.
- Potter, D. K., Corbett, P., Barclay, S., and Haszeldine, R.** (2004). Quantification of illite content in sedimentary rocks using magnetic susceptibility—a rapid complement or alternative to X-ray diffraction. *Journal of Sedimentary Research, Research Methods Papers Section*, vol. 74 (5), p. 730-735.
- Radan, S., Radan, S., and Catianis, I.** (2013). The use of magnetic susceptibility record as a proxy signature for the lithological composition of lake sediments: evidences from short cores in the Mesteru-Fortuna Depression (Danube Delta). *Geo-Eco-Marina*, vol. 19, p. 77-105.
- Rauen, A., Soffel, C., and Winter, H.** (2000). Statistical analysis and origin of the magnetic susceptibility of drill cuttings from the 9.1-km-deep KTB drill hole. *Geophys. J. Int.*, vol. 142, p. 83-94.
- Roberts, A., and Weaver, R.** (2005). Multiple mechanisms of remagnetization involving sedimentary greigite (Fe₃S₄). *Earth and Planetary Science Letters*, vol. 231, p. 263-277.
- Roberts, A., and Turner, G.** (1993). Diagenetic formation of ferrimagnetic iron sulphide minerals in rapidly deposited marine sediments, South Island, New Zealand. *Earth and Planetary Science Letters*, vol. 115, p. 257-273.
- Roberts, A., Tauxe, L., and Heslop, D.** (2013). Magnetic paleointensity stratigraphy and high-resolution Quaternary geochronology: successes and future challenges. *Quaternary Science Reviews*, vol. 61, p. 1-16.

- Roberts, Chang, Rowan, and Florindo.** (2011). Magnetic properties of sedimentary greigite (Fe₃S₄): an update. *Reviews of Geophysics*, vol. 49, p. 1-46.
- Robinson, S.** Lithostratigraphic applications for magnetic susceptibility logging of deep-sea sediment cores: examples from ODP Leg 115. *From Hailwood, E. A. and Kidd, R. B. (eds), High Resolution Stratigraphy Geological Society Special Publication*, vol. 70, p. 65-98.
- Rogl, F., Steininger, F., and Muller, C.** (n.d.). Middle Miocene salinity crisis and paleogeography of the Paratethys (Middle and Eastern Europe). p. 985-990.
- Rowan, C., and Roberts, A.** (2006). Magnetite dissolution, diachronous greigite formation, and secondary magnetizations from pyrite oxidation: unravelling complex magnetizations on Neogene marine sediments from New Zealand. *Earth Planet Sci. Lett.*, vol. 241, p. 119-137.
- Rowan, C., Roberts, A., and Broadbent, T.** (2009). Reductive diagenesis, magnetite dissolution, greigite growth and paleomagnetic smoothing in marine sediments: A new view. *Earth Planet Sci. Lett.*, vol. 277, p. 223-235.
- Salcher, B., Meurers, B., Smit, J., Decker, K., Holzel, M., and Wagneich, M.** (2012). Strike-slip tectonics and Quaternary basin formation along the Vienna Basin fault system inferred from Bouguer gravity derivatives. *Tectonics*, vol. 31, p. 1-20.
- Scholger, R., and Stingl, K.** (2004). New paleomagnetic results from the Middle Miocene (Karpatian and Badenian) in Northern Austria. *Geologica Carpathica*, vol. 55 (2), 199-206.
- Schon, J.** (2011). Handbook of Petroleum Exploration and Production. Physical Properties of Rocks: A workbook. Amsterdam: Elsevier.
- Schoonen, M.** (2004). Mechanisms of sedimentary pyrite formation. *Geological Society of America Special Paper 379*, p. 117-134.
- Schwarzacher, W.** (1993). Cyclostratigraphy and the Milankovitch theory. Amsterdam: Elsevier.
- Scott, J.** (1988). Interpretation of Magnetic logs in basalt, hole 418A. *Proceedings of the Ocean Drilling Program, Scientific Results*, 102.
- Seifert, P.** (1996). Sedimentary-tectonic development and Austrian hydrocarbon potential of the Vienna Basin. *Wessely and Liebl: Oil and Gas in Alpidic thrustbelts and basins of Central and Eastern Europe. EAGE Special Publication*, vol. 5, p. 331-341.
- Snowball, I.** (1991). Magnetic hysteresis properties of greigite (Fe₃S₄) and a new occurrence in Holocene sediments from Swedish Lapland. *Physics of the Earth and Planetary Interiors*, vol. 68, p. 32-40.
- Sopkova, B., Skulova, A., Hlavata, J., and Kovac, M.** (2007). Sequence stratigraphy of the Late Badenian and Sarmatian (Serravallian) of the eastern part of the Vienna Basin - Deltaic to tidal flats environment. *Joannea Geol. Palaont.*, vol. 9, p. 101-103.
- Strasser, A., Hilgen, F., and Heckel, P.** (2006). Cyclostratigraphy – concepts, definitions, and applications. *Newsl. Stratigr.*, vol. 42 (2), p. 75-114.
- Strauss, P., Harzhauser, M., Hinsch, R., and Wagneich, M.** (2006). Sequence stratigraphy in a classic pull apart basin (Neogene, Vienna Basin). A 3D seismic based integrated approach. *Geologica Carpathica*, vol. 57 (3), p. 185-197.
- Tauxe, L.** (n.d.). Lisa Tauxe's Home Page. <http://magician.uscd.edu>
- Tauxe, L.** (1993). Sedimentary records of relative paleointensity of the geomagnetic field: theory and practice. *Reviews of Geophysics*, vol. 31 (3), p. 319-354.
- Ter Borgh, M., Vasiliev, I., Stoica, M., Knezevic, S., Matenco, L., Krijgsman, W.** (2013). The isolation of the Pannonian basin (Central Paratethys): New constraints from magnetostratigraphy and biostratigraphy. *Global and Planetary Change*, vol. 103, p. 99-118.

- Thibal, J., Etchecopar, A., Pozzi, P., Pochacard, J., and Barthes, V.** (1999). Comparison of magnetic and gamma ray logging for correlations in chronology and lithology: example from the Aquitanian Basin (France). *Geophys. J. Int.*, vol. 137, p. 839-846.
- Thompson, Battarnee, O'Sullivan, and Oldfield.** (1975). Magnetic susceptibility of lake sediments. *Limnol. Oceanogr.*, vol. 20, p. 687-698.
- Thompson, R., and Morton, D.** (1979). Magnetic susceptibility and particle-size distribution in recent sediments of the Loch Lomond Drainage Basin, Scotland. *Journal of Sedimentary Petrology*, vol. 49 (3), p. 801-811.
- Torrence, C., and Compo, G.** (1997). A Practical Guide to Wavelet Analysis. Boulder: *Bulletin of the American Meteorological Society*.
- Van Vugt, N., Langereis, C.G.; Hilgen, F.J.** (2001). Orbital forcing in Pliocene-Pleistocene Mediterranean lacustrine deposits: dominant expression of eccentricity versus precession. *Palaeogeography, Palaeoclimatology, Palaeoecology*. vol. 172, p. 193-205
- Vasiliev, I., Bakrac, K., Kovacic, M., Abdul Aziz, H., and Krijgsman, W.** (2007). Paleomagnetic results from the Sarmatian/Pannonian boundary in North-eastern Croatia (Vranovic Section, Nasice Quarry). *Geologia Croatica*, vol. 60 (2), p. 151-163.
- Vasiliev, I., de Leeuw, A., Filipescu, S., Krijgsman, W., and Kuiper, K.** (2010). The age of the Sarmatian–Pannonian transition in the Transylvanian Basin (Central Paratethys). *Palaeogeography, Palaeoclimatology, Palaeoecology*.
- Vasiliev, I., Dekkers, M., Krijgsman, W., Franke, C., and Mullender, T.** (n.d.) Greigite as recorder of paleomagnetic and palaeoenvironmental signals in the Pliocene sedimentary rocks of the Carpathian foredeep (Romania). Chapter 6 p. 109-130.
- Vasiliev, I., Dekkers, M., Krijgsman, W., Franke, C., Mullender, T., and Langereis, C.** (2007). Early diagenetic greigite as a recorder of the paleomagnetic signal in Miocene–Pliocene sedimentary rocks of the Carpathian foredeep (Romania). *Geophys. J. Int.*, vol. 171, p. 613-619.
- Vasiliev, I., Franke, C., Meeldijk, J., Dekkers, M., Langereis, C., and Krijgsman, W.** (2008). Putative greigite magnetofossils from the Pliocene epoch. *Nature Geoscience. Advance Online Publication*, p. 1-15.
- Vigliotti, L., Capotondi, L., and Torii, M.** (1999). Magnetic properties of sediments deposited in suboxic-anoxic environments: relationships with biological and geochemical proxies. In: *TARLING, D. H. and TURNER, P. (eds), Geological Society, London, Special Publications*, vol. 151, p. 71-83.
- Vrsaljko, D.** (1999). The Pannonian Palaeoecology and Biostratigraphy of Molluscs from Kostanjek - Medvednica Mt. Croatia. *Geology Croatia*, vol. 52 (1), p. 9-27.
- Vrsalko, D., Pavelic, D., Miknic, M., Brkic, M., Kovacic, M., and Hecimovic, I.** (2006). Middle Miocene (Upper Badenian/Sarmatian) Palaeoecology and Evolution of the Environments in the Area of Medvednica Mt.(North Croatia). *Geologica Croatia*, vol. 59 (1), p. 51-63.
- Wagreich, M., and Schmid, H.** (2002). Backstripping dip-slip fault histories: apparent slip rates for the Miocene of the Vienna Basin. *Terra Nova*, vol. 14 (3), p. 163-168.
- Waythomas, C.** (1991). Magnetic susceptibility of fluvial sediment, Lower Fox River, Northeastern Illinois, and implications for determining sediment source area. *U.S. Geological Survey*.
- Wei, G., Li, X.-H., Liu, Y., Shao, L., and Liang, X.** (2006). Geochemical record of chemical weathering and monsoon climate change since the early Miocene in the South China Sea. *Paleoceanography*.
- Weissenböck, M.** (1996). Lower to Middle Miocene sedimentation model of the Central Vienna Basin. *Wessely and Liebl: Oil and Gas in Alpidic thrustbelts and basins of Central and Eastern Europe. EAGE Special Publication*, vol. 5, p. 355-363.

- Wessely, G.** (1998). Structure and development of the Vienna Basin in Austria. *In Royden and Horvath: The Pannonian Basin. A study in basin evolution. AAPG Memoir*, vol. 45, p. 333-346.
- Yang, T., Gao, J., Gu, Z., Dagva, B., and Tserenpil, B.** (2013). Petrophysical Properties (Density and Magnetization) of Rocks from the Suhbaatar-Ulaanbaatar-Dalandzadgad Geophysical Profile in Mongolia and Their Implications. *The Scientific World Journal*, 2013.

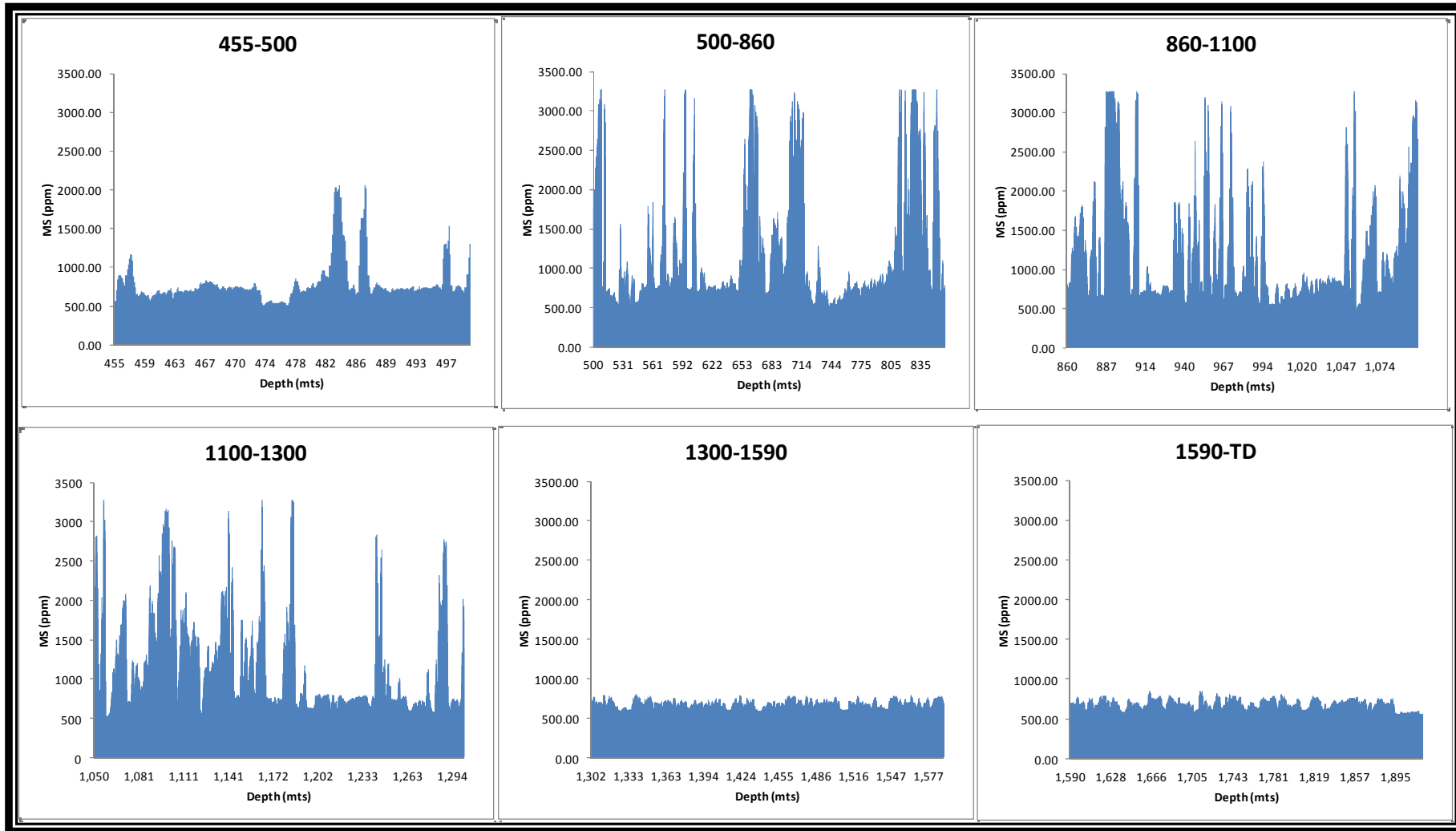
APPENDICES

LIST OF APPENDICES

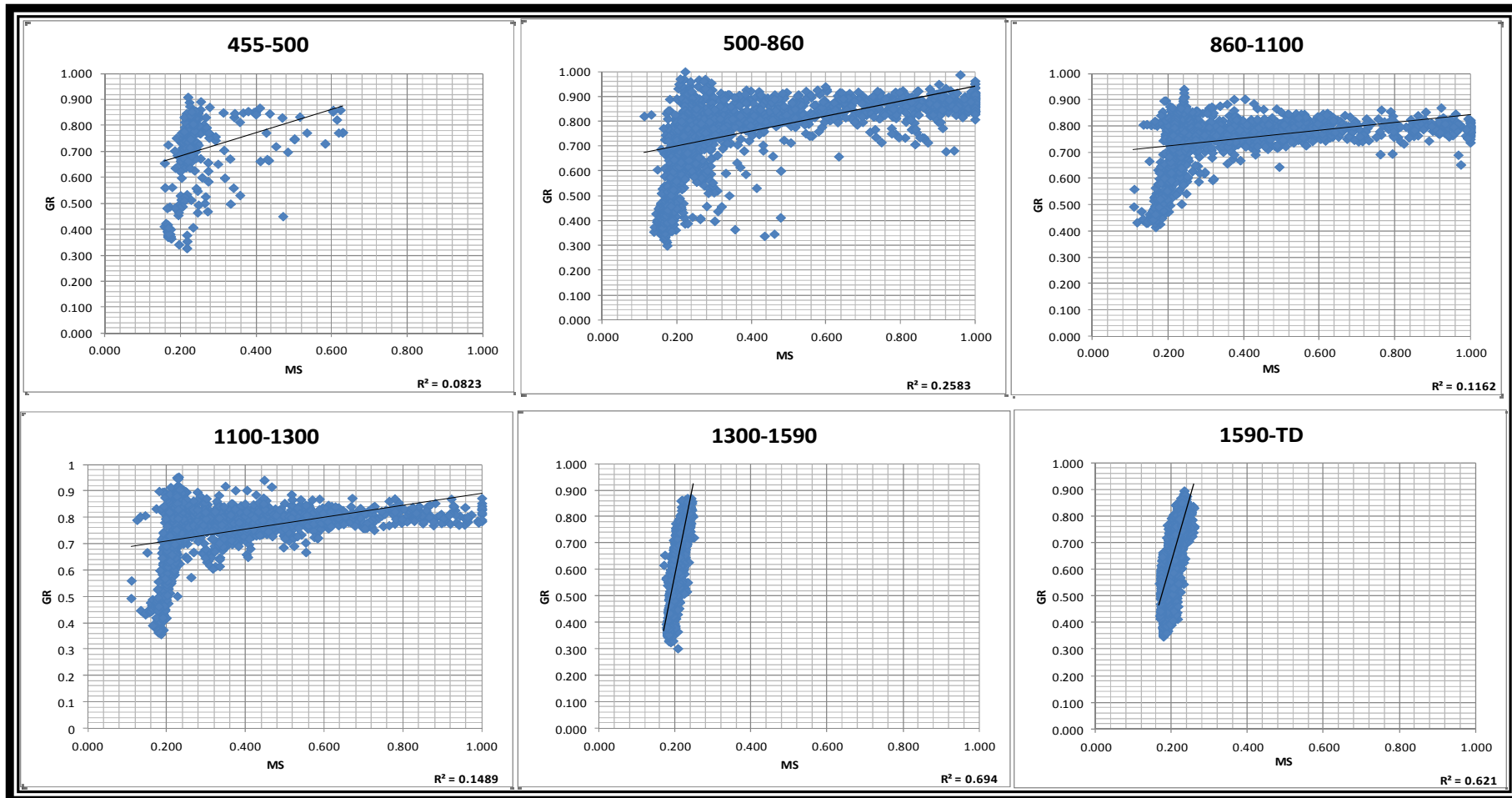
APPENDIX A: logging data Spannberg-21 _____	69
APPENDIX B: magnetic susceptibility per zone _____	70
APPENDIX C.1: GR vs. MS cross plot used for the correlation matrix _____	71
APPENDIX C.2: RHOZ vs. MS cross plot used for the correlation matrix _____	72
APPENDIX C.3: PEF vs. MS cross plot used for the correlation matrix _____	73
APPENDIX C.4: TNPH vs. MS cross plot used for the correlation matrix _____	74
APPENDIX D: depth intervals analyzed for acid test _____	75
APPENDIX E.1: XRD spectrum for Sample 1 and Sample 2 in compatible scales _____	76
APPENDIX E.2: XRD spectrum for Sample 3 and Sample 4 in compatible scales _____	77
APPENDIX E.3: XRD spectrum for Sample5 and Sample 6 in compatible scales _____	78
APPENDIX F.1: XRD spectrum for Sample 1, original report _____	79
APPENDIX F.2: XRD spectrum for Sample 2, original report _____	80
APPENDIX F.3: XRD spectrum for Sample 3, original report _____	81
APPENDIX F.4: XRD spectrum for Sample 4, original report _____	82
APPENDIX F.5: XRD spectrum for Sample 5, original report _____	83
APPENDIX F.6: XRD spectrum for Sample 6, original report _____	84
APPENDIX G.1: single elements and ratios for geochemistry analysis _____	85
APPENDIX G.2: single elements and ratios for geochemistry analysis _____	86

APPENDIX A: logging data Spannberg-21

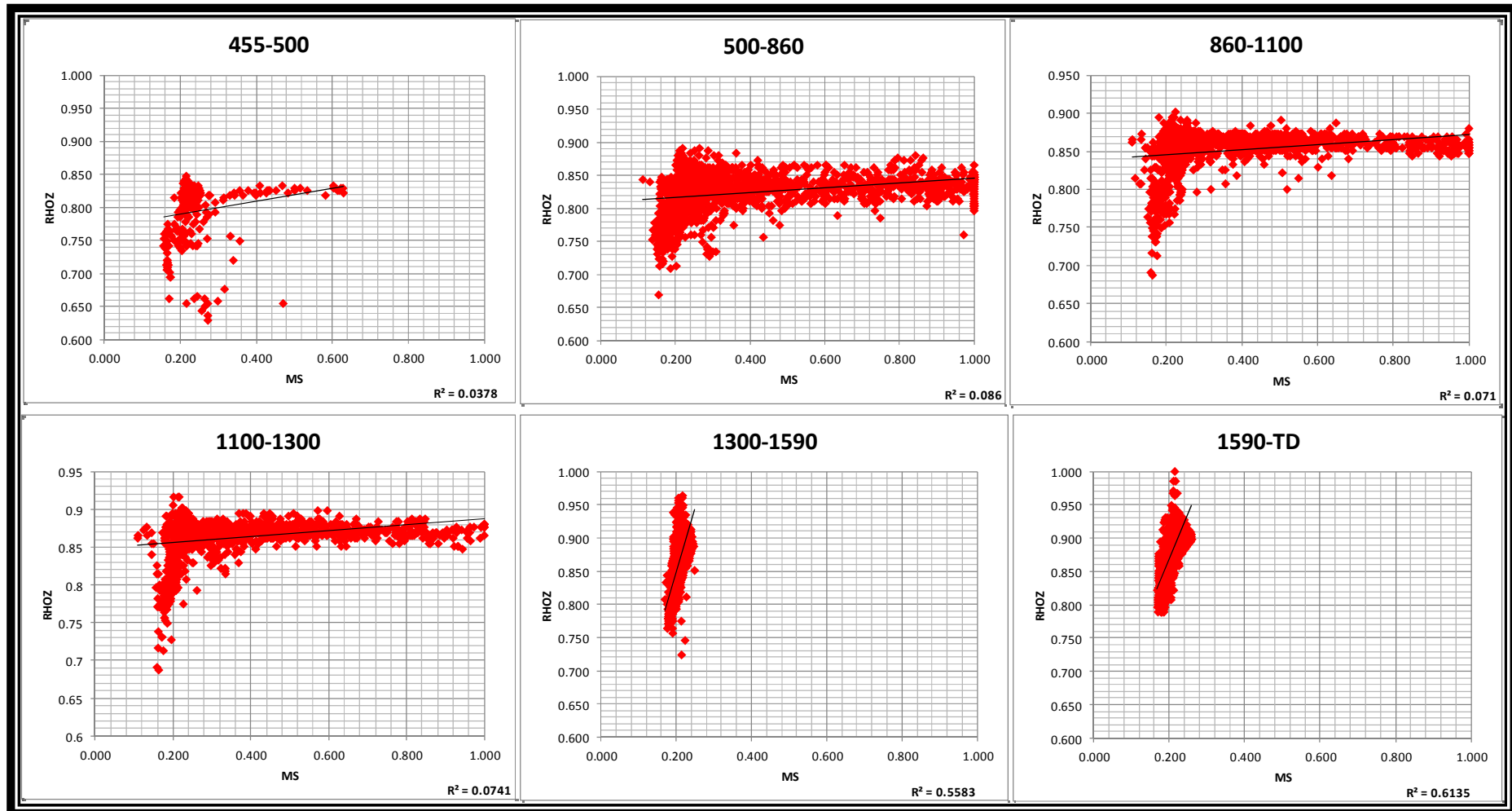
APPENDIX B: magnetic susceptibility per zone



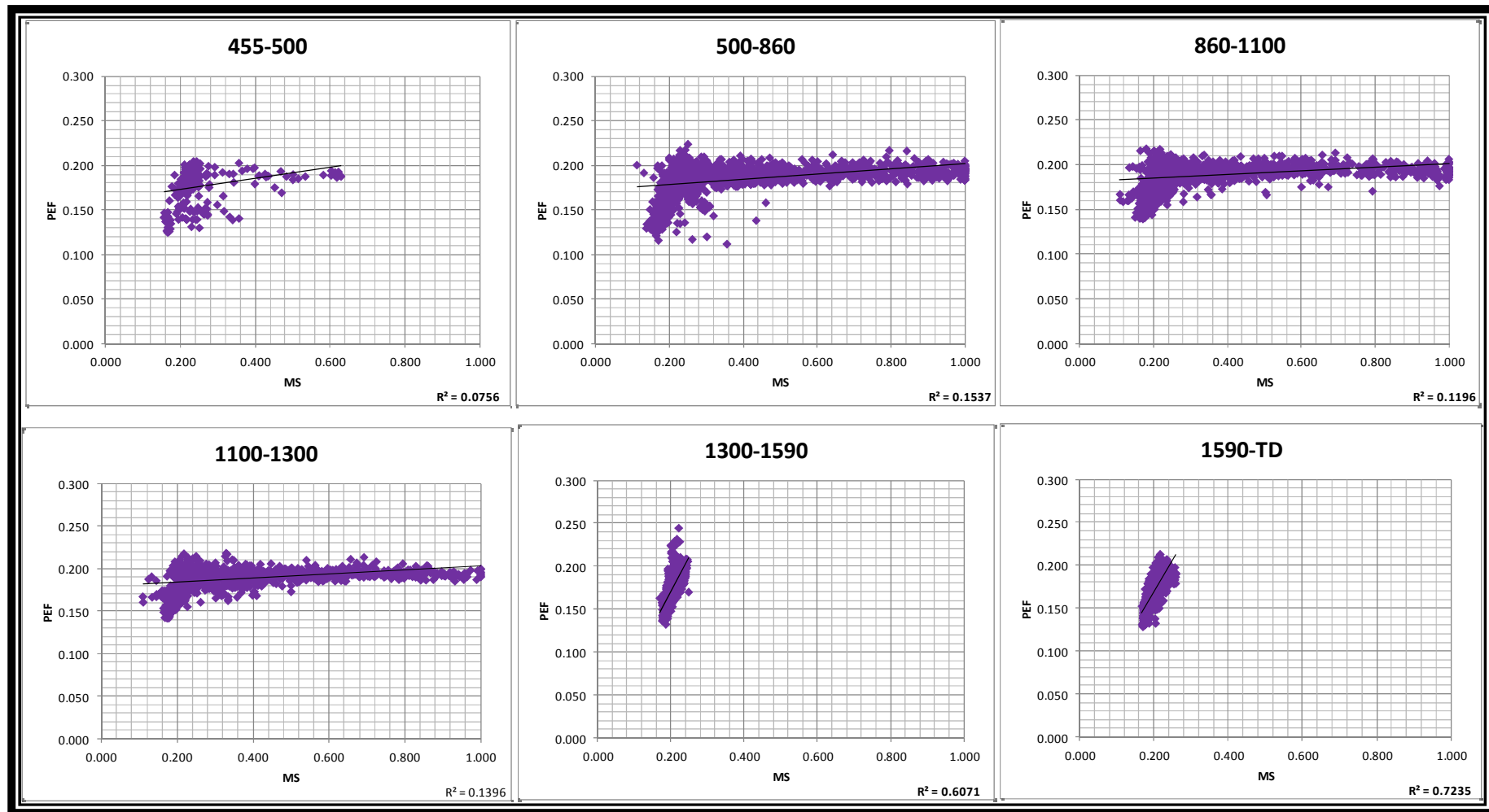
APPENDIX C.1: GR vs. MS cross plot used for the correlation matrix



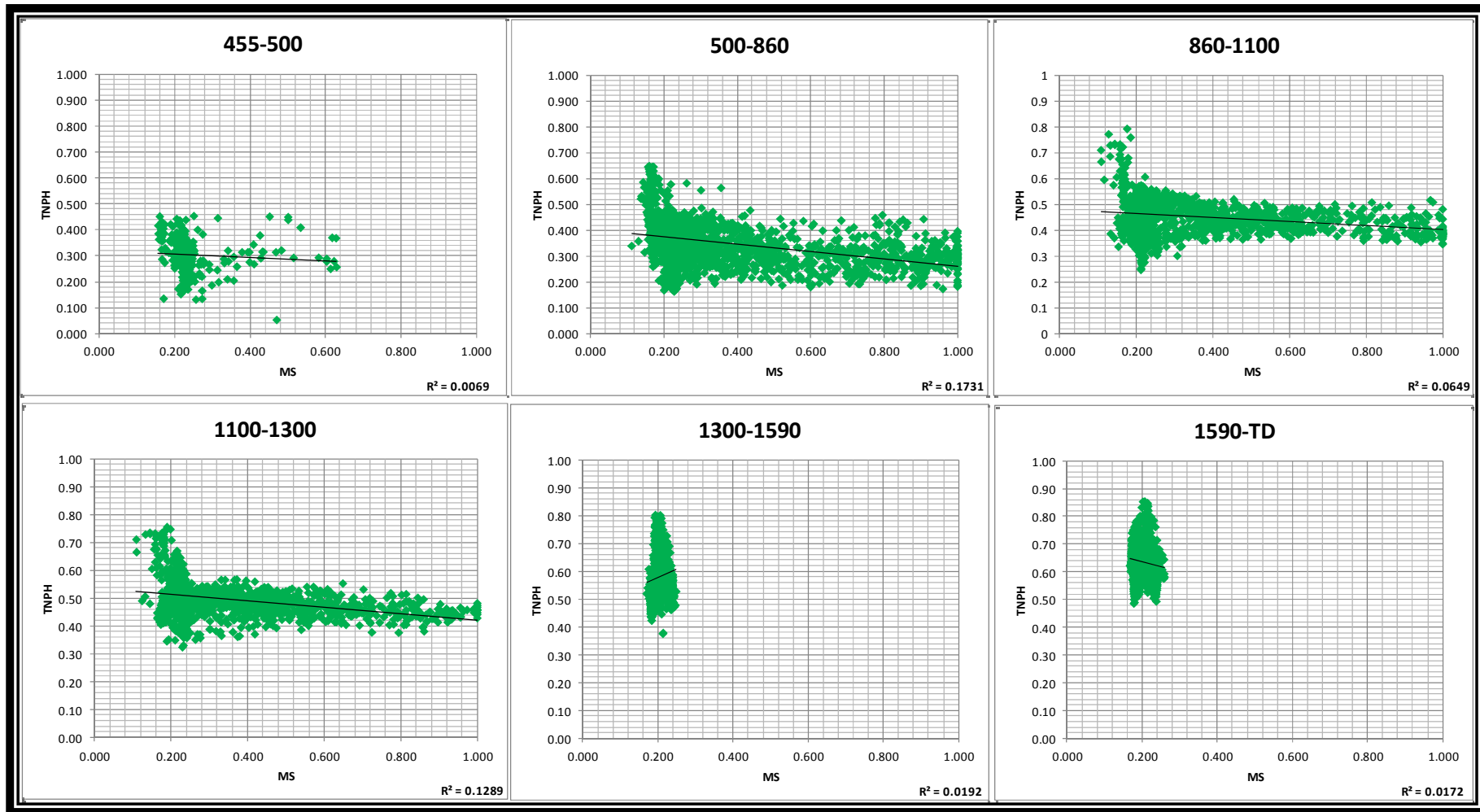
APPENDIX C.2: RHOZ vs. MS cross plot used for the correlation matrix



APPENDIX C.3: PEF vs. MS cross plot used for the correlation matrix



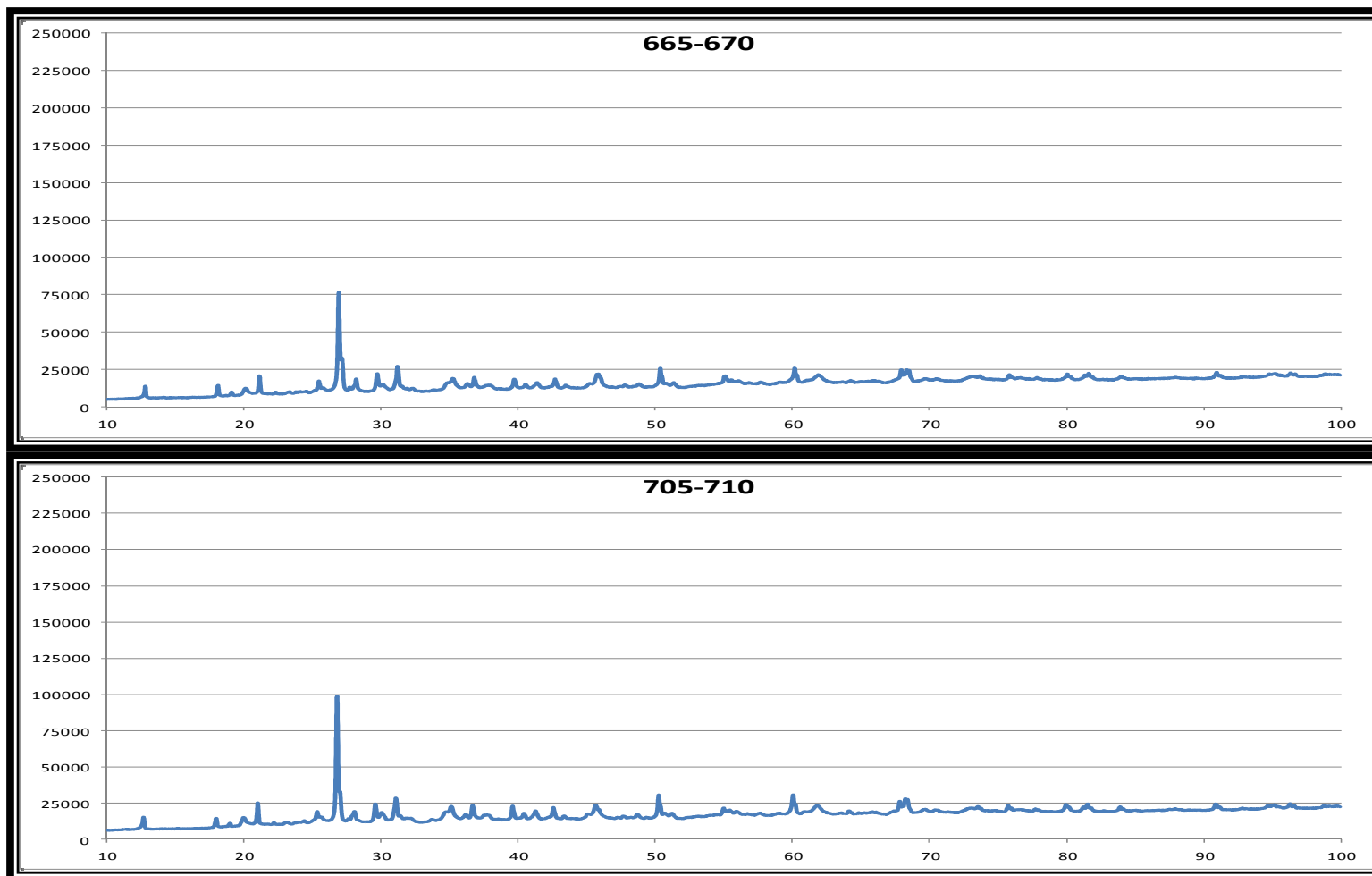
APPENDIX C.4: TNPH vs. MS cross plot used for the correlation matrix



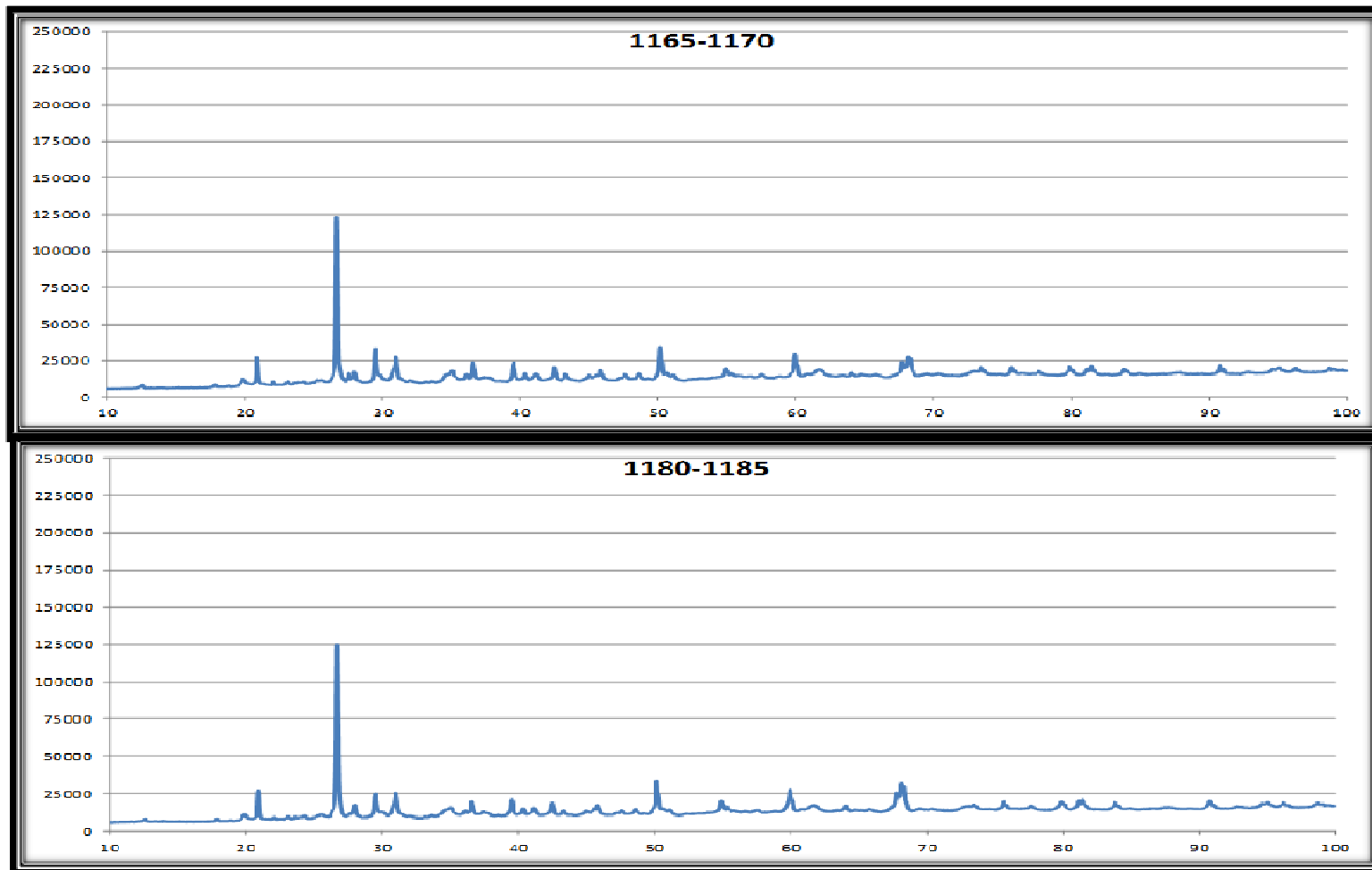
APPENDIX D: depth intervals analyzed for acid test

Depth (mts.)		
460-465	880-885	1340-1345
465-470	910-915	1350-1355
480-485	925-930	1355-1360
490-495	930-935	1370-1375
495-500	1035-1040	1400-1405
500-505	1050-1055	1440-1445
505-510	1070-1075	1465-1470
530-535	1090-1095	1505-1510
545-550	1095-1100	1640-1645
555-560	1100-1105	1640-1645
590-595	1105-1110	1670-1675
600-605	1115-1120	1680-1685
615-620	1130-1135	1700-1705
615-620	1155-1160	1715-1720
635-640	1165-1170	1740-1745
655-660	1185-1190	1760-1765
680-685	1210-1215	1770-1775
690-695	1225-1230	1780-1785
790-795	1240-1245	1795-1800
815-820	1250-1255	1810-1815
815-820	1270-1275	1820-1825
825-830	1280-1285	1820-1825
830-835	1285-1290	1830-1835
840-845	1285-1290	1840-1845
850-855	1290-1295	1855-1860
855-860	1295-1300	1880-1885
860-865	1300-1305	1930-1935
865-870	1315-1320	1987.5-1990
865-870	1325-1330	

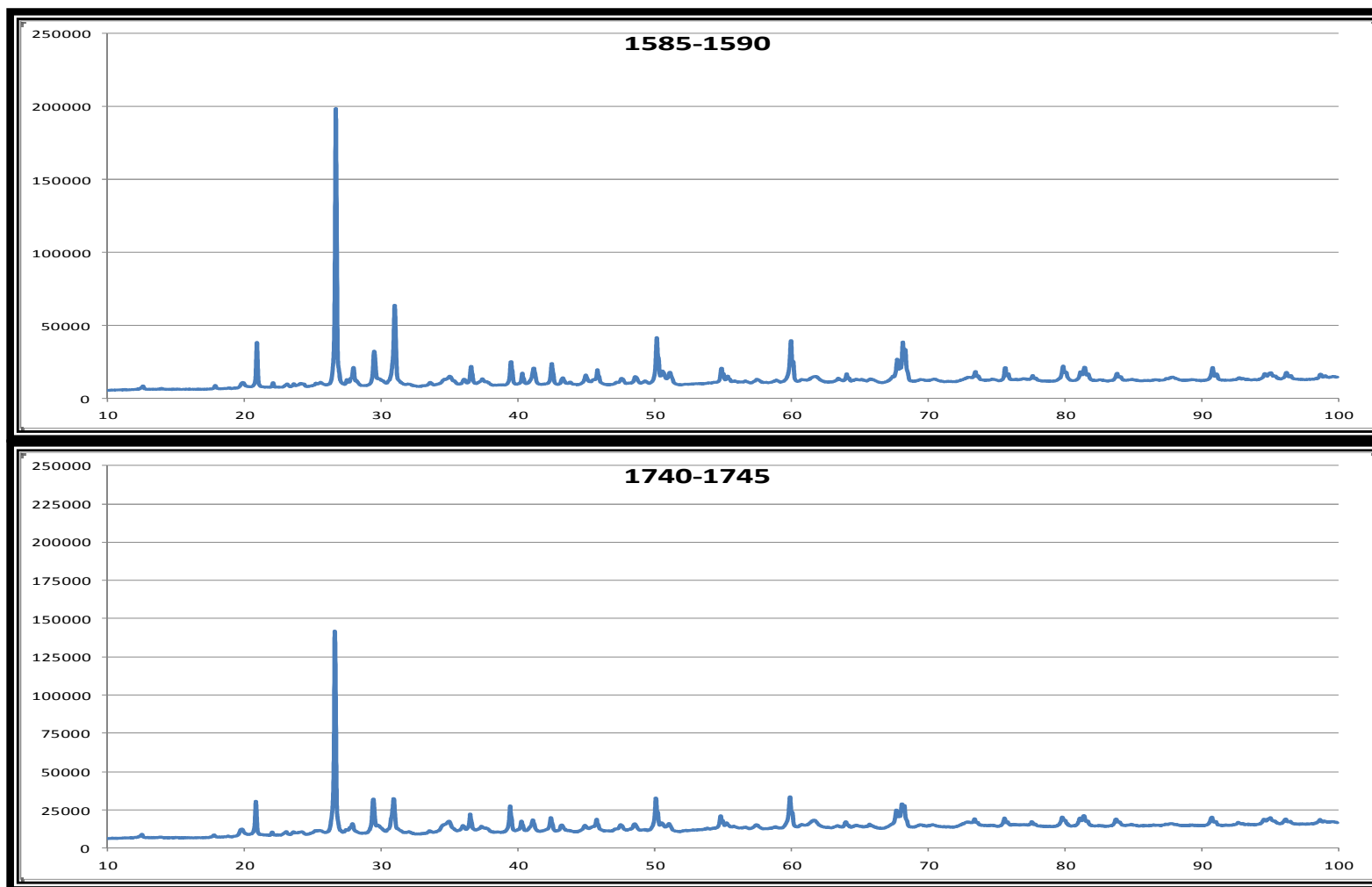
APPENDIX E.1: XRD spectrum for Sample 1 and Sample 2 in compatible scales (counts vs. 2θ)



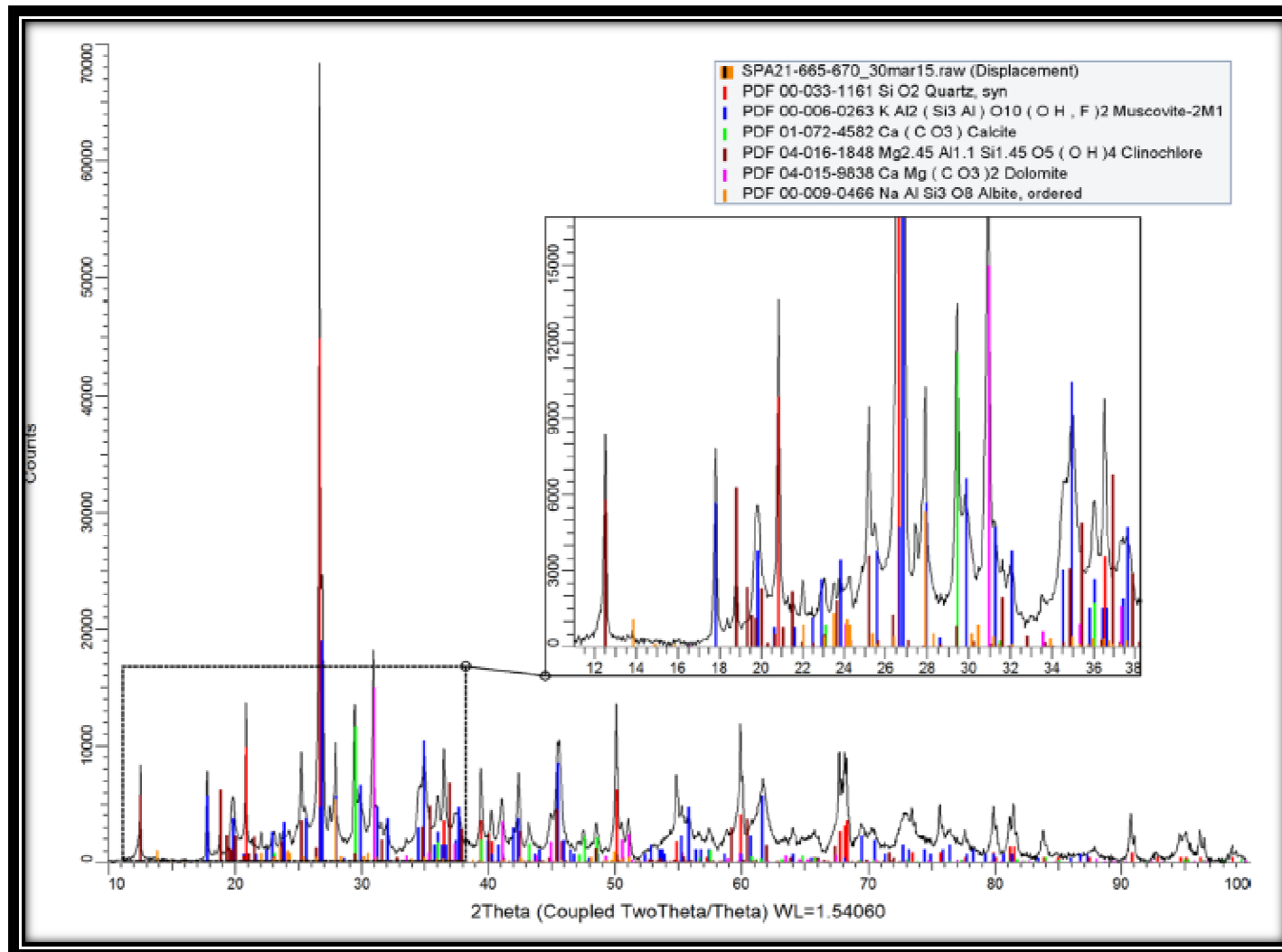
APPENDIX E.2: XRD spectrum for Sample 3 and Sample 4 in compatible scales(counts vs. 2 θ)



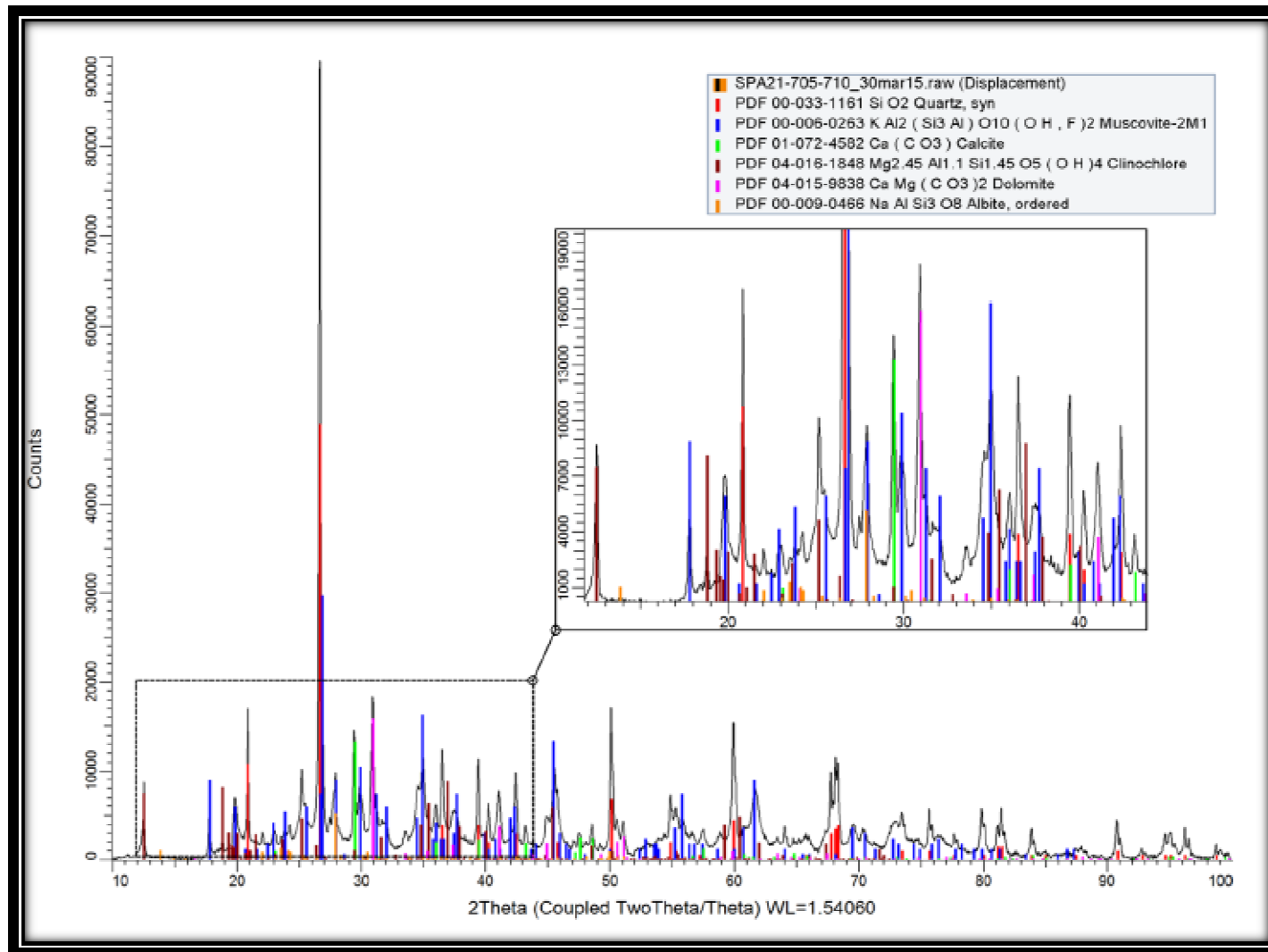
APPENDIX E.3: XRD spectrum for Sample 5 and Sample 6 in compatible scales (counts vs. 2θ)



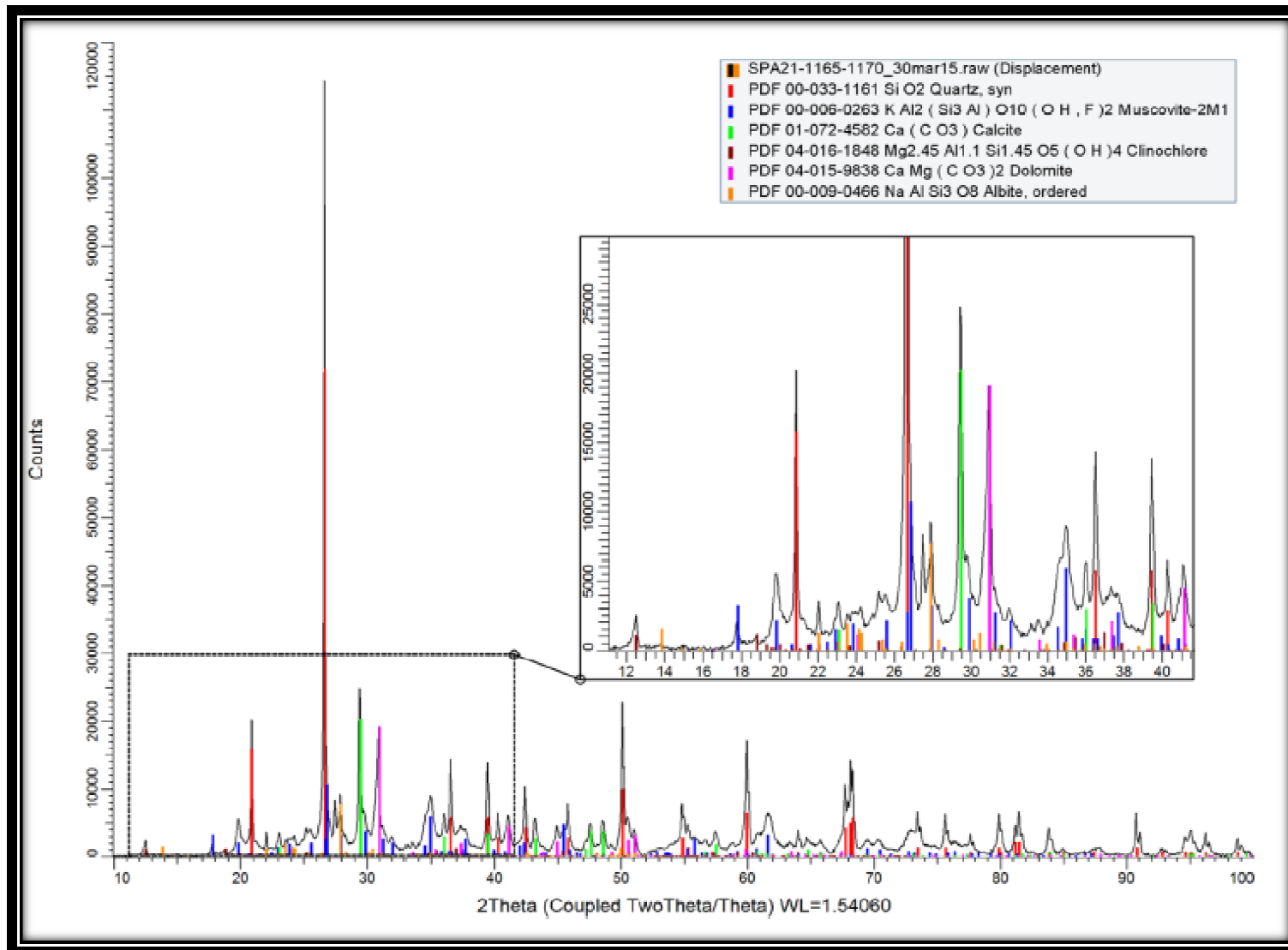
APPENDIX F.1: XRD spectrum for Sample 1, original report



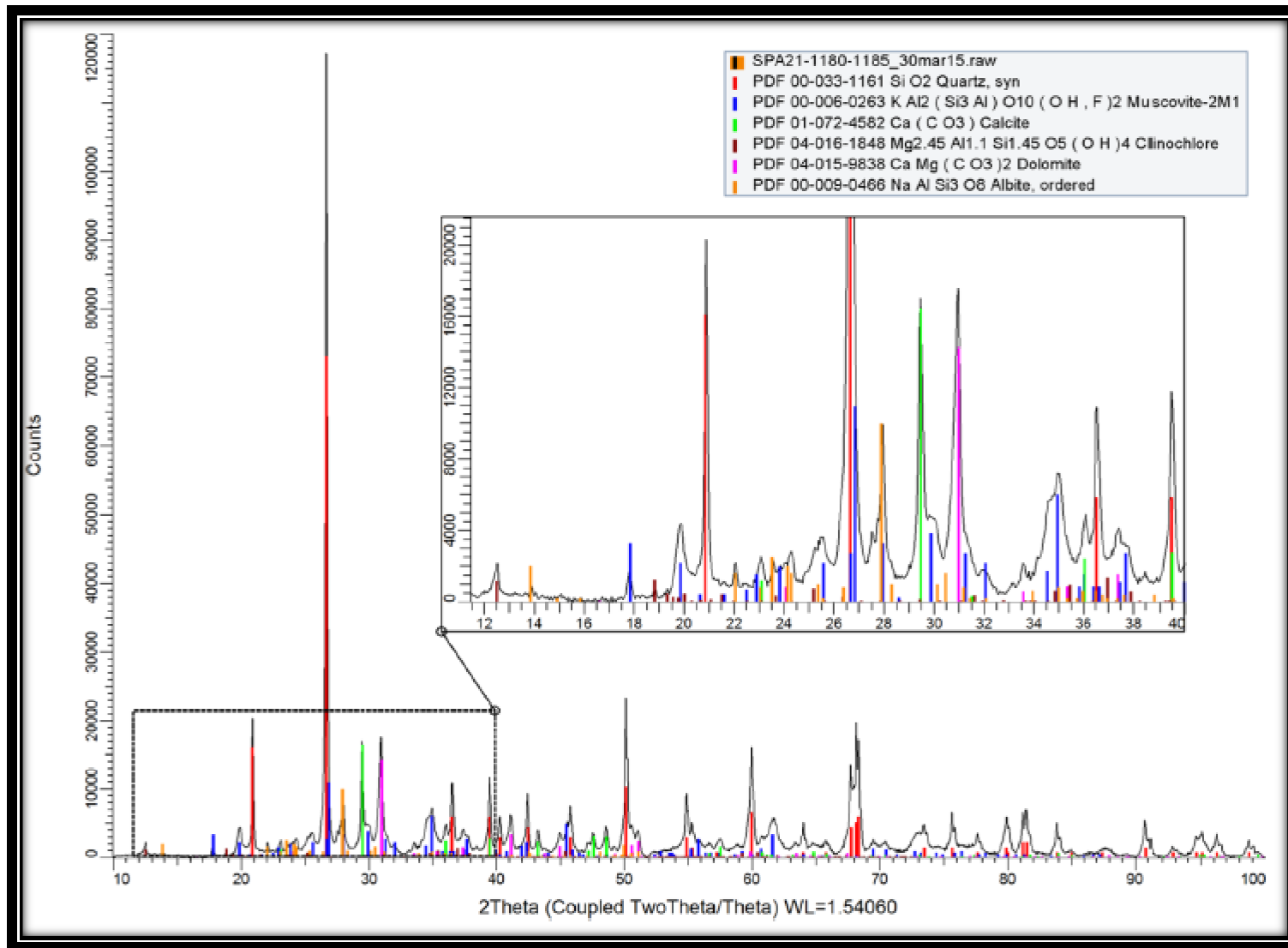
APPENDIX F.2: XRD spectrum for Sample 2, original report



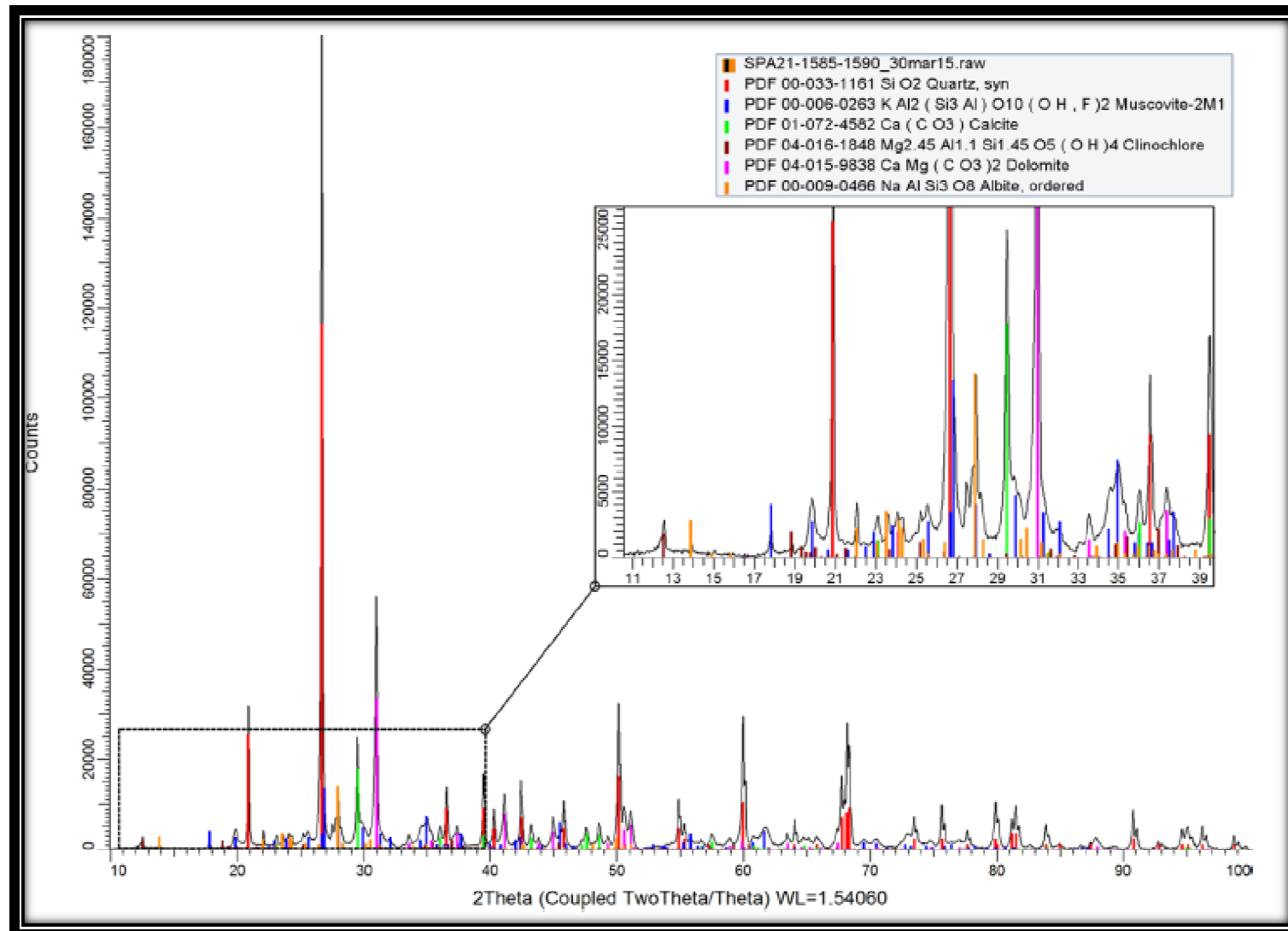
APPENDIX F.3: XRD spectrum for Sample 3, original report



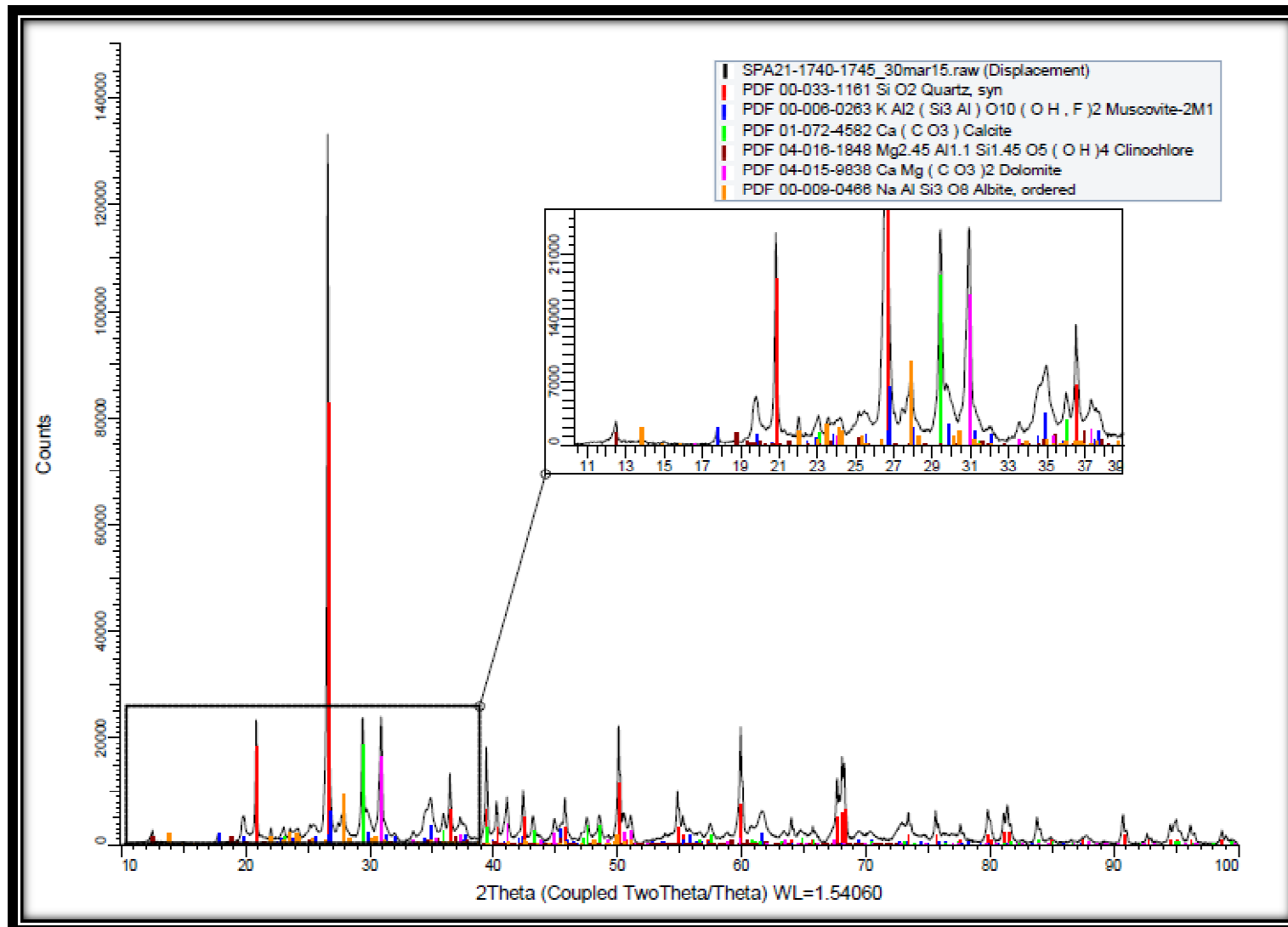
APPENDIX F.4: XRD spectrum for Sample 4, original report



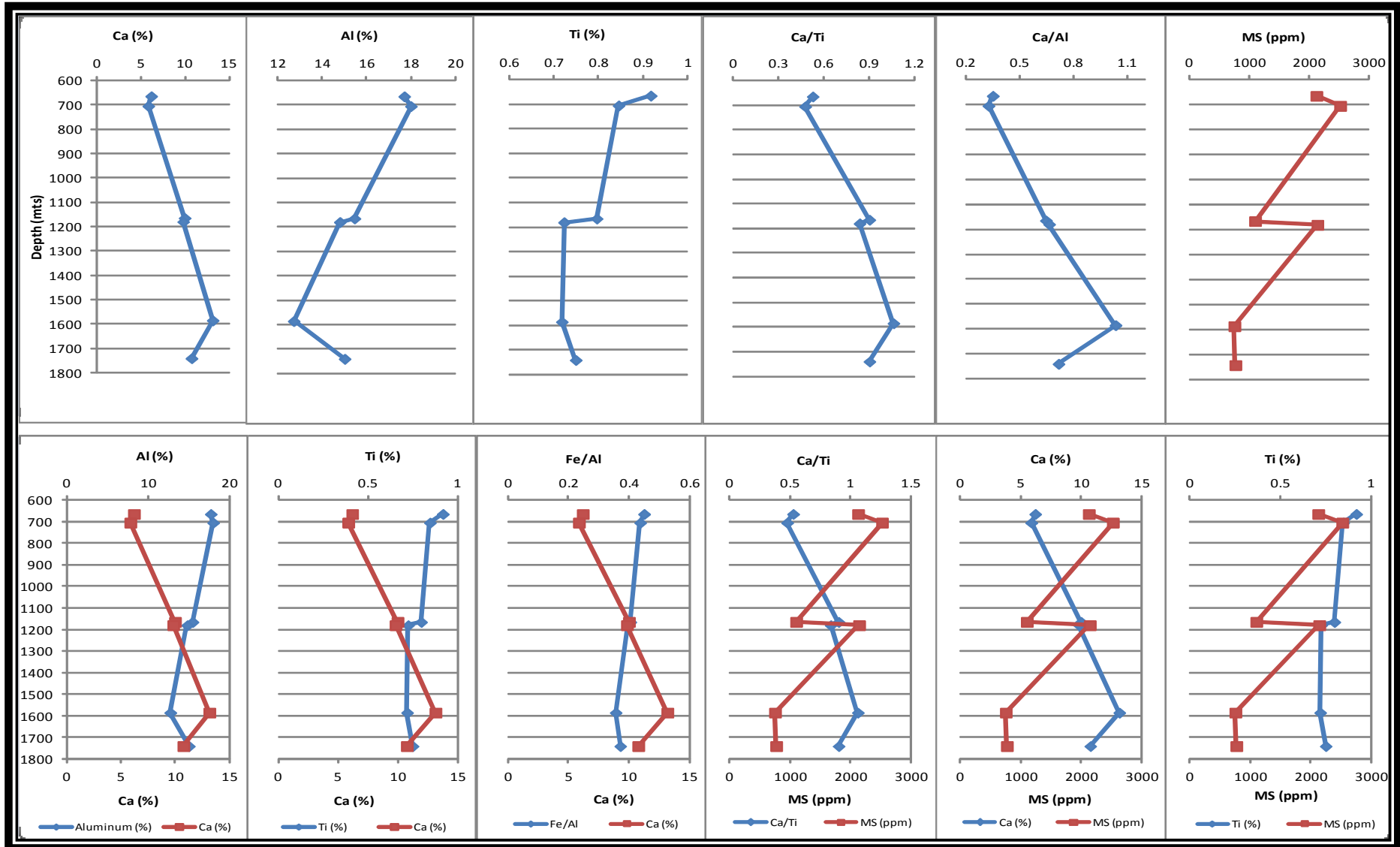
APPENDIX F.5: XRD spectrum for Sample 5, original report



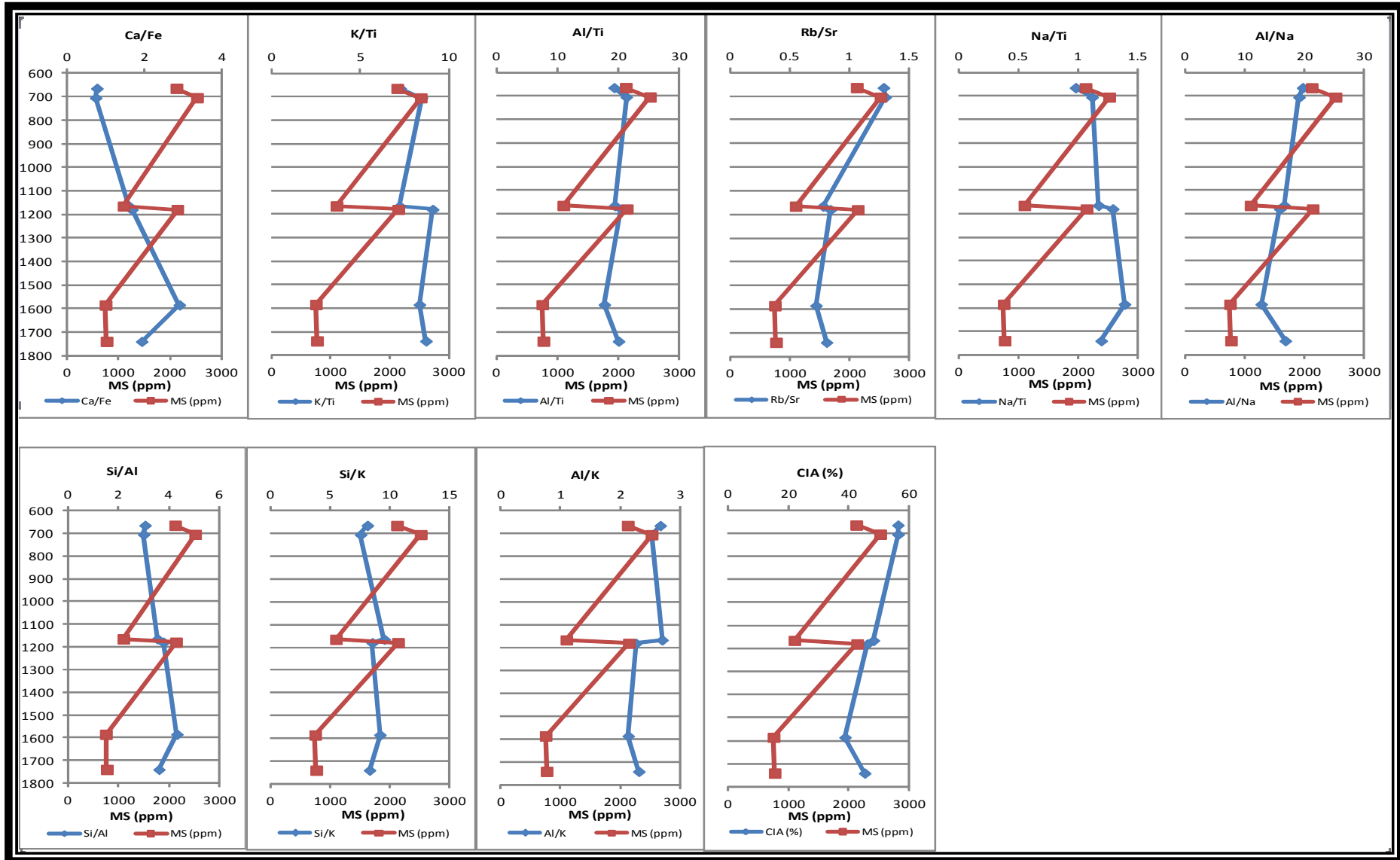
APPENDIX F.6: XRD spectrum for Sample 6, original report



APPENDIX G.1: single elements and ratios for geochemistry analysis



APPENDIX G.2: single elements and ratios for geochemistry analysis



GLOSSARY

GLOSSARY OF TERMS

Anhyseretic remanent magnetization (ARM): a laboratory remanence that results from applying a small DC magnetic field (~50–100 μ T) to a sample in the presence of an alternating magnetic field that is decreased from some peak value to 0. In most laboratories, the peak field is about 100 mT. A partial ARM can be applied by only switching on the DC field over a limited range of alternating field during the decrease from a peak alternating field value.

Authigenic: An authigenic mineral is one that formed in place, rather than being transported from another location.

B_{1/2}: is defined as the field at which half of the SIRM is reached.

CIA: The Chemical Index of Alteration was proposed by Nesbitt and Young (1982) as a measure of the role played by chemical weathering in the production of clastic sediments. The ratio $CIA = (Al_2O_3/Al_2O_3 + CaO^* + Na_2O + K_2O) \times 100$ (where CaO* is the calcium content of silicates) is based on the assumption that the dominant process during chemical weathering is the degradation of feldspars and the formation of clay minerals.

Coercivity of remanence (B_{cr}): The direct reversed magnetic field that must be applied and then removed to demagnetize to zero the saturation remanent magnetization that was imparted in the opposite direction.

Curie temperature (T_c): As temperature increases in a ferromagnetic material, interatomic distances increase, and the magnetic exchange interaction becomes weaker. At T_c, thermal energy overcomes the exchange energy, and magnetic moments become independent so that the material becomes paramagnetic. Named for the French scientist Pierre Curie (1859–1906).

Cyclostratigraphy: the study of periodic behavior of the properties of a sequence of sedimentary rocks.

Dispersion parameter DP: is the width of the distribution, given by one standard deviation of the logarithmic distribution.

DTA: Differential thermal analysis is a thermo analytic technique, similar to differential scanning calorimetry. In DTA, the material under study and an inert reference are made to undergo identical thermal cycles, while recording any temperature difference between sample and reference. This differential temperature is then plotted against time, or against temperature (DTA curve, or thermogram).

Eccentricity: the deviation of the Earth's elliptical orbit around the Sun from circularity. An eccentricity of 0 is a circular orbit, an eccentricity of 1 is a parabola. Earth's orbital eccentricity has ranged from 0.0034 to 0.058 over the past several hundred thousand years.

GAPI: API gamma ray units. A unit defined by the American Petroleum Institute for gamma ray log measurements.

IRM/SIRM: Remanent magnetism resulting from short-term exposure to strong magnetizing fields at constant temperature is referred to as isothermal remanent magnetism (IRM). In the laboratory, IRM is imparted by exposure (usually at room temperature) to a magnetizing field generated by an electromagnet. The maximum remanence that can be produced is called the saturation isothermal remanent magnetization (SIRM).

LWD: it stands for Logging While Drilling. is a technique of conveying well logging tools into the well borehole downhole as part of the bottom hole assembly (BHA). LWD tools work with its measurement while drilling (MWD) system to transmit partial or complete measurement results to the surface via typically a drilling mud pulser or other improved techniques, while LWD tools are still in the borehole, which is called "real-time data".

Magnetosome: A magnetic nanoparticle produced by, and found in, magnetotactic bacteria. Magnetosomes are usually aligned in chains and are encased by a thin cellular membrane. These chains act like a compass needle to orient magnetotactic bacteria in the geomagnetic field. Magnetosomes commonly consist of magnetite or greigite.

Magnetotactic bacteria: A class of bacteria discovered in the 1960s that contain ferrimagnetic crystals within cell structures that enable the bacteria to navigate along geomagnetic field lines.

Multidomain (MD): As a magnetic particle increases in size, its magnetic energy increases. In order to minimize this energy, a particle will begin to nucleate domain walls at a critical grain size threshold. These walls divide the particle into two or more magnetic volumes or domains. The magnetization is uniform in each domain, but it differs in direction from domain to domain. MD grains are less effective paleomagnetic recorders than single-domain grains.

Natural remanent magnetization (NRM): The magnetic remanence of a geological sample prior to laboratory treatment. The NRM is typically composed of more than one component acquired at different times during a sample's history. Magnetization components are usually identified in the laboratory using stepwise thermal or alternating field demagnetization.

Obliquity: In astronomy, axial tilt, also known as obliquity, is the angle between an object's rotational axis and its orbital axis, or, equivalently, the angle between its equatorial plane and orbital plane. It differs from orbital inclination.

Precession: is a change in the orientation of the rotational axis of a rotating body. In astronomy, "precession" refers to any of several slow changes in an astronomical body's rotational or orbital parameters, and especially to Earth's precession of the equinoxes.

Pseudo-single-domain (PSD): A magnetic structure intermediate between the single-domain (SD) and multidomain states in which particles contain more than one domain but exhibit many of the stable magnetic properties typical of SD particles. PSD grains can have stable remanent magnetizations over geological time scales and can therefore be paleomagnetically important.

RES_BS: shallow button resistivity for the LWD tool.

RES_BM: medium button resistivity for the LWD tool.

SEM (scanning electron microscopy): is a type of electron microscope that produces images of a sample by scanning it with a focused beam of electrons. The electrons interact with atoms in the sample, producing various signals that can be detected and that contain information about the sample's surface topography and composition.

Single-domain (SD): A uniformly magnetized magnetic particle with a single magnetic domain. Noninteracting SD grains are ideal recorders of paleomagnetic information. In most magnetic minerals, stable SD grains are extremely small (the SD size range in magnetite is ~30–80 nm).

Superparamagnetism (SP): Class of magnetic behavior exhibited by very small particles (<30 nm in magnetite) that have relaxation times on laboratory time scales (typically <100 s). For these particles, atomic magnetic moments align in a magnetic field to produce a strong induced magnetization that can be rapidly destroyed by thermal vibration soon after removing the field (seconds to minutes).

TEM (transmission electron microscopy): is a microscopy technique in which a beam of electrons is transmitted through an ultra-thin specimen, interacting with the specimen as it passes through. An image is formed from the interaction of the electrons transmitted through the specimen; the image is magnified and focused onto an imaging device. SEM focuses on the sample's surface and its composition whereas TEM provides the details about internal composition.

TGA: Thermo gravimetric analysis or thermal gravimetric analysis is a method of thermal analysis in which changes in physical and chemical properties of materials are measured as a function of increasing temperature (with constant heating rate), or as a function of time (with constant temperature and/or constant mass loss). TGA can provide information about physical and chemical phenomena such as second-order phase transitions, including vaporization, sublimation, adsorption, absorption, and desorption.

WL: it stands for Wireline. the term wireline usually refers to a cabling technology used by operators of oil and gas wells to lower equipment or measurement devices into the well for the purposes of well intervention, reservoir evaluation, and pipe recovery. Tools inserted into the well for both workover and logging efforts, wireline and slickline are very similar devices. While a slickline is a thin cable introduced into a well to deliver and retrieve tools downhole, a wireline is an electrical cable used to lower tools into and transmit data about the conditions of the wellbore called wireline logs.

**High-resolution magnetic susceptibility
data interpretation in a well through
the Miocene of the Vienna Basin**